



UNIVERSITÀ DEGLI STUDI DI TRIESTE

XXXIII CICLO DEL DOTTORATO DI RICERCA IN

INGEGNERIA INDUSTRIALE E DELL'INFORMAZIONE

finanziato da Electrolux Professional S.p.A.

**ADVANCED INTELLIGENT SYSTEMS FOR PROCESS
IMPROVEMENTS IN PROFESSIONAL LAUNDRIES**

Settore scientifico-disciplinare: ING/IND13 MECCANICA APPLICATA ALLE MACCHINE

**DOTTORANDO / A
FEDERICO FURLAN**

Federico Furlan

**COORDINATORE
PROF. FULVIO BABICH**

Fulvio Babich

**SUPERVISORE DI TESI
PROF. PAOLO GALLINA**

Paolo Gallina

ANNO ACCADEMICO 2019/2020

*“If you do not believe in
yourself, no one will do
it for you”*

Kobe Bryant

Abstract

This thesis presents theoretical and experimental studies on the improvement of the cleaning process for professional laundries, from sorting to drying phase. The research focuses on three areas, which can be enhanced to obtain benefit for both customers and workers. Sorting of garments, based on the washing program, is a time-consuming and risky job, as the workers are exposed to possible contaminations and bacteria, which proliferate in dirty clothes. In particular, this is very important in the hospitals business, where the clean rooms must be separated from the contaminated areas. In these places, an automation of the process is needed, along with an intelligent system able to correctly recognize and categorize the items for the subsequent sorting. After that the loads are divided into different baskets, they are washed in professional appliances. The dewatering process is an important step of the washing cycle, because it permits to short the post drying operations in tumble dryers and thus to save energy and time in the entire laundry process. Moreover, to guarantee the best performance possible during the extraction, it is important that the washing machine can detect and predict the amount of water content in the load during the extraction cycle, based on the type of load, the dimension of the drum, the spinning time and speed. For these reasons, an experimental three-dimensional model is developed, which depends on the drum speed and the extraction time. Finally, the garments need to be dried before to send back the items to the laundries' customers. The moisture measurement, during a drying cycle, is important for knowing the trend of the water evaporation and to stop the appliance at the right point, based on the program selected by the user. The sensors that are today used in the professional appliances are not accurate when the loads are near to the dry conditions, so the cycles last some minutes more to correctly evaporate the water from the textiles. It is fundamental to have sensors accurate in the entire range of the drying cycle, especially when the garments are almost dry, as it let to reduce the energy consumption, by avoiding the over drying. Since an improvement is needed especially in this area, a textile moisture content sensor based on

self-capacitance technology is proposed, with an experimental evaluation on four different fabric types. The solutions proposed in this thesis are the results of a research on the last advances in artificial intelligence and electronics, with a focus on their application for the professional business. The devices developed, verified with real functioning prototypes, show excellent results and are applicable for the laundry business. The research here proposed covers the entire cleaning process and is able to improve three areas that are today critical for the business.

Contents

List of Figures	XI
List of Tables.....	XIX
Chapter 1: Introduction	1
1.1 Professional Laundry Appliances.....	1
1.1.1 Washing machine	3
1.1.2 Tumble Dryer	10
1.2 Cleaning process in laundries	19
1.3 Contributions of the thesis	24
1.4 Structure of the thesis.....	27
Chapter 2: Autonomous Laundry Sorting	29
2.1 Introduction.....	30
2.2 Image Acquisition Hardware.....	35
2.3 Image Classification	40
2.3.1 State of the art.....	40
2.3.2 Deep Network Architectures	44
2.3.3 Custom Database	47
2.3.4 Transfer Learning Parameters Optimization.....	49
2.4 Garments features extraction	70
2.4.1 State of the art.....	70
2.4.2 Methodology for garments features.....	72
2.4.3 Color extraction and gripping point selection.....	75
2.5 Washing program selection	83
2.6 Automatic Sorting System	87
2.6.1 Robotic sorting prototype.....	89
Chapter 3: Water Retention Model.....	93
3.1 Introduction.....	94
3.2 Water Retention models.....	95
3.2.1 Numerical models	95
3.2.2 Analytical models	96
3.2.3 Experimental models.....	97
3.3 Water retention in washing machines.....	99
3.4 Experimental method	100
3.4.1 Experimental setup	100
3.4.2 Experimental procedure	102
3.5 Experimental model results.....	106
3.5.1 Time-analysis repeatability.....	106
3.5.2 Proposed empirical model.....	109

3.5.3 Model scaling.....	112
Chapter 4: Advanced Moisture Measurement	117
4.1 Introduction.....	118
4.2 Textile moisture sensors.....	121
4.3 Capacitance on lifter.....	124
4.4 Sensor development.....	127
4.4.1 Measuring circuit board.....	128
4.4.2 Sensor design	131
4.4.3 Shield.....	136
4.5 Experimental validation	139
4.5.1 Textile test	140
4.5.2 Harsh conditions test	148
Chapter 5: Conclusions and Future Works.....	153
Bibliography	159
Appendix A	175

List of Figures

Figure 1. Examples of laundry appliances manufactured in the plant of Ljungby, Sweden.	3
Figure 2. First washing mechanism created by Jacob Christian Schäffer [3].	4
Figure 3. Bull's patent that illustrates the first washing machine with a hand operated drum [4].	5
Figure 4. Thor washing machine, the first manufactured by a company that provided an electric motor connected to a rotating drum (1910).	5
Figure 5. Washing machines manufactured by Electrolux Professional AB are characterized by a stainless-steel frame to guarantee reliability in severe environments.	7
Figure 6. Cycle of Sinner represents the four variables that influence the cleaning results.	9
Figure 7. Clothes dryer patented by George T. Sampson in 1892 [14].	11
Figure 8. A modern dryer sold by Hamilton Manufacturing company in 1956.	12
Figure 9. Entire portfolio of dryers manufactured by Electrolux Professional. Image courtesy of Electrolux Professional AB.	13
Figure 10. Airflow in a vented tumble dryer. Blue arrows are environmental air, red arrows are heated air. Image courtesy of Electrolux Professional AB.	15
Figure 11. Clock of garments' falling, depending on the sense of rotation of the drum.	15
Figure 12. Three phases of the drying process, with temperature referred to the outlet air.	16
Figure 13. Semi-axial airflow on the left and radial airflow on the right. Image courtesy of Electrolux Professional AB.	16

Figure 14. Moisture levels for cotton (left) and polycotton (right) at the standard drying points. In blue the values with bone dry as reference, in red the values with condition dry as reference.....	17
Figure 15. Residual Moisture Content (RMC) circuit for the moisture content estimation during the drying process. Image courtesy of Electrolux Professional AB.....	18
Figure 16. An industrial laundry in the early of 20 th century [17]......	19
Figure 17. Distribution of professional laundries in western countries [17]......	20
Figure 18. In modern laundries there are a need of automatize processes for increase productivity and lower risks for workers [17]......	21
Figure 19. Coin operated laundry.	22
Figure 20. Typical human and computer vision pipeline for objects classification.....	31
Figure 21. Basic model of a Convolutional Neural Network (right) which is similar to the human brain structure (left) [21]......	32
Figure 22. Difference between CCD (left) and CMOS (right) sensors.....	36
Figure 23. Industrial color camera selected for the image acquisition. ..	37
Figure 24. Relation among working distance, focal length, field of view, and sensor size.....	39
Figure 25. Field of view calculation at a working distance of 500 mm. ..	39
Figure 26. Industrial camera, coupled with a wide optic, used to acquire images for the automatic sorting system.....	40
Figure 27. AlexNet architecture, the input image has size 227x227x3 [74].	44
Figure 28. ResNet50 architecture [82]......	46
Figure 29. Garments custom database composition created for the classification task The red horizontal line highlight that all the categories have 400 images at least.	47
Figure 30. Example of the images part of the custom database.	48
Figure 31. Streamline of the classification system using transfer learning methodology.	50

Figure 32. Framework proposed for training parameters and for their analysis.....	52
Figure 33. Training progress of ResNet50. Blue lines are the training progress, orange lines are the loss progress, black dots are the validation points connected by a dashed line to highlight the trend.....	55
Figure 34. Accuracy with learning rate variation using ADAM optimizer.	56
Figure 35. Accuracy with learning rate variation using SGDM optimizer.	56
Figure 36. Accuracy with drop variation using ADAM optimizer.....	57
Figure 37. Accuracy with drop variation using SGDM optimizer.....	58
Figure 38. Accuracy with regularization variation using ADAM optimizer.	60
Figure 39. Accuracy with regularization variation using SGDM optimizer.	60
Figure 40. Accuracy and average training time normalized on batch for the best performing CNNs.....	61
Figure 41. Accuracy and loss of the best performing architectures.	62
Figure 42. Accuracy and prediction time relative to the fastest network of each architecture.	63
Figure 43. Confusion Matrix of ResNet50 fine-tuned with Transfer Learning on the custom database.	65
Figure 44. Results from Bayesian optimization. The blue line is the minimum value of the objective function obtained so far; the green line is the relative estimated value from the optimizer. The brown line is the best accuracy reached from the network so far.....	69
Figure 45. Streamline to extract the garments color from the original RGB image using Class Activation Map to localize the item.....	74
Figure 46. Class Activation Map applied to three images randomly chosen from the database. On the left the original image, on the right the CAM applied to the picture, with the top-3 class predicted by the network. ...	76
Figure 47. Streamline for color extraction applied to three database images. a) original image; b) CAM; c) grayscale image; d) entropy filter; e)	

entropy borders with CAM border; f) borders inside CAM area g) area for color extraction..... 77

Figure 48. Color accuracy summary for each garment category. Blue bars are the image analyzed for each category, orange bars are the number of images with the wrong color extracted, the gray points are the color accuracy in percentage. 80

Figure 49. Gripping point accuracy for each category. Blue bars are the centroid of the CAM areas, gray bars are points of the maximum activation. 81

Figure 50. Two examples of gripping point errors. a) are the CAM centroids; b) are the maximum activation points. 82

Figure 51. Touch user interface of Professional Washing Machine, line 6000. The washing programs are based on garments' categories. 85

Figure 52. Washing program accuracy on random images taken from the database. The blue bars are the washing program final accuracy for each category, the gray bars remove the error that with a less aggressive cycle. 87

Figure 53. Coordinates conversion between camera and robot reference frames, from pixel to millimeters. 89

Figure 54. Robotic sorting system in an indoor environment. The baskets are placed around the cobot, that grabs the items onto a conveyor belt. There is one basket for every washing program presented in 2.5. The only sensor used is a camera. 90

Figure 55. Automatic sorting system flowchart, which connects all the modules developed. 91

Figure 56. Professional washing machines used for the experimental testing of water retention during the extraction phase. a) is WH6-6 with 6 Kg of capacity; b) is WH6-7 with 7 kg of capacity; c) is WH6-13 with 13 kg of capacity. 101

Figure 57. Picture (a) and sketch (b) of the experimental setup used to perform the water retention tests. 101

Figure 58. Flow chart to prepare the load before the test series through a stabilization, normalization, conditioning and weight process. 103

Figure 59. Flow chart describing the test procedure followed to test the dewatering performances of washing machines..... 104

Figure 60. Customized washing cycle used to perform water retention tests. 105

Figure 61. Water retention time history of the towels inside the drum during a spinning cycle considering a specified extraction speed, fill factor coefficient and drum dimension and shape..... 108

Figure 62. Repeatability of water retention tests at fixed spinning speed and washing machine. The blue line is the repeatability test number 1, the dashed red line represents test number 2 and the black dotted line the number 3..... 108

Figure 63. Water retention surface fitted on experimental data by a fifth order polynomial equation for a professional washing machine. 111

Figure 64. Data residual of the fitting polynomial equation respect to the experimental data for a professional washing machine..... 111

Figure 65. Comparison of water retention variation among the machines as a function of G-acceleration after one minute (a) and eight minutes (b) of spinning time. Each line denotes the absolute difference of water retention between two washing machines. The blue line shows the absolute variation between *WM1* and *WM3*, the black dotted line between *WM2* and *WM3*, and the red dashed line between *WM1* and *WM2*..... 114

Figure 66. Difference between mutual capacitance and self-capacitance. 119

Figure 67. Lifter used as a capacitance sensor. In a) the positioning of the lifter in respect to the drum which is grounded, in b) a focus on the lifter, which is hollow and have the space for the capacitance measurement circuit..... 125

Figure 68. Capacitive meter Agilent U1733C connected to the lifter and to the drum..... 125

Figure 69. Range for capacitance measurement using the lifter as sensor. 126

Figure 70. Accuracy for capacitance measurement using the lifter as sensor. 126

Figure 71. Design flow of the measurement system for moisture sensing.	127
Figure 72. Sigma-Delta modulator.....	128
Figure 73. In a) the Cypress measurement circuit board, in b) the Bluetooth module to communicate with an external device far from the sensor.....	129
Figure 74. Equivalent resistor model.	130
Figure 75. Sensor layouts for analysis. a) pad electrodes and hatch ground; b) trace electrode and hatch ground; c) trace electrode and ground.....	133
Figure 76. Frequency sweep of the sensor PCB c) without overlay.....	134
Figure 77. Cables comparison using sensor a) coupled with both no overlay and quartz glass overlay.....	135
Figure 78. Overlay comparison using sensor a) connected with both gray and black cable.....	136
Figure 79. Sensor layouts comparison using gray cable with 30 cm length.	136
Figure 80. Electric field lines between the sensor (ch) and the ground (gnd) without (left) and with (right) the shield [178].....	137
Figure 81. Shielding configurations for cables.....	138
Figure 82. Shield signal compared to the switching signal driven by the Sigma-Delta modulator.....	139
Figure 83. Sensor for moisture measurement (a) with the hatched shield on the back (b).	139
Figure 84. Test bench for testing different types of textiles in a steady condition.....	141
Figure 85. Measurement procedure for textiles moisture evaluation...	142
Figure 86. Test results normalized, using cotton.....	143
Figure 87. Test results normalized, using polycotton.....	144
Figure 88. Test results normalized, using wool.....	145
Figure 89. Test results normalized, using pure polyester.....	146
Figure 90. Experimental test results normalized, using four different textiles.	146

Figure 91. Experimental test results with absolute values, using four different textiles..... 147

Figure 92. Residual analysis of the four regression models on normalized data 148

Figure 93. Climatic chamber used for harsh condition test. 149

Figure 94. Temperature variation analysis at low relative humidity. ... 150

Figure 95. Temperature variation at high relative humidity..... 150

Figure 96. Comparison between the two temperature variations at different relative humidity..... 151

List of Tables

Table 1. Annual energy, water and detergent consumptions using professional washing machines [9].....	8
Table 2. Learning Rate selection with default training parameters.	53
Table 3. Accuracy [%] results with the learning rate value variations. ...	55
Table 4. Accuracy [%] results with the drop period and factor variations.	57
Table 5. Accuracy [%] results with L2 regularization variations using ADAM as optimizer.	59
Table 6. Accuracy [%] results with L2 regularization variations using SGDM as optimizer.	59
Table 7. Training parameters using Transfer Learning that results from the optimization using SGDM.	64
Table 8. Parameters selected for Bayesian Optimization, with the range for the values evaluation.....	67
Table 9. Iterations details of the Bayesian optimization with ResNet50. The objective function shows the error on the validation dataset. Learning rate, drop period and factor, regularization and momentum used for every training are reported.....	68
Table 10. Color misclassification for the category of garments. No garment class is not part of this table, because the category does not contain any item.....	79
Table 11. Gripping point errors for each category.....	81
Table 12. Washing program assignation based on garment's category and color.....	86
Table 13. Results of pixel to robot coordinates conversion. Points 1 and 2 are used for the constants determination, result is presented for the Check Point.	92
Table 14. Sample features.	102

Table 15. Comparison of water retention repeatability results at three different speeds for all the washing machines (WMs) considered. 109

Table 16. Value of the coefficients of fifth order fitting polynomial expression..... 110

Table 17. Statistical parameters to evaluate the accuracy of the model for the three washing machines..... 112

Table 18. Shape factor coefficient of the washing machine considered. 114

Table 19. Reference weights of the textiles used for the experimental tests. 141

Introduction

One of the most repetitive tasks regularly performed in all homes concerns laundry, which involves sorting, washing, and drying. When we move to professional sector, higher volumes of items must be processed in a short time, with the needs of more performing and durable appliances compared to the domestic ones. This thesis presents the result of a study on how to improve the process in professional laundries at any level, starting from sorting until drying. More specifically, this research aims to introduce artificial intelligence, automation and new sensors to improve the appliances and reduce the human presence in risky areas, where is important to avoid contamination and enhance the workers' conditions. For this reason, the thesis unfolds between different topics, but linked by the common intent to improve the process in the professional world.

In the next section, an overview of laundry products manufactured by Electrolux Professional will be given, as a background is fundamental to understand the environment where the research has been deployed. Then, the cleaning process in professional laundries will be analyzed, with the identification of the weak points where an improvement is needed. Finally, three projects will be presented, which focus on sorting, washing and drying.

1.1 Professional Laundry Appliances

Electrolux Professional is one of the leaders in providing appliances for food service, beverage, and laundry, serving a wide range of customers

globally, from restaurants and hotels to healthcare, educational and other service facilities. The products are manufactured in twelve facilities located in seven countries around the world and sold in approximately 110 nations [1].

Professional's long history dates back more than 100 years when companies such as Wascator, Zanussi and Cecilware, that were subsequently acquired by Electrolux AB, were founded. The professional business in the main Electrolux Group started in 1962, with the acquisition of Elektro Helios. Some years later, in the early of 70's, the professional business was expanded also to laundry. The business area within Electrolux Group was established for the first time in 1989, integrating all the professional activities that had been acquired throughout the years. These operations comprised market leaders in specific segments, such as food service, laundry system, commercial refrigeration and cleaning. It is only recently that the professional business has been expanded also to the beverage sector with the acquisition of Grindmaster-Cecilware in the United States in 2017. Then, one year later, SPM in Italy and, finally, UNIC from France, were added to Electrolux Group. Starting from 2020, Electrolux Professional has become an independent company with a spin-off from the main Group, and autonomously listed on Nasdaq Stockholm since march [2].

Electrolux Professional is divided into two segments: Food & Beverage and Laundry. The latter provides a wide range of equipment for professional laundry operations. In addition to the product offering, aftermarket services are provided to customers throughout the equipment lifecycle. Laundry products represents the 36% of the company net sales in 2019 [1]. Electrolux Professional manufactures a wide range of appliances for laundries, that are mainly divided into washers, dryers, and ironers. The focus of the thesis is to improve the process from sorting items until drying, for this reason the first two types of appliances will be explained in the next sections. The main R&D development and production center for washing machines and tumble dryer is located in Ljungby, Sweden, while the production is also present in Thailand and in France. In Figure 1, some of the new professional laundry products manufactured in Ljungby is presented.



Figure 1. Examples of laundry appliances manufactured in the plant of Ljungby, Sweden.

1.1.1 Washing machine

1.1.1.1 History

Washing machines are the appliances that, together with refrigerators, are the commonest present in every households. The need of washing clothes goes back to earliest civilizations, first performed in streams of running water and then using tanks and more sophisticated mechanisms. Washing garments by hand is one of the most laborious domestic tasks that exist. The clothes were rubbed on stones or wooden planks with sand, to remove dirt and stains. Then, the water was removed hitting the items with a wooden beater. As this was a tiresome chore, especially for washerwoman, there was a need for a mechanism to automatize the process, maintaining the same procedure.

The first invention of washing machines dates back to the 16th century, when a first idea was sketched by Jacob Christian Schäffer, with a mechanism probably created for the use in the textile manufacturing. It was composed by a tank, filled with hot water, with a lever was turned to wash the items that were finally wringed between two rollers to remove as much water as possible. The mechanism is shown in Figure 2.



Figure 2. First washing mechanism created by Jacob Christian Schäffer [3].

The first British patent listed under the category of Washing and Wringing Machine is the number 271, dated 22nd August 1691, by John Tyzacke. There is no diagram available and the description is about an invention for “washing of cloathes”. A second patent, issued to Hugo Oxenham in February 1774, deals with wooden rollers held together by metal springs. The main function was to press and iron the clothes, however, have also been used to remove water from clothes after washing. This problem is still studied today, and a section of this thesis will deal with the dewatering process.

During the 19th and 20th centuries, the washing machine was developed from being a simple primitive mechanism to a sophisticated domestic appliance. The first drum washing machine appeared in 1905 but was still hand operated. In Figure 3, an illustration from a patent registered by Bull is shown, with a drum inside a tank filled with water [4].

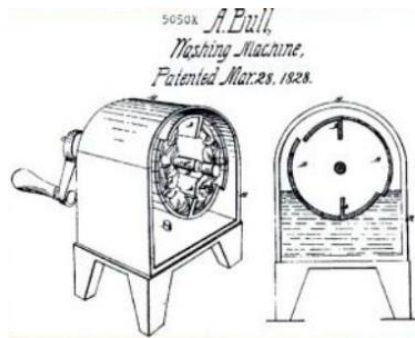


Figure 3. Bull's patent that illustrates the first washing machine with a hand operated drum [4].

Several other patents came in succession during the following years. The most relevant invention that enabled the washing machine to become a common household appliance is the introduction of the electrical motor. Henry Sidgier equipped for the first time the rotating drum with a motor, then Alva J. Fisher registered a patent with such automation in 1910 [5]. The concept was later improved from the same inventor, using a shaft coupling system to directly connect the electric engine to the drum of the appliance [6]. This solution was implemented in a product manufactured by the Hurley Machine Company of Chicago and called "Thor washing machine". It is shown in Figure 4.



Figure 4. Thor washing machine, the first manufactured by a company that provided an electric motor connected to a rotating drum (1910).

At that time, only the turning mechanism was electric, all the remaining controls were still automatic. The operator could manually control the filling and emptying of the water in the tub. The development was very rapid, by 1920 more than 1300 companies were producing washing machines [7]. It was only in 1930 that pressure switches, thermostats and timers were included in the appliances. Starting from the 80s, the introduction of electronics lets to introduce new advanced features with the adjustments of washing parameters such as water level and spinning speed [4].

1.1.1.2 Washing process

Over the years, the technological development has greatly improved the design and functionalities of washing machines, making them more reliable and cheaper. The economic growth, with the industrial needs of washing many items in a short time, pushed the development of appliances that can be operated in harsh environments with the possibility of having high loads to be washed in a single cycle. Professional washing machines are specifically designed for industrial applications where longer life, high load capacity, robustness and fast cycles become relevant. These products have to improve the durability and washing performances when compared to the domestic ones, handling high load capacity that can reach up to 400 Kg. Smaller appliances are typically used to wash uniforms clothing while the larger ones are dedicated for hotel and hospital linens. The machine consists of an internal stainless-steel metal drum which is perforated with many holes. The drum sits within a heavy metal frame which can be bolted to the ground when the dumpers are not provided. All the machines have springs to help prevent "shakes" on the extraction cycle. There are connections at the back or side of the machine for the chemical pumps, a drain outlet, and a lockable door. The extraction force required is therefore higher, as the drum dimension is much bigger than household machines, and the quality of materials and assembling must be high to guarantee a long-term operation. Professional washing machines are designed for a wide usage in laundry shops, hotels, and apartment buildings. Business working areas in these places typically run from 6 a.m. to 10 p.m., with stores that usually occupy between 1000 and 5000 square feet. Focusing on coin operated laundry, in the United

States there are about 29500 shops that generate nearly 5 billion dollars in gross revenue annually, with the business that increases proportional to the population number [8]. These data explain why, unlike domestic appliances, the professional sector demands reliable products that can operate continuously in diverse environmental conditions. Indeed, as these appliances are sold around the world, the washing cycle have to be the same performances independently of water temperature and hardness, air humidity, type of detergent, plant layouts etc.. Professional washing machines, as shown in Figure 5, has a robust frame with panels, doors and the main structure built is stainless-steel instead of cheaper materials as in the domestic products.

As laundry has a great impact on energy and water consumptions, new regulations impose limits to lower the environmental impact. The relative consumptions of professional washing machines can be divided in categories based on three energy needs: for water heating, for motor action and for supply all the electric and electronic components [9]. In Table 1 is shown the annual water, energy and detergent consumptions of professional washing machines based on the washing capacity.



Figure 5. Washing machines manufactured by Electrolux Professional AB are characterized by a stainless-steel frame to guarantee reliability in severe environments.

Washing Capacity [Kg]	Laundry [Kg/year]	Energy [kWh/year]	Water [liters/year]	Detergent [kg/year]
<15	14400	3026	233280	330
15÷40	42200	10973	740610	798
>40	194400	81648	3265920	4199
Barrier washer	56300	26461	1080960	1216
Washing tunnel	3825000	1606500	27540000	41310

Table 1. Annual energy, water and detergent consumptions using professional washing machines [9].

As the resources required for washing items is high thanks to the wide global diffusion of professional washing machine, it is important to improve the efficiency maintaining the cleaning performances. There are four factors have to be balanced to achieve optimal cleaning results: temperature, time, chemistry and mechanical action. These variables are part of the “Cycle of Sinner”, invented in 1959 by Dr. Herbert Sinner, which is shown in Figure 6.

The functioning of the cycle is that one action can be privileged in respect to others increasing the size, but the total area has to be preserved to not change the energy necessary to perform the cleaning process. Increasing the size of one factor automatically means that the total of the other variables becomes smaller. On the contrary, reducing the size of a factor increases the size of the others [10]. For example, if a high temperature is used to remove stains, there is a lower need to use high cycle times, mechanical action or detergents as the temperature is helping more than the other variables to clean the items.

Every variable has a different effect on the cleaning process. Temperature accelerates the activation of the chemicals of detergents and speeds up the removal of the soil, in particular grease and fat. The longer the cycle time, the better the cleaning performance: prolonged washing and interim soak phase have a positive effect on the final result. Detergents have the purpose of removing and then suspending the soil. Targeted chemicals ensure cleaning and hygienic performance on particular type of soils, the right dosage should be used to avoid any

damage on the load. Mechanical action, which is obtained during the rotation of the drum, ensures that soil is removed from the surfaces of crockery [11]. However, the Cycle does not consider the textiles' type and the consumer behavior. Following the trend of the last years, the mechanical action and the time are preferred to reduce the energy consumption and environmental impact, which are primarily caused by the temperature and the detergents.

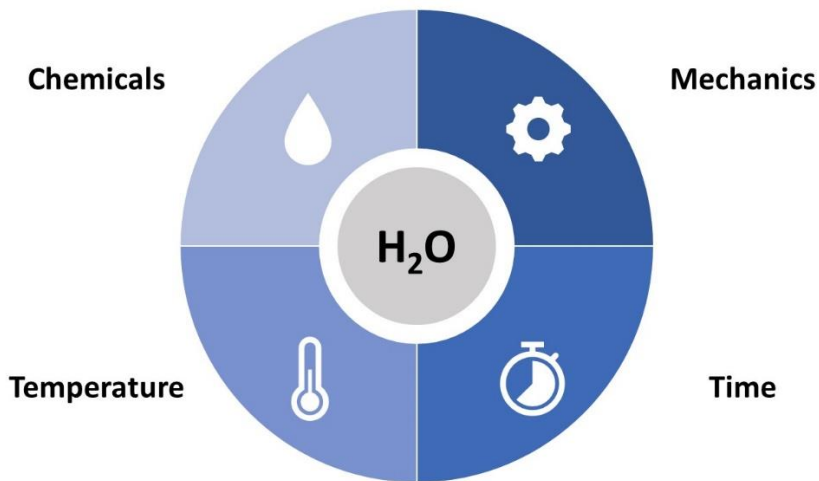


Figure 6. Cycle of Sinner represents the four variables that influence the cleaning results.

Professional washing machines are programmed with different washing cycles, specifically designed for different textile types, garments categories and soil level. Among the others, the most used in professional laundries is the “60° cotton” cycle, which is composed by a sequence of main wash, drain, extraction and rinse phases. During the main wash phase, the drum is filled with water previously heated to the desired temperature and mixed with detergents and softener. The tub rotates clockwise and counterclockwise at low speed to blend the load and to provide the rubbing of the clothes, important for the mechanical action. The main wash is followed by the drain phase where the residual water not absorbed by the laundry is drained out from the machine in few seconds. Sometimes, an intermediate short and low speed extraction phase is required to decrease the water content inside the load before that the successive rising phase starts. This allows the removal of detergents and dirty particles dissolved in the water and to finally refresh the washed

items. A series of drain, extraction and rinse cycles are performed in succession after the main wash, depending on the textile type and amount of load. The final step is always the extraction cycle, defined also as spinning, in which the revolution speed of the drum increases up to the defined speed, which is usually high. The items are subjected to the centrifugal force that drains out the water.

The dewatering process is fundamental, because it leads to shorter post drying operations in tumble dryers and thus to save energy and time in the entire laundry process. As discussed in [12], the energy necessary for drying textiles strongly depends on the final residual moisture content. To guarantee the best performance possible during the extraction, it is important that the washing machine can detect and predict the amount of water content in the load during the extraction cycle, based on the type of load, the dimension of the drum, the spinning time and speed. Many parameters influence this process, such as the type of textile, the appliance capacity, the amount of load and its aging, the quantity and chemical composition of detergents, the principal fluid parameters (water temperature and hardness), the spinning speed and washing programs [13].

1.1.2 Tumble Dryer

1.1.2.1 History

Before the advent of the drying systems, the only way to have the garments dried was to hang out the items to the sunlight. This method was time consuming, as every clothes has to be stretched or hung, and requires a lot of space available outdoors. With the advent of professional laundries, where many items are needed to be processed quickly, it is important to have appliances that dry high loads in a short time.

The first drying machine has been created by Pochon, a French inventor, that creates in 1799 a drum with holes where to place the garments. The items were dried over an open fire with a hand cranking system. The design of such machine was working but has several disadvantages: the garments were smelling of smoke and occasionally were dusted in soot [7]. Around 100 years later, in 1892, George Sampson improved the initial idea of Pochons, using a metal drum with a rack but

located away from the main source of heat [14]. Furthermore, a fundamental difference in its variation is the use of a stove instead of an open fire, to improve the safety of the user. The figure of the system patented is shown in Figure 7.

As the technology was rapidly advancing in the early of 90s, in 1915 was already possible for consumers to purchase an early design of tumble dryers for their homes. However, the price was still high, and the appliances were affordable only of a small elite of people. In 1938, an American company “Hamilton Manufacturing” started to sell a cheaper version of driers based on the improvement of J. Ross Moore, which introduced for the first time both a gas and an electric model. The model was called “June Day” [15].

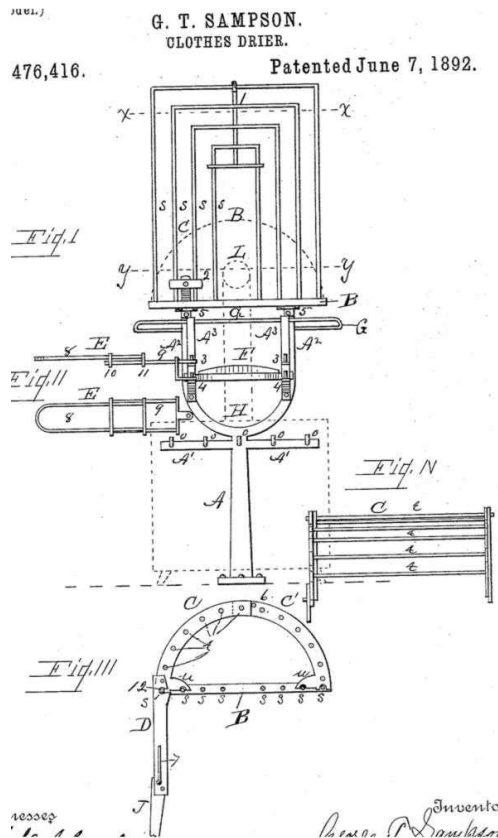


Figure 7. Clothes dryer patented by George T. Sampson in 1892 [14].

Some years later some sensors were added, and the mechanism was improved. Temperature controls, timers and a cooling cycle were implemented during the 40s, and the first dryness sensor was invented in the 50s. The latter innovations were fundamental, as the dryer was automatically switched off based on the garments' moisture content. In 1956, Hamilton manufacturing company was already selling a dryer with temperature control and several cycles implemented for different fabric types [16]. The appliance is shown in Figure 8. Further advances were developed in the next years, with the introduction of the electronics inside the machine.

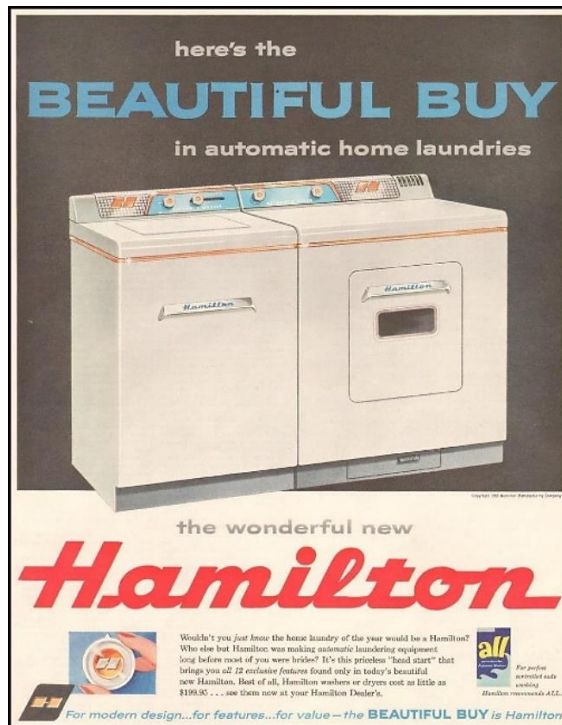



Figure 8. A modern dryer sold by Hamilton Manufacturing company in 1956.

As for washing machines, also professional tumble dryers have to guarantee reliability and robustness to operate in severe environments. The frame is built in stainless steel and the drum are bigger compared to the domestic ones, to dry high loads in a short time. Today, tumble dryers' models can be divided into three categories: vented, condenser and heat pump. In vented models, the hot and damp air is pumped out through a

flexible hose to the outside, so the dryer needs to be placed close to a wall or a window. This is the more traditional type of dryers, and the source of energy for the heater can be either gas or electricity. The condenser models do not need to connect a hose to eject the air to the outside, as the moisture extracted from the load is condensed into a removable tank. The containers can be emptied into the sink when full and most appliances have an indicator to let the user know when the tank needs to be emptied. A hose can also be connected to drain to avoid emptying the container. Heat-pump models are the most expensive but also energy-efficient dryers available on the market. They use a heat pump to heat the air before it flows into the dryer and then to cool down it for the moisture condensation into a tank.

1.1.2.2 Drying Process

Electrolux Professional manufacture standard, low-energy and condenser dryers with electrical, gas and heat pump options. The condenser dryer and heat pump dryer have the particularity that they do not need any exhaust outlet through external walls. Stacked dryers can also be found in the product range and they are useful to save space. These models are electrically heated with a drum volume between 130l and 190l. Dryers in Electrolux Professional portfolio are available in a range from 130l to 1200l (7 kg to 60 kg of load), in Figure 9 all the models manufactured by the company are shown.



	T5130-LAB	TD6-6	lagoon TD6-7	T5190 T5190LE	lagoon TD6-14	T5290 slimline	T5300S	lagoon TD6-20	T5425S	T5550 slimline	T5675 slimline	T4900	T41200
Drum volume	130	130	135	190	255	290	2x300	360	2x425	550	675	900	1200
Electric	x	x	x	x	x	x	x	x		x	x	x	x
Heat Pump			x	x	x			x					
Gas			x	x	x	x	x	x	x	x	x	x	x
Steam					x	x		x		x	x	x	x
Stacked							x		x				
Condense		x											

Compass Pro Selecta

Figure 9. Entire portfolio of dryers manufactured by Electrolux Professional. Image courtesy of Electrolux Professional AB.

Professional dryers are in the market above the semi-professional and the domestic market. The differences between those segments are the longer lifetime, the higher load processed and a better finish with fewer creases. They have shorter drying program, bigger heating systems and 3-phase connection. With that kind of dryers, it is possible to dry up to 2 loads per hour which led to a time and economical saving. A professional dryer has a lifetime around 30000 cycles compared to 3000 for a household dryer. The capacity is also higher from 5,5 kg to 60 kg compared to 5 to 8 kg. The drying program is around four times shorter and the processed load of an eight hours working day is up to 150 kg, six times higher than a domestic one. This type of machine also offers a high flexibility and programmability to the user. A professional dryer has a lifetime of approximately 10 years, meaning 5 times longer compared to the household appliances.

Basic working principle for a vented tumble dryer is shown in Figure 10, where the arrows represent the airflow from the ambient air to the outlet of the dryer. Garments are inside the drum and float in the hot air stream while the drum is rotating. The inlet air is heated using one of technology available, as gas or electricity, and then blow inside the drum. To get an efficient drying, the lifters inside the drum moves the garments in a way that they are more in contact with the airflow. The hot airflow goes through the garments and absorbs the moisture, then the humid air passes the lint filter before being blown out the machine by the exhaust pipe. The drum is rotating at a special speed according to the program and to allow the garments to fall between 2 and 8 o'clock and 10 to 4 o'clock, as illustrated in Figure 11.

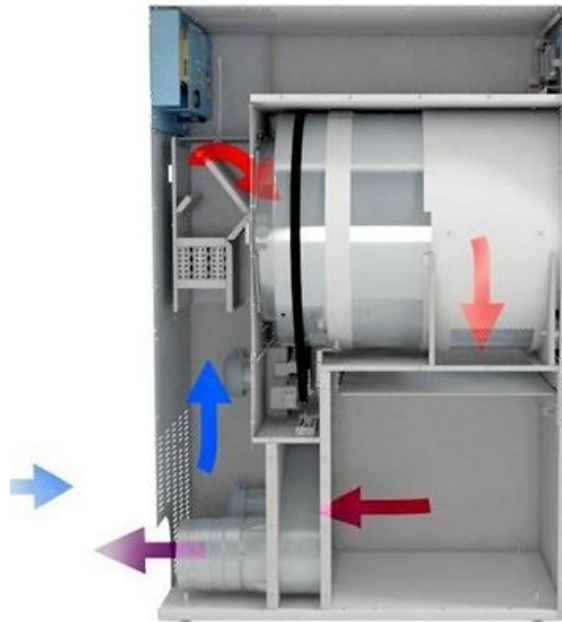


Figure 10. Airflow in a vented tumble dryer. Blue arrows are environmental air, red arrows are heated air. Image courtesy of Electrolux Professional AB.

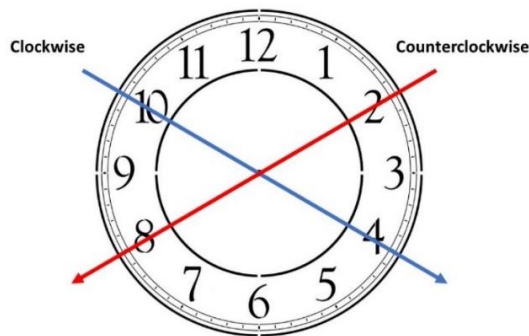


Figure 11. Clock of garments' falling, depending on the sense of rotation of the drum.

Three different stages can be recognized in the drying process, as is shown in Figure 12. The first step is the heating, which takes between 2 and 5 minutes to reach the temperature to which the moisture start to evaporate from the load. The time depends on the heating source and on the initial temperature of the wet garments. The second step is evaporation, which is the longest and takes between 20 and 30 min. The amount of 90 till 95% of the total water content is evaporated at a constant temperature of around 45°C. Finally, in the last stage, garments

will reach the dryness required, in case of a bone-dry cycle all the hidden moisture inside the pockets and zippers is removed.

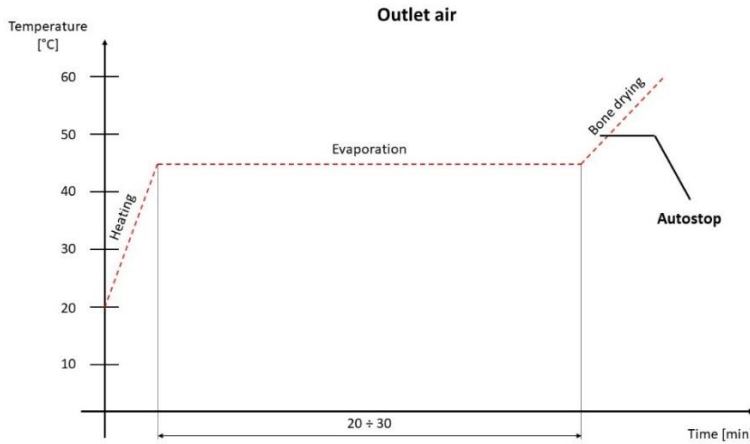


Figure 12. Three phases of the drying process, with temperature referred to the outlet air.

There are three directions to blow the hot airflow inside the drum: radial, axial or semi-axial airflow. In semi-axial airflow, which is illustrated on the left in Figure 13, the heating element is in the back of the appliance. In the radial airflow, on the right in Figure 13, the heating element is placed on the top of the machine. The axial airflow has also a heating source on the back. Gas and electricity can be used with all airflow configurations. In the last launched dryer line, the semi-axial airflow is the only option available, as it is the best performing among all the configurations. In this case, the air flows inside the drum axially and leaves it radially.

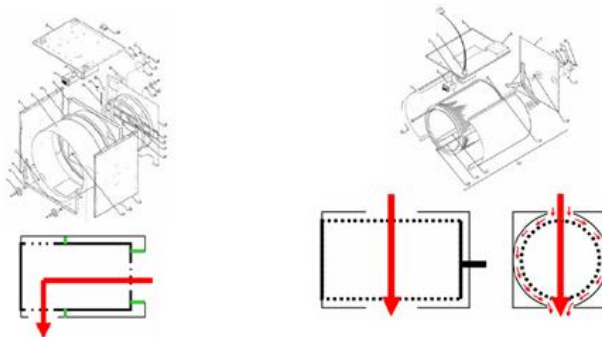


Figure 13. Semi-axial airflow on the left and radial airflow on the right. Image courtesy of Electrolux Professional AB.

At the end of the drying process, two actions are performed. The first is called “cool down”: the garments are cooled down to avoid any wrinkling and provide an anti-crease effect. It is also done to reduce the risk for the user to burn his hands and to avoid self-combustion of the garments. The second action is the “anti-crease”: the drum rotates in both directions at regular intervals to avoid wrinkling.

Three different references can take place when talking about moisture content inside textiles: iron dry, condition dry, bone dry. Usually, bone dry and condition dry are the most common references used in laundry standards. A real process is usually stopped at iron dry, condition dry or slightly over dried levels of moisture. Bone-dry is defined as the total absence of moisture at all inside the garments while condition dry has some moisture that comes from the air humidity. Depending on the textile types, these values can change as the fibers can retain different quantities of moisture. Condition dry can be calculated from the bone dry weight leaving the items in a climatic chamber at a certain air temperature and humidity for a fixed time, as defined from the standards. The moisture content expressed in percentage can vary based on the reference point used, which are typically condition dry or bone dry.

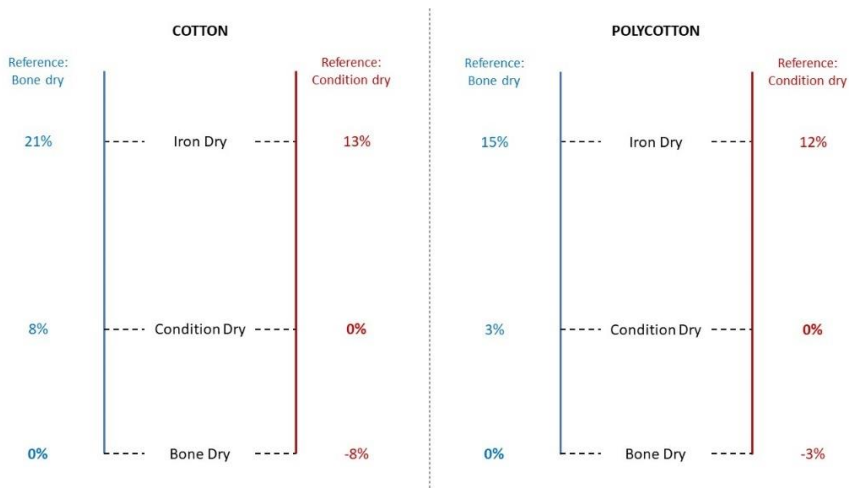


Figure 14. Moisture levels for cotton (left) and polycotton (right) at the standard drying points. In blue the values with bone dry as reference, in red the values with condition dry as reference.

In Figure 14, the moisture content for cotton and polycotton is shown depending on which reference base is used. Cotton is showed on the left, polycotton on the right. The values with bone dry as reference are displayed in blue, the ones with condition dry as reference are in red. For example, with bone dry as a reference, the moisture content of cotton at condition dry is 8% and 21% in iron dry. Instead, if condition dry is used as reference, iron dry is 12% of moisture content and bone dry is -8%.

At present, two different methods are used to measure the moisture content in the garments inside the machine, during a drying cycle. They are called Residual Moisture Content (RMC) and Autostop. The Autostop function stop the drying process when the outlet airflow temperature reaches a set temperature, as shown in Figure 12. The RMC function is based on the conductivity between the drum and the lifter and is illustrated in Figure 15.

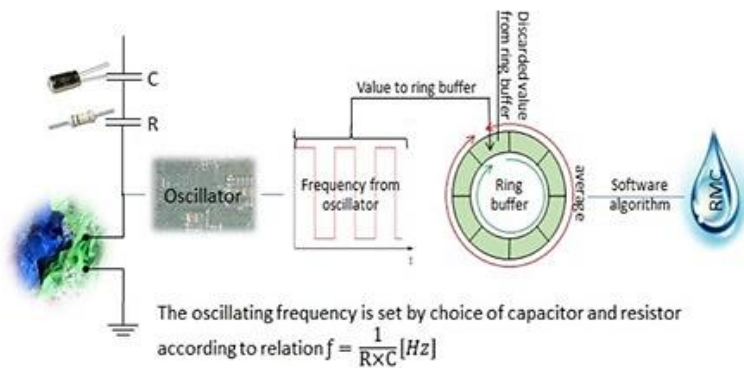


Figure 15. Residual Moisture Content (RMC) circuit for the moisture content estimation during the drying process. Image courtesy of Electrolux Professional AB.

In this system, the garments loaded in the drum are seen as an element of a RC circuit. They give to an oscillator different frequency, according to the fluctuation of the resistance of the circuit. A low frequency, that is related to a low conductivity, means that the garments are dry. This measurement system is accurate between 50% and 2% with reference to condition dry but cannot detect the moisture content down to bone dry. For this reason, an improvement is needed to accurately detect the moisture content in all the moisture range, for every type of textile. This is particularly important to reduce the energy consumption

and avoid the over-dry phenomena, as the garments are dried for an additional fixed time below the detection range of the actual measurement circuits. Moreover, the RMC circuit needs to be calibrated on the lifter' materials and size, with the consequence that is model dependent. A new sensor, that can be applied in every tumbler model, would be beneficial to avoid the tare and to improve the manufacturing process.

1.2 Cleaning process in laundries

As described in 1.1.1, during the beginning of the 19th century parts of the laundry processes were already mechanized. The heavy laundry work in households was hard, slow, and tedious. Large and numerous items were soaked in a boiling solution of water, lye and soap, with a great toll on the back, shoulders, arms and hands. It took to days to wash and dry all the household's clothes and five days later the task started all over again [17]. With the economical and industrial expansion, the needs of washing more and more garments brought to the born of industrial laundries, were to process high quantities of items in the shortest time possible. It was no possible to bring the same practices used in households into industries. Cleaning, well-maintained garments is a vital component for hotels, restaurants, hospitals of all sizes and standards. In some cases, the linens are owned by the customer and laundered externally and in others by the laundry operator, who rents and clean the items for the customer.



Figure 16. An industrial laundry in the early of 20th century [17].

Professional laundries today are large buildings with several complex flows of items, dozens of specialized machines and up to several hundred people engaged in the operations. The industrialization has made the running cost of small laundries, which are tied to a single customer, too high compared with the benefits that can be gained by centralizing the laundering from many customers in a unique site. The simple equation that the more items to spread the investments over, the better equipment you can invest in, has transformed the laundries in larger plants able to serve more and more customers [17]. In concrete figures, the relative distribution of industrial laundries in western world countries is shown in Figure 17.

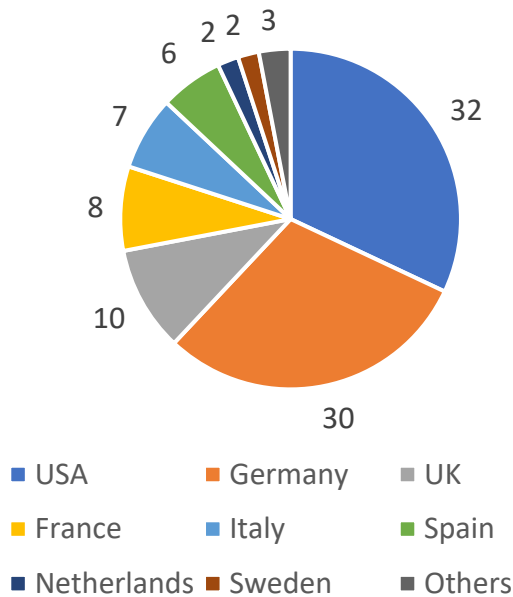


Figure 17. Distribution of professional laundries in western countries [17].

The modern laundries, the garments pass through a series of sequential process steps, which are all created to increase the productivity per working or clock hour. Each splitting up of the entire process has been done with the purpose of specialization and automation. The operations are characterized by a typical structured flow with include:

- Collection of soiled linen from source
- Sorting of items based on stains and washing programs

- Washing
- Drying
- Finishing
- Final inspection
- Ironing and folding
- Storage and transportation back to the customer.

To complete all these operations, there are different staff employed with different functions: sorters, washmen, tumbler dryer and ironer operators, folders [18]. The layout of the laundry and the workplaces are based on the phases previously described. The starting point is the soiled uncategorized items storage, followed by different areas for sorting, washing, drying, finishing. Advanced professional laundries are characterized by a high degree of specialization and automation, while older plants have still manual processes and low productivity. In technical terminology, laundries that are on the same location as the customer, called On-Premises Laundries (OPLs), are distinguished from sites that are far from their clients, called Central Laundries. The former is typically found in hotels, hospitals, residential homes, and factories. Moreover, Heavy Duty Laundries (HDLs) are distinguished from the smaller Professional Laundries (PLs), with the limit that is 15 metric tons of work per week. PLs are typically college rooms and coin operators, where the machines are smaller than HDLs but bigger than the domestic ones. An example of Heavy-Duty Laundries is shown in Figure 18 while a coin operated Professional Laundry is in Figure 19.



Figure 18. In modern laundries there are a need of automatize processes for increase productivity and lower risks for workers [17].

When soiled items arrive at the laundry for the cleaning, it is important to sort the garments before the washing take place. Different items are washed at different temperatures, at diverse water levels and chemicals. The sorting expedites the successive processing, and the items are kept separate for an easier identification. The machine programs have an influence on the sorting, as the garments have to be distinguished among:

- Article, the individual piece of linen
- Category, a group of articles that can be processed together
- Program, the appliance setting for a specific category.



Figure 19. Coin operated laundry.

The purpose of sorting is to make decisions on garments' treatments to process equally the items belonging to the same category. Soiled garments should always be kept separate from clean ones to avoid the risk of a potential cross-contamination. When they arrive to the laundry, they are transported using bags or trolleys which are then manually emptied in most cases. Then, garments are placed in a stainless-steel sorting table or, in HDLs, in a conveyor belt. The sorting process are conducted by

individuals or a team of sorters. There are some criteria that are usually followed for the sorting:

- Colored items are separated from the white ones
- Linens are separated by fiber type or category
- Items are divided according to the degree of soil.

In the guidelines described by [18], items are sorted based on categories: sheeting, pillowcases, duvet covers, towels, colored towels, bathrobes, cleaning clothes and mops, table linen. The categories are defined based on the customer sector of belonging and on the washing programs of the appliances used in the laundry.

The sorting stage is the riskiest place for workers in laundries, as they are in direct contact with dirty and potentially contaminated items. In some countries, as Germany, the authorities do not allow to handle contaminated textiles while dirty. All sorting and categorization are either done already at the customers' site or in the laundry plant after the washing, which is problematic for the program selection. The advantage of pre-sorting is that it is possible to categorize several loads to control what is washed together and to remove any foreign objects before washing. It is also an advantage for controlling the batch volumes. For this reason, this is the preferred options in countries where it is admitted [17].

When sorting items, the workers must take several precautions are they are exposed to a potential contamination. They must wear protective clothing, also if hotel linens are not as potentially infectious as hospital linens. The protective wear includes a hospital-style gown which ties at the back or a plastic apron, rubber gloves and even a face mask. The face mask is worn to protect the worker from the dust which becomes airborne. Soiled towels that are in contact with all parts of the human body can be contaminated with potentially infectious body fluids. In case the workers have abrasions or cut on their hands, these must be covered by a protective waterproof dressing to prevent the entry of bacteria to the wound. In any case, the hands should be washed regularly with an antimicrobial soap both before and after the job.

In order to reduce the risk for people that work in sorting areas, which is particularly important also in this period of Covid-19 pandemic spread, an automation of the process is needed. The sorting principles should be

defined according to the washing program and the garments that has to be cleaned, and a final system must be developed with a fully automatic platform. This has also the advantage to free workers both from heavy clothing and from a repetitive and time-consuming job, in order to have them available for other tasks in different areas. The sorting system is particularly important for hospitals, where the contaminated area is separated from the clean rooms to avoid any cross-contamination coming from the linens.

1.3 Contributions of the thesis

The aim of the thesis is to improve the whole process of the laundry cleaning, starting from sorting until drying. The goal is to take advantage from the last advances in artificial intelligence and electronics, with a deeper research on the weak points of these technologies for a successful application into professional products. More specifically, the present study has been focused on three areas of the cleaning process: sorting of garments, extraction phase at the end of the washing cycle, and moisture measurement during the drying run. These topics are important both to free workers from risky jobs, as in contaminated places for sorting, and to enhance the washing and drying cycle with the final objectives to improve the energy consumption and the final cleaning results for customers.

The principal contributions of the thesis can be summarized in the following points:

- *Image classification system development*

An autonomous classification system, based on deep Convolutional Neural Networks, has been developed with the final assignation of an input image into one of the 16 categories defined by the author. Several CNNs has been compared and trained using the Transfer Learning technique, with a novel pipeline to select the best training parameters. A new custom database, with more than 8000 images, has been built for the training purpose. A final network, able to categorize the images into one of the 16 categories, has been selected based on the laundry requirements.

- *Garments color and gripping point extraction*

Based on the results coming from the Convolutional Neural Network used for the classification of images, other two useful information for the laundry business has been extracted. Instead of using the popular object detectors already available from other research, in this work the activations of the neural network are used to extract color and gripping point, for the first time according to the author's knowledge. The areas with the highest activations are selected from the original image, then the color is recognized using some Image Processing technique. The gripping point is selected, using either the maximum activation point or the centroid of the selected area based on the garment's category.

- *Prototype of an autonomous sorting platform*

The recognition system has been applied to a fully autonomous prototype for the sorting of garments, based on the washing program. The information coming from the classification network and its activations are computed to assign a washing program to each item present in an image. The novel platform developed is able to sort the garments based on class and color information. The system comprises:

- a conveyor belt, to move the garments
- an industrial camera, to acquire images of the items
- a collaborative robot, to pick and sort the garments into one basket assigned to a washing program.

- *Water retention value forecast*

The value of the residual water content during the extraction, based on drum speed and cycle time, is forecasted based on a regression model. An experimental analysis, using three professional washing machines, has been carried out with a final model on three axes.

- *Moisture measurement sensor*

A novel sensor, based on self-capacitance, has been developed to measure the textile moisture content during the drying

process. The system developed is able to measure the moisture in the entire drying range, from 70% till 5%, with bone dry as reference. The final accuracy obtained meets the requirements for the professional tumble dryers.

- *Publications*
 - The research on the training parameters setting, with a comparison among five Convolutional Neural Network, has been condensed in the paper *“Transfer Learning for Garments Classification with Deep Neural Networks Parameters Optimization”* submitted to *Applied Artificial Intelligence* published by Taylor & Francis.
 - The work on the autonomous garments sorting system, based on category and color, has been condensed in the paper *“Garments Category and Colour Extraction with Grip Point Detection for Robotic Sorting Systems”* submitted to *International Journal of Intelligent Robotics and Applications* published by Springer.
 - The research on the water retention three-dimensional model has been condensed in the paper *“Empirical model of textile water retention in professional washing machines”* submitted to *The Journal of the Textile Institute* published by Taylor and Francis.
 - The work on the moisture sensor development, based on self-capacitance, has been condensed in the paper *“Design and experimental validation of a novel self-capacitance sensor to estimate textile moisture content”* submitted to *Sensing and Imaging* published by Springer.

1.4 Structure of the thesis

The thesis is structured in 5 chapters.

- *CHAPTER 1 – INTRODUCTION*

This chapter gives an overview about the professional appliances and the cleaning process in laundries. The purpose is to provide general information regarding the products evolutions, with an history of the main achievements reached during the many years of developments. The focus then moves to the weak points that requires further investigations, with the final goal of simplify the customers usage and improve the usability and the general efficiency. More specifically, the areas identified are the sorting before the cleaning process, the extraction phase of the washing cycle and the moisture measurement during the drying run. Finally, a summary of the main contribution given by the present thesis is presented, also with a list of publications submitted to international peer-reviewed journals.

- *CHAPTER 2 – AUTONOMOUS LAUNDRY SORTING*

This chapter first presents a survey regarding the traditional and more recent methodologies for image classification and object recognition. Then, a focus on Convolutional Neural Networks and Transfer Learning technique is presented, which are the most promising way to perform the garments classification into the classes defined for the washing program selection. A novel pipeline for the learning parameters optimization and for the CNNs comparison is described, with the final accuracy of the algorithms analyzed. All the information needed for the washing program are extracted from the same network, using the Class Activation Map and some Image Processing techniques. Once the garment's color and the gripping point are extracted, a washing program is assigned to each item. Finally, a fully automatic sorting system is presented, with a real application on a prototype and a trial on new garments previously unseen by the network.

- *CHAPTER 3 – WATER RETENTION MODEL*

This chapter explain the water retention three-dimensional model built up starting from experimental data collected on several tests. First, an overview is given, focusing on the retention calculation in porous media and three possible ways to address the problem. Then, the experimental methodology followed to conduct the test is presented, with a detailed explanation of the test bench built. Finally, the retention model is shown, which consist of a surface on three axes: retention, centrifugal force, and extraction time. A scaling analysis about the different drum dimensions is performed, showing that the results achieved are independent by the drum dimension.

- *CHAPTER 4 – ADVANCED MOISTURE MEASUREMENT*

This chapter first present the state of the art of moisture sensors, which are based on different technologies. The advantages of the capacitance measurements are presented, with an in-depth explanation on the self-capacitance. The capacitance technology is first evaluated on the tumble dryer, to have an indication about the range and the resolution of the measurement needed for the development. Then, the acquisition circuit is explained together with the sensor design, which is tested using an impedance analyzer. The overall system is tested on a test bench using four different textiles, in the moisture range processed by the professional tumble dryers. Finally, the sensor is tested on a climatic chamber under harsh environmental conditions, to prove the functioning also in extreme conditions like inside the tumble dryers' drum.

- *CHAPTER 5 – CONCLUSIONS AND FUTURE WORKS*

The overall conclusions of the study are presented, to evaluate the results obtained for each of the projects presented in the thesis. Based on the outcomes, the areas for possible future improvements are presented, with some ideas on how to solve the most difficult problematics that are highlighted.

Autonomous Laundry Sorting

Sorting garments is a time-demanding operation and a risky job for workers, that are exposed to soiled and contaminated garments. Therefore, this process needs an automation for laundry business, with the automatic sorting of the items based on the washing program. In this chapter, an automatic laundry sorting system is proposed, with the usage of a collaborative robot (cobot). The developed system acquires the images from an industrial camera placed over a conveyor belt, then the algorithms perform the classification and the localization of the items. Image analysis is based on a single deep convolutional neural network, able to both classify and extract features from the images thanks to its activations.

Deep Neural Networks (DNNs) are increasing their popularity thanks to the great performances achieved on classification of images in several fields. Different DNN architectures are compared, to classify garments into 16 defined categories and to evaluate the influence of training parameters in the overall accuracy. Five well-known and powerful architectures are used: AlexNet, GoogLeNet, VGG16, ResNet50 and Inception v3. The transfer learning technique is applied to train these networks for the new classification task, starting with the existing pre-trained weights from ImageNet database. Firstly, a custom database is created, downloading images available on the internet and manually labelled into the defined categories. Data augmentation with common transformations like rotation, translation and scaling is applied in every training epoch to reduce the risk of overfitting. Then, because of the lack

of information in literature about the training parameters to be set, a new framework is built to allow the evaluation of their impact on the final accuracy. Two optimization algorithms are selected to update the weight values: stochastic gradient descent with momentum (SGDM) and adaptive moment estimation (ADAM). For each algorithm, the parameters are adjusted and optimized following the framework steps. Finally, both an analysis of the impact of each training parameter, related to the architectures and the optimization algorithms, and an investigation of the network performances are carried out.

Garments are then located into the image using the activations of the network previously chosen for the classification. Class Activation Maps and Image Processing techniques are used for the image analysis, to extract two useful parameters: color and gripping point for the robot. Using the classification and color of garments coming from the previous steps, a washing program is assigned to the image. Finally, the vision system is evaluated for a sorting application using a cobot in an indoor environment, with garments never processed before by the model developed. The final accuracies confirm the validity of the proposed new methodology adapted, that can be further expanded for sorting of garments in pile.

The task is challenging because the clothes, lying on a conveyor belt, can be highly wrinkled and self-occluding. Garments are deformable objects that can take on infinite possible configurations, so that learning a generalized representation and extract useful features from limited training data is difficult. Moreover, the proposed sorting system is flexible and can be used under different light conditions in indoor environments, with a good generalization on new garments that are not part of the database. To the best of the author's knowledge, it is the first time that such streamline has been proposed and that CAM are used as an affordable tool also for the robot picking point.

2.1 Introduction

Recognize, localize, and classify garments is a very simple task for humans, but poses hard challenges to artificial intelligence, which is

extremely necessary when an automation of processes is needed. During the last years, the development of several Image Processing algorithms and the spread of deep learning methodologies allow the identification of many types of objects, leading to an increasing accuracy as the models become more and more complex. Garments recognition is gaining particular attention during the last years because clothes are present in everyday life and some repetitive tasks can be automated, thanks to the growing presence of robots in industries. Intelligent algorithms for category recognition and object detection are necessary to solve different challenges. Firstly, clothes classification is applied in the fashion industry both in developing marketing strategies and for helping customers during the choice of products in shopping websites [19]. Secondly, laundry operations involve washing, drying and sorting continuously. Washing and drying are executed by professional appliances, but sorting is still a manual and repetitive job, which is labor-intensive [20]. The development of an autonomous garments sorting system can be useful to free human resources from repetitive jobs and to avoid being in direct contact with dirty clothes in risky areas as hospitals.

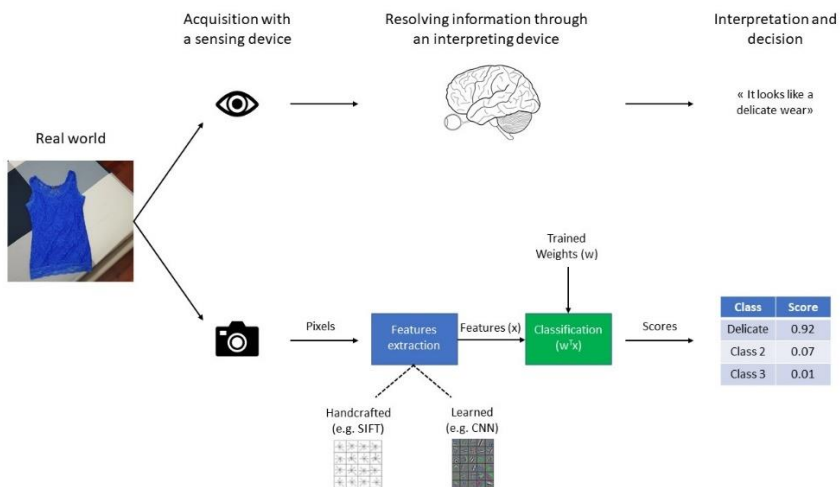


Figure 20. Typical human and computer vision pipeline for objects classification.

The first step is the development of the recognition system. In recent years, CNN architectures became popular to solve recognition problems, relying on the high accuracy results achieved in many research fields when compared to traditional Computer Vision classifiers. In CNNs,

features are automatically extracted, whereas in the classical machine learning strategy they are manually chosen using instructed algorithms, often resulting in lower accuracy for the last ones. The difference is shown in Figure 20.

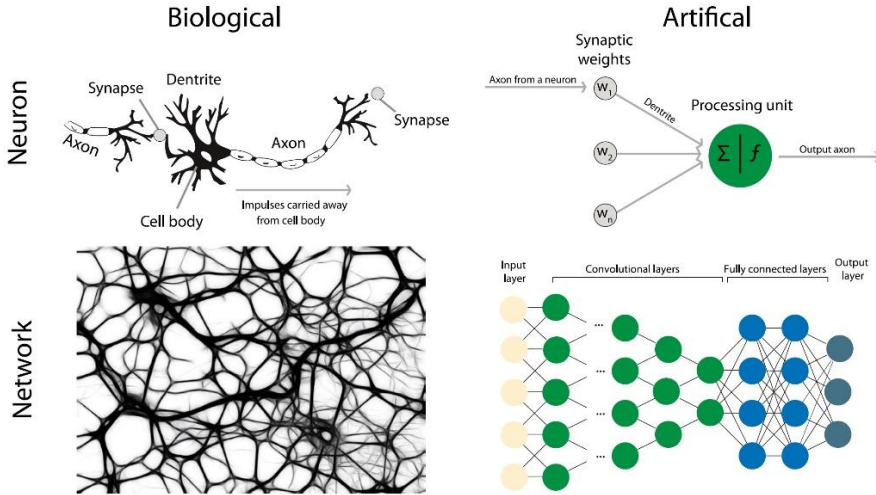


Figure 21. Basic model of a Convolutional Neural Network (right) which is similar to the human brain structure (left) [21].

Artificial Neural Networks automate the feature extraction step by learning a suitable representation of the data from a collection of examples and developing a robust model themselves. The great success achieved by deep learning can be explained thanks to their nonlinear functions distributed in a multi-layer structure which led to high accuracy without a manual features design [22]. Deep learning builds upon mathematical models using learning models inspired by biological neural networks, the central nervous system of animals. The human brain contains an average of 86 billion neurons [23]. Each neuron produces an output along its axon, which can influence the dendrites of another neuron across junctions called synapses. Some of them generate a positive effect in the dendrite encouraging its neuron to fire while others discourage the neuron from firing. Convolutional Neural Networks tries to imitate this structure, as shown in Figure 21. Unlike a human brain, where each neuron can connect to any other within a certain distance, in CNNs the structure consists of a finite and predefined number of layers and

connections [21]. The leftmost layer is called *input layer*, the rightmost is the *output layer* while the layers in between are the *hidden layers*.

In the past years, clothes classifiers were developed based on manually generated descriptors. Semantic attributes and low-level features were extracted from unsimilar images and combined with a classifier, using Support Vector Machine (SVM) algorithms [24]–[27]. Another strategy consists in the automatic segmentation of images by learning geometric constraints and shape cues combined with HOG [28] or SIFT [29] features extraction. Bag of Visual Words (BOW) recognizes recurrent attributes at different levels and was widely used for garments classification followed by SVM classifiers [30]–[34].

Recently CNN architectures overcome the accuracy obtained with traditional machine learning strategies thanks to convolutional layers. These networks can be built either from scratch [35]–[39] or starting from some common and popular architectures with modifications on their last layers, for the classification purposes [40]–[43]. The need of many images to train these networks from scratch, and the high computational resources required, have driven the research to find a solution adapting to the desired task networks already pre-trained.

Transfer learning is the approach that aims to fine-tune the existing CNN architectures to obtain a network able to classify images on a new problem. The architecture is first pre-trained on a large dataset and finally retrained on a smaller target dataset. Since first layers extract low level features like edges and color blobs, they can be reused for several classification tasks without big changes. The last layers, on the contrary, are typically problem dependent and focus on high level features [44]. For this reason, when transfer learning is applied, the weights of the first layers are kept frozen while the last ones are trained. This results in a faster learning process having a high accuracy at the same time. Previous research has shown that this methodology improves the performances of the networks over random initialization, when a small amount of images are available [44].

While the first layers of the CNN extract simple features from the images, the last ones focus on complex structures typical of the classification problem under consideration. The activations of the nodes

can be used to provide explanations to the classification class output from the network, highlighting the important regions of the image for the prevision. This technique, known as Class Activation Mapping (CAM), was originally used to check the area where the network focus for the classification, but is also able to localize the objects also if no location information is given during the training process [45]. The advantage is that is possible to easily extract an area from the image without the additional work of designing a bounding box for each image part of the database. The sensed area from the CAM can be later used for the extraction of other additional features, without a dedicated training.

In this thesis, an Artificial Intelligence AI-based robotic sorting system for garments is introduced. A new system has been developed to automatically detect the garment lying on a conveyor belt, classify it into 16 categories, extract its color and gripping point and sort it, using a cobot, in one of the baskets around it. The entire system is based on a Convolutional Neural Network, ResNet50 which have shown a good balance between high classification accuracy and short recognition time. Compared to other systems, the proposed methodology is fast because is based on only one CNN, works under any light conditions without the need of an external light source, recognize garments not part of the database and is easy to update, because there is no need of drawing any bounding box to localize the garment.

The robot vision streamline proposed is made up of four modules: (1) image acquisition system, (2) image classification based on ResNet50 and Transfer Learning, (3) features extraction, that in this case are color and gripping point, and (4) robot sorting platform, which detects the garment, stop the conveyor belt and move the robot according to the previous information. The garments are finally sorted by the cobot to the basket previously assigned to a washing program. All the analyses are performed using a mobile workstation equipped with an Intel i7-6820HQ CPU, with 16GB RAM, and a mid-range Nvidia Quadro M1200 4GB video card for the training. The software used is MatLab 2019b.

2.2 Image Acquisition Hardware

Before starting with the image classification algorithm, the first action to perform is to take the images of the garments to classify. For this reason, a camera has to be selected from a catalogue. When selecting a camera for an application, three factors have to be taken into account: the performance of the sensor, the camera features, the interface protocol for the transfer of the images.

A camera acquires images that are projected into an internal sensor. This data must be read and transferred to another device for storage, display, or analysis. During the last years, sensor technologies has made huge advances, due to the development of Charge Coupled Device (CCD) and, more recently, Complementary Metal Oxide Semiconductor (CMOS). With the recent developments, it is possible to obtain high resolution images at high frame rates. Until few years ago, CCD were the preferred sensor technology because of the best image quality. Recently, CMOS are becoming more popular because they can acquire good images at a lower price.

CCD sensors consist of multiple arrays of light sensitive semiconductor elements. Each element is a photo detector, which converts the light, in the form of photons, into electrons. During the exposure time to the light, all the electrons that are released by the elements are collected in a potential well. The accumulated capacity is proportional to the amount of the incident light and the exposure time. The fundamental difference with the CMOS sensor is the conversion from charge to voltage, as shown in Figure 22. In a CCD sensor, every element's charge is transferred through a limited number of output nodes. As all the pixels are devoted to the light capture, the uniformity is high. In a CMOS sensor, each pixel converts the charge to voltage, with the consequence that the complexity is higher and the space for the light capture is smaller. Also, the uniformity of the image acquired is lower, but they have a higher speed when many images have to be transferred. The increasing interest on the latter sensor type is because of a lower power consumption and manufacturing cost, with an overall quality that is close to the CCD with the last improvements.

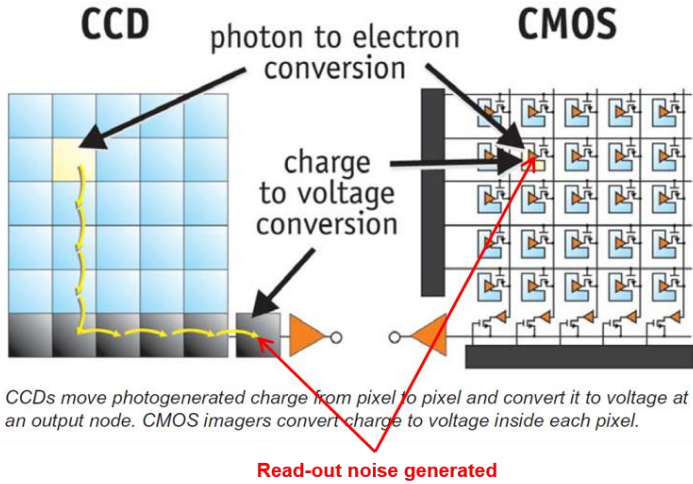


Figure 22. Difference between CCD (left) and CMOS (right) sensors.

The way in which the information is collected from each pixel, determines the difference between global and rolling shutter. The former exposes the pixel to the light all simultaneously for a defined period, in the latter the exposition happens sequentially. In case of fast-moving objects, the rolling shutter has the disadvantage that distorts the objects but is cheaper than the global one as the electronics is simpler [46].

When two cameras are used together, which is particularly common in robotic and picking applications, we talk about stereo or 3D cameras. This allows the simulation of the human vision, also giving the depth information that is not available with one planar camera. The images captures are three-dimensional, but the cost is higher as two sensors are involved for the acquisition.

To successfully design a vision application, a list of requirements should be established before buying and prior to installation. It is good practice to ensure there is spare processing capacity as it is common for the applications requirements to grow one the integration phase of the project is underway [46]. For the garments sorting application, the initial requirements are:

- A color camera, to extract the useful information to set the temperature for the washing program
- A global shutter camera, to avoid the distortion of objects as they are moving into the conveyor belt

- A low frame rate, as a unique image has to be taken and then processed in the recognition system, which takes some times, on the order of tenths of seconds
- A big sensor size, to capture as much light as possible which is particularly important in indoor environments
- A communication protocol compatible with MatLab software, used for the image analysis.

The camera chosen, based on the previous requirements, is a Basler acA-2500 60uc, color, with a resolution of 5 MP, and based on USB3 Vision communication protocol. The big 1" sensor allows to capture a great amount of light, so that an extra LED ring is not needed to illuminate the scene. The maximum frame rate of 24 fps in color mode is enough for the sorting application. The camera is shown in Figure 23.



Figure 23. Industrial color camera selected for the image acquisition.

Once a camera is selected, a lens has to be coupled to collect the light that is scattered from the surface of an object. The lens reconstructs this light as an image on a sensitive area behind it, which is represented by a CCD or a CMOS sensor. The parameters that impact the quality of an image are:

- the construction of the lens, e.g., lens radii or distances between optics
- the distance between object and lens, called working distance
- the distance between the lens and the sensors.

The ratio between the object reproduction, that is the image, and the object is called magnification. The focal length of an optics defines its magnification. Lenses that are made up by fixed elements have an unchangeable working distance and magnifications and are called fixed

focal lenses. Selecting the correct lens has a direct relationship to the sensor of the chosen camera. The lens has to be able to illuminate the complete sensor area in order to avoid shading and vignetting. The pixel size has to be resolved by the optic, so that the better the optical resolution of a lens, the more detailed structure can be reproduced. Finally, in order to resolve the details of an object and to ensure definite edge detection, the detail should be reproduced across 4 pixels. Pixel size varies from camera to camera, depending on the size and the resolution of the sensor, that is the number of pixels. The smaller the pixels, the higher the resolution required from the lens [46].

The working distance defines the space between the object and the leading edge of the lens. Standard lenses are generally designed to focus an object from infinity to a minimum object distance, defined as MOD. If the distance between the camera sensor and the lens is increased, the MOD can be decreased [46]. By focusing the lens for different working distances, differently sized Angular Fields of View (AFOV) can be obtained. The focal length of a lens defines its angular field of view. For a given sensor size, the shorter the focal length, the wider the angular field of view. This means that, to have a wide scene taken by the camera at a small working distance, a short focal length is needed. The relation among these variables is illustrated in Figure 24 and expressed by Equation (1):

$$AFOV[^\circ] = 2 \cdot \tan^{-1} \left(\frac{h}{2f} \right) \quad (1)$$

where h is the sensor size, f the focal length, $AFOV$ the angular field of view measured in degrees [47].

Fixed a working distance of 500 mm, the minimum field of view required for a correct framing of garments is 900x700 mm. The calculated focal length of the lens for the Basler acA-2500 60 uc is 6 mm, as illustrated in Figure 25. The field of view obtained from this configuration is 1024x809 mm, in the range defined in the initial requirements. The chosen optic is a wide lens Kowa LM6HC, with a manual focus and a focal length of 6 mm, that lets to have a horizontal angle of view of 92.1°. The minimum working distance of the optic is 100 mm, 5 times lower than the

fixed distance. The lens has to resolve a sensor pixel size of $4.8 \mu\text{m}$, as described in the Basler datasheet [48]. From the conversion between the sensor size and the lens resolution, obtained using Equation (2), the minimum resolution is 104 [lp/mm] . From the Kowa datasheet, the lens resolution is 120 [lp/mm] , which is above the requirement of the image sensor.

$$\text{Lens resolution} \left[\frac{\text{lp}}{\text{mm}} \right] = \frac{1000}{2 \cdot \text{pixel size} [\mu\text{m}]} \quad (2)$$

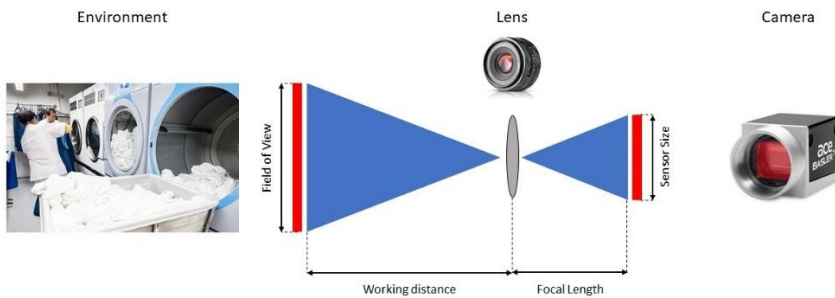


Figure 24. Relation among working distance, focal length, field of view, and sensor size.

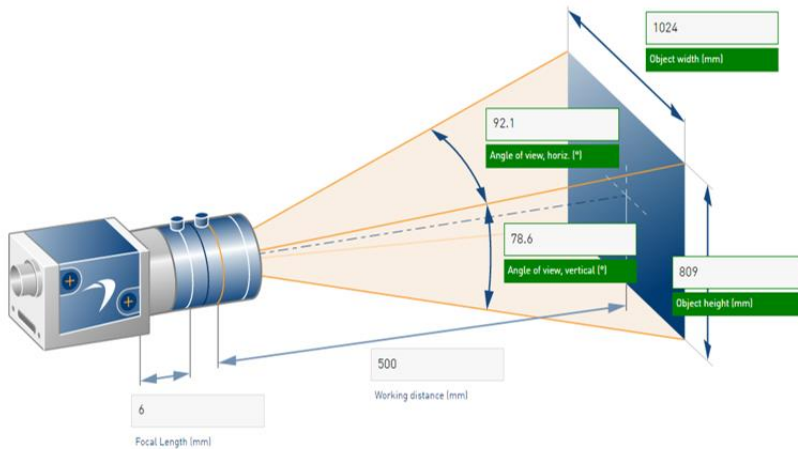


Figure 25. Field of view calculation at a working distance of 500 mm.

The entire Image Acquisition System, which comprises the industrial camera and the wide lens is fixed on a support over the conveyor belt and connected to the PC for the image analysis. The camera, coupled with the lens, is shown in Figure 26.



Figure 26. Industrial camera, coupled with a wide optic, used to acquire images for the automatic sorting system.

2.3 Image Classification

Two classify images, two are the possible ways: using traditional machine learning-based techniques or the more recent Convolutional Neural Network. In order to decide what is the best solution for the application on garments classification, a survey regarding the classification techniques is presented.

2.3.1 State of the art

2.3.1.1 Traditional Computer Vision and Neural Networks

Over the past years, a significant number of publications on garments classification were based on traditional computer vision techniques that analyze the images with manual features extraction, preprocessing and supervised learning. Garments may be identified by sets of category-

specific features as fabric type or garment elements like buttons, pockets, toes and the like [49]. Early approaches to garments classification have considered the use of edges to compare the shape, also using different views of the same item to increase the final accuracy. Images are compared using different features to determine a match score [26]. A more detailed description about the objects can be obtained by learning meaningful semantic attributes. Some of them are binary, to check the presence of some features, while others are multi-class, like colors. The items are then classified using a Supervised Multi-Class (SVM) algorithm based on the extracted features [24], [25]. More advanced approaches use segmentation as a pre-processing technique to first isolate the clothes in the images and then to extract the attributes for the final classification. The segmentation can be initialized by learning geometric constraints and shape cues followed by either a color histogram combined with HOG features [28] or a promising region analyzer [29]. The SVM classifier, that is predominantly used in clothing perception, can also be substituted by a multi-class Gaussian Process classifier that is based on a probabilistic approach [27].

In subsequent years the research focuses on the features extraction phase to allow higher accuracy and best attribute selection. Among all kinds of feature extractors developed for image classification, Bag of Words (BOW) and its variations become popular. They have been widely studied on account of their efficiency, simplicity and invariance to the viewpoint [50]. Compared to low-level features, the attributes have better robustness to clothing variations and carry semantic meanings as high-level image representation [31]. When it is compared to other techniques, BOW seems better suited to cope with the challenges of detecting and classifying flexible objects since it does not impose a geometry as template matching does [51]. For this reason, the methodology is used in several tasks related to garments. Automatic clothes search in consumer photos [30], recognition of clothing categories, both from videos [32] and from a pile of laundry [34] are developed based on BOW. It can be also used in combination with 3D descriptors to sort garments with a robotic interaction, outperforming the classification performance of new clothing items [33].

Recently, the use of deep learning algorithms and CNNs has become a subject of great interest because they have shown much better performances and features representation compared to traditional classifiers with manual annotation or attribute extraction, which may not be satisfactory for various tasks. These architectures overcome the accuracy obtained with traditional machine learning strategies thanks to successive convolutional layers. The parameters of these layers are fully learnable to identify low and high level patterns through supervised training [52]. The network architecture can be either created from scratch or already available in literature for generic recognition assignments.

A simple architecture is created in [39] with only two convolutional layers to classify ten categories taken by a well-known database: Fashion-MNIST [53]. The classification accuracy is higher compared to the classical CV techniques but is tested on small and simple images. A deeper model is proposed in [35] and consists of four convolutional layers able to classify images of size 128×128 into 16 categories. In [37] the layer number is gradually increased until no significant improvement is present. The final network has five layers with learnable parameters, where the first three layers are convolutional while the remaining two are fully-connected. In this case the network can output only three clothes categories, used for a subsequent robot manipulation. Custom CNNs are useful also when a depth camera is used, for which no standard architectures are developed. Four convolutional layers are used both in [54] and in [38] with image acquired by a Kinect sensor and a RGB-D camera. The training is done using both real images, acquired with a robotic manipulation, and synthetic ones.

When a single RGB image is available for the classification, it is convenient to use some well-known existing architectures already optimized for general recognition tasks. According to literature findings, the networks used for garments classification with a training done from scratch are LeNet [55], AlexNet [41], VGG16 [40], [42] and SqueezeNet [43]. These architectures have shown a high classification rate for pictures with diverse background and complex garments.

2.3.1.2 Transfer Learning

The training process of a CNN architecture is an extremely complex optimization problem that needs a lot of data and computational power. When a network is designed from scratch, the weights are usually randomly initialized starting from a Gaussian distribution. In this case, a lot of training images are necessary in order to reach a great accuracy, especially when the architecture consists of many layers. Transfer Learning is an effective technique to improve the performance of a classification system given only few labelled images in the target domain, which greatly reduces the training time and the computational cost. This method takes a network already trained on a wide dataset and then retrain it on a smaller target set, with a small modification of the last classification layers. In this way, the architectures are adapted to the new, but similar, recognition task to be solved. Instead of starting the training from random weights, the parameters previously learned can be reused, resulting in a reduced training time and complexity [56]. With this technique, a CNN architecture can be retrained from any layer, the previous one will be frozen and the weights are not changed during the optimization [57].

Transfer Learning is spreading recently thanks to the availability of several CNNs developed mainly to take part in the ImageNet competition, that includes a dataset of millions of images automatically sourced from the Internet [58]. Starting from the networks pre-trained on the ImageNet database with 1000 categories, the knowledge can be transferred to solve tasks in many different fields. For example, it is used in the medical area to automatically diagnose malignant and benign breast masses [59], [60] or in the field of digital pathology [61]. Also multi-label attribute classification for facial recognition can be performed, using VGG16 as reference network [62], and to match pedestrians across non-overlapping multiple cameras [63]. In [64], transfer learning is used to classify different materials in natural settings, while [65] recognizes gears, connectors and coins. Different transfer learning models for deep neural network are investigated for classification of plants [66], [67], flowers [68], leaf [69], crops and weeds [70], fruit [71]. In plants recognition this methodology is widely used because of both the availability of many databases and the difficulty in the classification of many different species,

which is challenging also for non-expert humans. Deep transfer learning models are also applied to recognize clothes in unconstrained images of people with limited training data available [72]. Finally, a clothing classification tool is developed based on Inception v3 for the classification into 7 categories with high accuracy [73].

2.3.2 Deep Network Architectures

Five well-known CNN architectures are considered to evaluate the impact of training parameters on the transfer learning performances, when applied to garments classification problem. These networks are AlexNet, GoogLeNet, VGG16, Resnet50 and Inception v3.

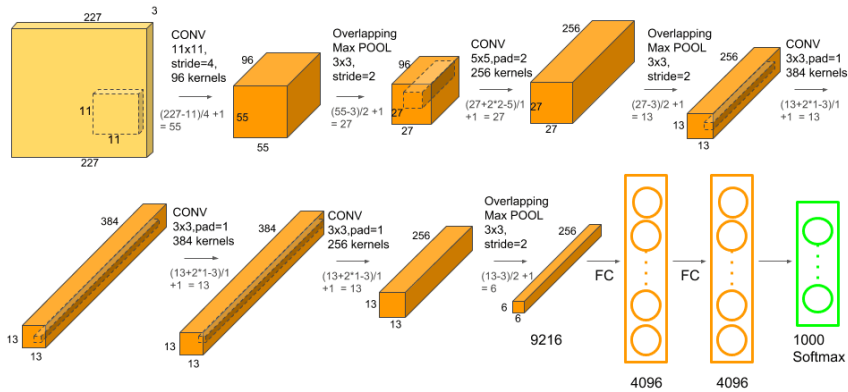


Figure 27. AlexNet architecture, the input image has size 227x227x3 [74].

AlexNet

AlexNet model [75] is the first deep convolutional neural network and won the 2012 edition of the ImageNet Large-Scale Visual Recognition Challenge (ILSVRC) [76]. The architecture has about 61 million parameters and 650.000 neurons distributed in 8 layers. The input image size is 227×227 . The model is relatively simple compared to more recent architectures; it is made up of 5 convolutional layers and 3 fully connected layers. In this study, the AlexNet latest version is used with dropout regularization method [77] and Rectified Linear Units (ReLU) for the activations. This architecture was used to achieve a top 5 test error rate of 15.4%, that represents a huge improvement when compared to the best

previous result of 26.2%. Since 2012, the use of CNNs models became standard, instead of traditional Computer Vision algorithms to compete for ILSVRC contest. The architecture is shown in Figure 27.

GoogLeNet

GoogLeNet model won the ILSVRC competition in 2014 with a top 5 error rate of 6.7 %. The input image size is 224×224 in the RGB color space. The architecture is made up of 6.8 million parameters distributed in 22 layers. The big improvement compared to the previous networks is the inception module that implements the multi-scale idea and dimension reduction layers. This allows to have a more efficient computation because the convolution layers, with different filter size, are in parallel with a max pooling operator, so the network becomes progressively wider, not deeper. GoogLeNet uses the dropout regularization in the fully-connected layer and rectified linear activation functions in all the convolutional [78].

VGGNet

This model was created to compete in ILSVRC 2014 and to study the effect of increased convolutional network depth on performance. It is made up of 19 layers with 144 million parameters and it strictly uses 3×3 filters with stride and pad of 1 [79]. There are different versions of the same network with the only difference of the number of convolutional layers implemented in the architecture. In this study, VGG16 is analyzed, which is built with 13 convolutional layers and 3 fully connected layers. This network has a greater number of parameters compared to AlexNet and GoogLeNet, which makes it more expensive from the computational point of view.

ResNet

ResNet model [80] won the ILSVRC competition in 2015 with a remarkable error rate of 3.6%, that is lower than a typical human error. The architecture is made up of 152 layers and accepts input images of 224×224 , the same as GoogLeNet and VGG. The novelty of this network is the use of residual blocks to solve the vanishing gradient problem [81]. As the gradient is back propagated to previous layers, it becomes smaller, with the consequence that the first layers learn slower than the last ones. This

problem tends to be amplified with the use of very deep networks that are made up of a high number of layers. To solve the problem, in residual blocks the original input is added to the output of the convolutional stack. In this way, every module compute only a small change of the original input. The authors argue that it is easier to optimize the residual mapping than the original one, with an improvement of the general efficiency of the network. Multiple versions are developed according to the number of layers. In this thesis ResNet50 is analyzed, with 50 layers and 25.6 million parameters.

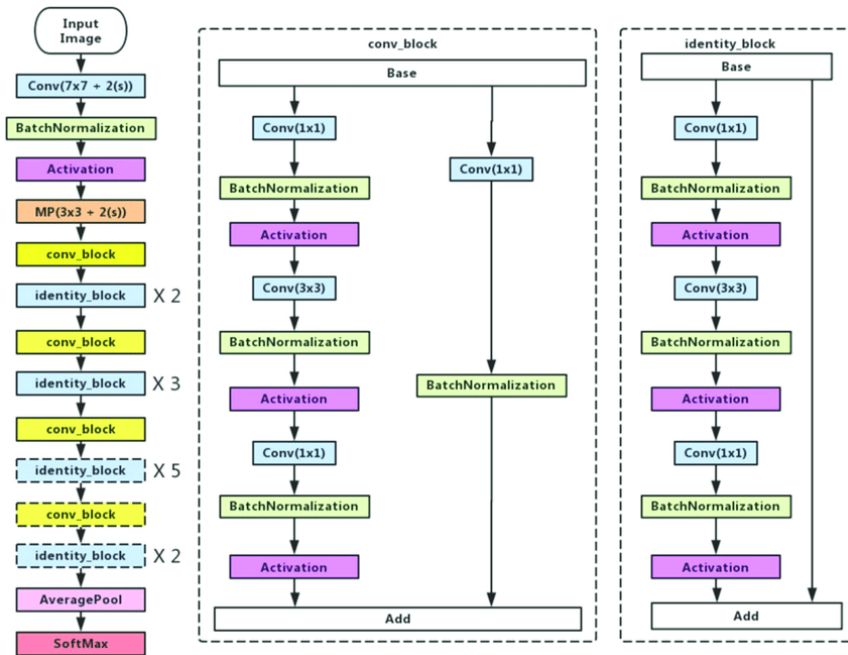


Figure 28. ResNet50 architecture [82].

Inception v3

This network is an improvement of the original GoogLeNet inception architecture and of the Inception v2. The traditional 7×7 convolution is factorized into three 3×3 convolutions, the classification layer is regularized with the introduction of Label Smoothing to prevent the overfitting, and the batch normalization is used in the auxiliary classifiers. The computation time is higher than with GoogLeNet, but the efficiency is much greater than VGGNet. The accepted image input size is 299×299 and the architecture has 23.9 million parameters distributed in 48 layers [83].

2.3.3 Custom Database

In the present study, a new database with 16 categories has been created, 15 of which are garments classes, and one is devoted to the identification of people that stand in front of a camera without holding garments. The latter category is called “no garments”. The database is fundamental for the training and the analysis of the five CNNs presented in 2.3.2 and the categories selected are based on the washing program to assign at each garment. The total number of images is 8391 and each category has at least 400 pictures. The details of the new database composition and the defined classes are shown in Figure 29.

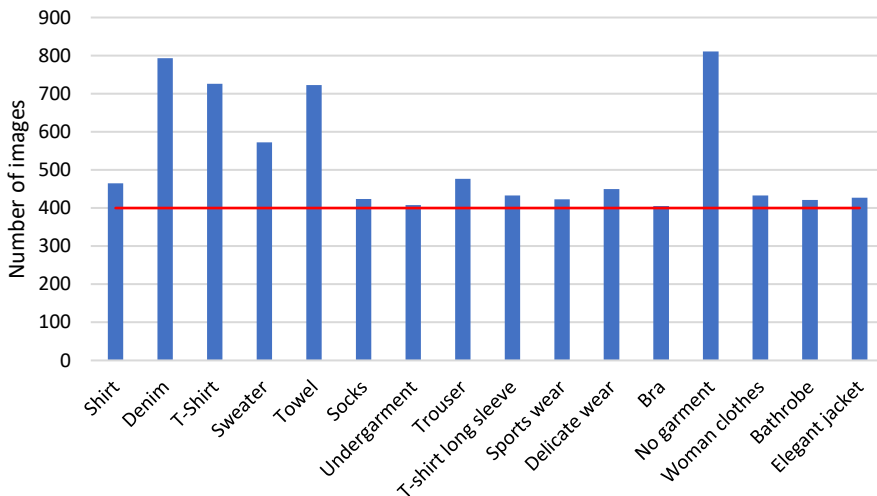


Figure 29. Garments custom database composition created for the classification task. The red horizontal line highlight that all the categories have 400 images at least.

All the images are RGB with a minimum resolution of 300×300 pixels and were collected both from the internet and from other databases already available online. Every file has different backgrounds, light conditions and item configurations to generalize as much as possible in order to make the network focuses on learning details that relevant to garments. Pictures are then manually labelled into the 16 categories. The existing databases used are Clothing part dataset [33], ImageNet [58] and CloPeMa [84]. Other images are downloaded from Google Images with a Python code [85] and from Instagram [86] by using keywords such as the

2.3.4 Transfer Learning Parameters Optimization

The goal of the proposed system is to classify an isolated single garment that is shown in front of a camera but without recognizing clothes worn by people. For this type of problem, a large database that contains only pictures of garments without being worn is not available and it is tough, and time expensive, to create a new one from scratch with an extensive number of images. Hence, transfer learning seems the best methodology to be applied to adopt the knowledge that has been learned in other contexts, since a lower number of images is required for the training. Two common transfer learning strategies are: feature extraction, which consist in the substitution of the final classification layer with a ML classifier, and parameters fine-tuning, which adapt the last layers to the new classification classes. It has been already demonstrated that the accuracy of the first strategy is lower than the second one [66]. With the fine-tuning, the first layers of the pretrained network can be fixed in a way that only the last layers learn the properties of the new dataset. This is because in the lower layers, more general features are extracted, and these can be transferred to other tasks as well. Moreover, to use a pre-trained network for transfer learning, the number of classes of the final classification layers must be modified to match the new dataset. The default networks have 1000 output classes, while in the presented case involves just 16.

2.3.4.1 Streamline for parameters optimization

The streamline of the proposed approach, using the transfer learning technique, is shown in Figure 31 and consists of several steps. First, a pre-trained network on the ImageNet database is selected among the five described in Section 2.3.2. The network is modified to replace the final classification layer with a new one that has 16 neurons, the same number of the categories to recognize. The model is then trained using all the images collected in a new database, specifically built for the garments classification purpose, and manually labelled into pre-defined categories. To train the network, several parameters and an optimization algorithm must be selected however there are no general rules for the transfer learning technique. For this reason, a dedicated framework that allows the comparison and the analysis of the parameters, is built. By means of this framework, it is possible both to optimize the parameters to reach the

maximum accuracy for each architecture and to check the impact of each constant analyzed on the classification. All the results of accuracy are collected and finally examined to have a performance evaluation among all the networks with the same training parameters.

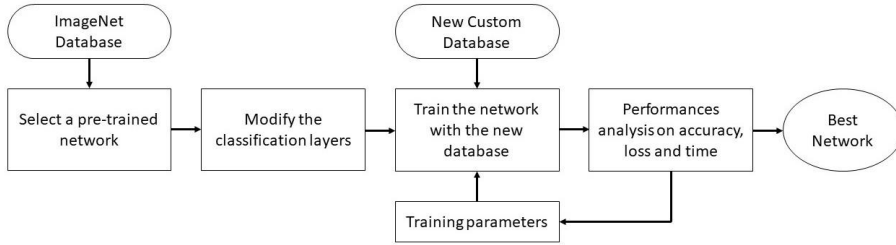


Figure 31. Streamline of the classification system using transfer learning methodology.

Training is the most important and difficult part of the entire streamline where the network learns to classify the new images of the database. Convolutional neural networks are generally trained minimizing an objective function, that usually is the prediction loss [89]. Having the input image x , related to the output label y , the function will iteratively minimize the following expression:

$$E(w) = \frac{1}{N} \sum_{i=1}^N L(f(w; x_i), y_i) + \lambda R(w) \quad (3)$$

where N is the mini-batch number, that is the number of images processed in every iteration, L is the loss function, f is the network output that depends on the current weights w , R is the regularization with the Lagrange multiplier λ .

The loss function is minimized using the Stochastic Gradient Descent algorithm (SGD) that updates the network internal parameters by taking small steps at each iteration:

$$w_{i+1} = w_i - \alpha \nabla E(w_i) \quad (4)$$

where $\alpha > 0$ is the learning rate. The weights w are randomly initialized in a network trained from scratch, while they are set to the pre-trained values in fine-tuning with transfer learning methodology. The stochastic gradient descent uses only a subset of the training data for each iteration, that is called mini-batch. Each time the entire training set is presented to the network, we are talking about one epoch. In this thesis two versions of the SGD are used for the performance evaluation on the five CNNs: Stochastic Gradient Descent with Momentum (SGDM) and Adaptive moment estimation (ADAM).

SGD algorithm can oscillate along the path toward the optimum value. To reduce this oscillation, a term, that is called momentum, is added to the Equation (4):

$$w_{i+1} = w_i - \alpha \nabla E(w_i) + \mu(w_i - w_{i-1}) \quad (5)$$

where μ is the momentum which determines the contribution of the previous gradient step to the current iteration [90].

While SGDM uses a single learning rate for all the internal parameters, ADAM improves the network training by automatically adapting α to the loss function to be optimized. The latter keeps a moving average of both the loss gradients and their squared values to update the network parameters:

$$w_{i+1} = w_i - \frac{\alpha m_i}{\sqrt{v_i + \varepsilon}} \quad (6)$$

with:

$$m_i = \beta_1 m_{i-1} + (1 - \beta_1) \nabla E(w_i) \quad (7)$$

$$v_i = \beta_2 v_{i-1} + (1 - \beta_2) [\nabla E(w_i)]^2 \quad (8)$$

where β_1 and β_2 are the decay rate of the moving average and ε is a small constant. If the gradients contains noise, the moving average becomes small and, consequently, the parameter updates are small too [91].

Before starting to train the networks, some parameters must be chosen and then adjusted to increase the final accuracy and the general performances. Different parameters have different impact, depending on the network's architecture, and strategies to obtain the best accuracy possible are often heuristic. According to the author's knowledge, an in-depth analysis in the literature of the most important constants impact on the network training, relying on both the optimization algorithm and the network architecture, is missing. For this reason, a new framework is presented to compare the same training parameters, when applied to different architectures, as in Figure 32. The parameters selected for the evaluation are the learning rate α , its drop period $\alpha_{d,p}$, the drop factor $\alpha_{d,f}$ and the L_2 regularization. The drop period represents the number of epochs after which the learning rate is decreased. Every time the specified epochs are evaluated, the global learning rate is multiplied by a drop factor smaller than one. This lets to reduce the initial value of α as the training progress, according to a pre-defined schedule. While the minimum of the loss function is approached, the step size defined by the learning rate should be reduced to get closer to the optimum point progressively. The reduction of the learning rate, when the fine tuning is applied, is beneficial as is pointed out in [92], but it is still needed a structured analysis of its effect with a comparison between two different optimizers. Finally, L_2 regularization is the penalty term R added to the cost function in (3) to reduce the overfitting problem.

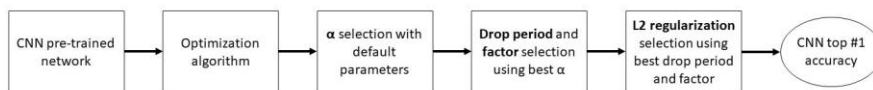


Figure 32. Framework proposed for training parameters and for their analysis.

Different values of these terms are tested for each of the five CNNs with both ADAM and SGDM optimization algorithms, keeping frozen other

values. The maximum epochs number is set to 12, the batch size is fixed to 32 as suggested in [89], the validation frequency is half of the number of iterations of one epoch, and the training data is shuffled at the beginning of each epoch. The network training is stopped before the maximum epoch number if the loss value on the validation set is larger or equal to the smallest recorded loss for five consecutive times. This term, called Validation Patience, is useful to stop the training process when the network does not improve anymore.

As is shown in Figure 32, firstly a CNN architecture is selected among the five presented previously in 2.3.2. Then, for each of the two optimizers ADAM and SGDM, the best initial learning rate α is selected maintaining fixed the drop period, the drop factor and the regularization term to the default values. The α values examined, with the default terms, are presented in Table 2.

Optimizer	Learning Rate α	Drop period	Drop Factor	L2 Regularization	Max Epochs
ADAM	0.0006	3	0.1	0.0001	12
	0.0003				
	0.0001				
SGDM	0.006	3	0.1	0.0001	12
	0.003				
	0.001				

Table 2. Learning Rate selection with default training parameters.

The learning rate is one of the most important parameters to tune in a CNN. It is selected at the beginning of the training process before to set other terms. It reflects the step size that the algorithm takes to reach the minimum and it is connected to the optimizer, the architecture used and the task to be solved. The selected α is the one that returns the network with the highest accuracy. Three couple of values are analyzed:

- Period 3, Factor 0.1
- Period 2, Factor 0.7
- Period 1, Factor 0.8

Then, according to the structure presented in Figure 32, there is an evaluation of the impact of the drop period and factor using the α chosen in the previous step. The evaluation is carried out for both the optimizers. Finally, L_2 regularization is modified with several values (0.0001, 0.0003, 0.001, 0.03, 0.01) to reduce the overfitting problem using the combination of drop period and factor that gives the highest accuracy. For the higher $\alpha_{d,p}$, a small $\alpha_{d,f}$ is selected while, for lower periods, the factor is increased. This means that, in the first case, α is maintained constant for more epochs and then it is considerably decreased. In the last case, α is dropped in every epoch but with a small amount.

The analysis suggested in the presented structure is important to standardize the study in order to evaluate the impact of each parameter on the training, when transfer learning is used. This approach let us to find a relation, if there is one, between the training parameters and both the architecture and the optimizer used. Moreover, this framework let us to optimize the parameters according to the accuracy results for each network.

2.3.4.2 Analysis of the parameters

First, the learning rate impact on the final accuracy is evaluated. Then, the drop period and factor are analyzed and selected before the L_2 regularization investigation. The optimization algorithms are compared based on the previous modification of the parameters. Finally, the overall network performances on accuracy and time are evaluated and compared.

An example of the training process is shown in Figure 33. On the top, the training accuracy is displayed while on the bottom the loss is plotted. The black points represent the calculation on the validation set. The blue dotted line is the training accuracy, while the orange dotted line is the loss. These data are filtered with a smoothing function to remove the training oscillations and show more clearly the trend (solid line).

After several trials, it was not possible to train VGG16 using ADAM optimizer because the architecture has too many weights to set and this algorithm is computationally more computational demanding compared to SGDM. Even reducing the batch size until the category number, the GPU used for this study does not support the training process. For this reason,

in the following Section, only the results with SGDM will be presented for VGG16.

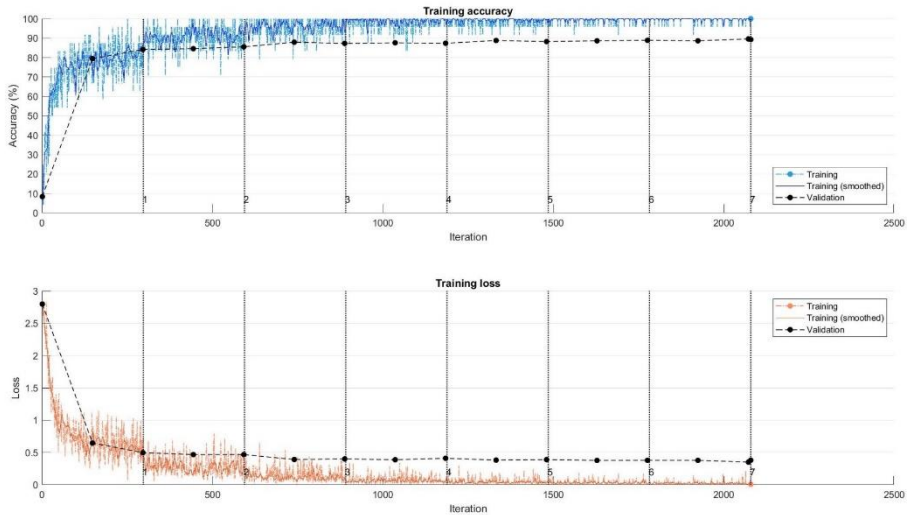


Figure 33. Training progress of ResNet50. Blue lines are the training progress, orange lines are the loss progress, black dots are the validation points connected by a dashed line to highlight the trend.

Learning Rate

The summary of the accuracy obtained modifying the learning rate value is presented in Table 3. As explained in the previous section, the ADAM values for the VGG16 network are not present and the highest value of α tried with SGDM does not permit the convergence of the optimization.

	ADAM			SGDM		
	0.0006	0.0003	0.0001	0.006	0.003	0.001
AlexNet	52.66	76.61	80.70	77.40	78.97	77.84
GoogLeNet	83.74	85.60	85.01	84.43	82.57	79.92
VGG16	-	-	-	-	85.31	88.56
ResNet50	86.74	88.96	90.79	89.12	89.28	89.20
Inceptionv3	89.20	89.75	91.58	90.87	92.06	89.99

Table 3. Accuracy [%] results with the learning rate value variations.

The same results are separated based on the optimizers and graphically presented in Figure 34 when ADAM optimizer is used and in Figure 35 with SGDM. ADAM increases the accuracy with a decrease of α in all the architectures except for GoogLeNet. The biggest difference is provided using AlexNet and ADAM with a delta of 28.04%, while ResNet50 seems to be insensitive to α when SGDM is used. VGG16 shows a considerable improvement when the learning rate is reduced. AlexNet, GoogLeNet and ResNet50 perform better with ADAM while Inception v3 has the best accuracy with SGDM.

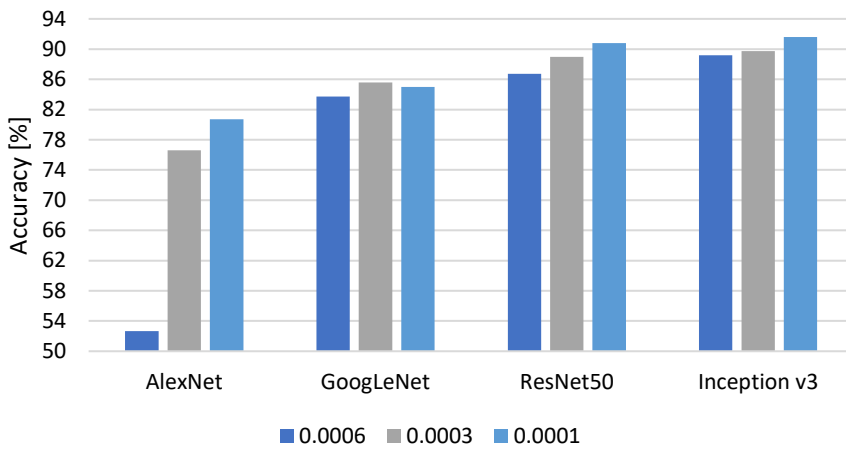


Figure 34. Accuracy with learning rate variation using ADAM optimizer.

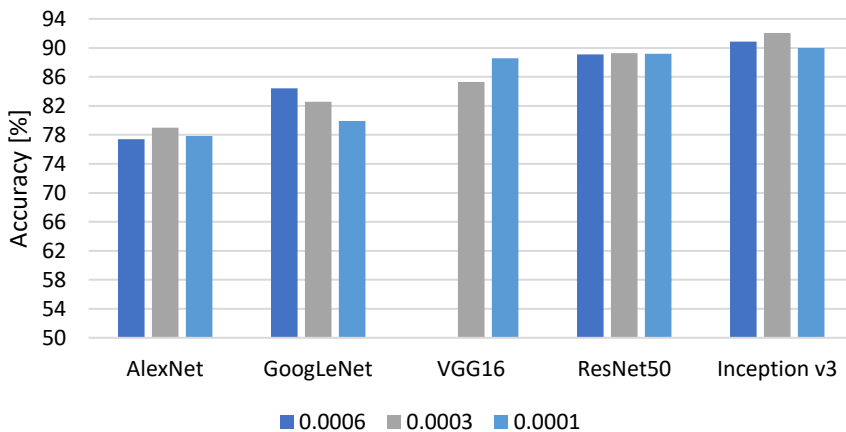


Figure 35. Accuracy with learning rate variation using SGDM optimizer.

Drop period and Drop factor

After the learning rate selection is carried out for each optimization algorithm, using the values that show the best accuracy, the drop is analyzed. Three solutions are tried for each optimizer:

- Drop 1: period 3, factor 0.1
- Drop 2: period 2, factor 0.7
- Drop 3: period 1, factor 0.8

The outcome is summarized in Table 4.

	ADAM			SGDM		
	Drop 1	Drop 2	Drop 3	Drop 1	Drop 2	Drop 3
AlexNet	80.70	80.58	81.49	78.97	79.79	80.26
GoogLeNet	85.60	85.39	85.42	84.43	85.15	84.81
VGG16	-	-	-	88.56	88.40	87.77
ResNet50	90.79	88.96	90.23	89.28	90.15	90.63
Inceptionv3	91.58	91.58	90.87	92.06	91.74	90.63

Table 4. Accuracy [%] results with the drop period and factor variations.

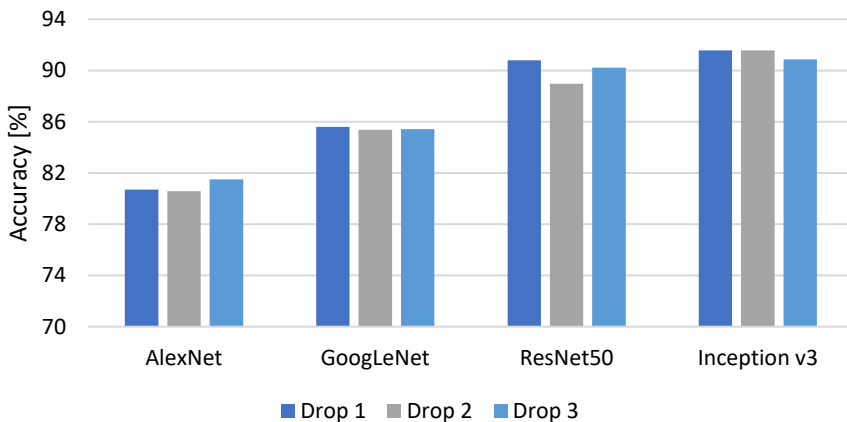


Figure 36. Accuracy with drop variation using ADAM optimizer.

The results with ADAM are shown in Figure 36. AlexNet performs better with drop 3 while all the others give better accuracy with high drop period and low drop factor. With the exception of AlexNet, no network performs well when α is dropped in each epoch. When focusing on SGDM (see Figure 37), some general trends can be extracted. AlexNet and ResNet50 increase the accuracy when decreasing the drop period, while VGG16 and Inception v3 behave in the opposite way. Finally, GoogLeNet has the best performance with drop 2.

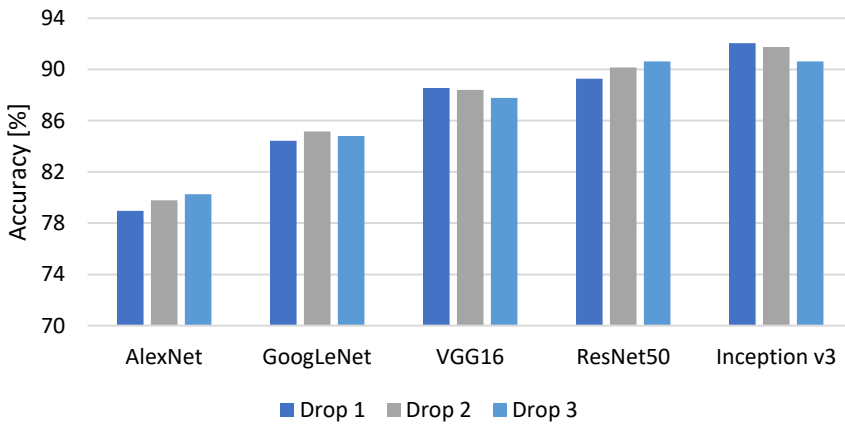


Figure 37. Accuracy with drop variation using SGDM optimizer.

Regularization

In previous paragraphs the learning rate and its drop were analyzed to select the best step size to reach the optimal point for each architecture, following the path defined by the framework. A relevant question is how to modify the regularization and to quantify the benefit in terms of classification accuracy. The analysis is carried out using the combination of learning rate, drop period and factor that led to the best results. For each optimizer, the same regularization values were tried. The first value in Table 5 and Table 6 is the default one and the results come from the previous section. Other four values are tried, with a multiplication factor of approximately three between each of them. Results for ADAM are given in Table 5 while Table 6 shows the values with SGDM.

ADAM					
	0.0001	0.0003	0.001	0.003	0.01
AlexNet	81.49	80.20	80.74	80.80	81.00
GoogLeNet	85.60	86.00	85.64	85.56	83.30
ResNet50	90.79	89.28	89.67	89.99	89.12
Inceptionv3	91.58	91.58	91.66	90.95	91.10

Table 5. Accuracy [%] results with L2 regularization variations using ADAM as optimizer.

SGDM					
	0.0001	0.0003	0.001	0.003	0.01
AlexNet	80.26	80.46	80.64	81.14	80.18
GoogLeNet	85.15	84.71	84.51	85.17	84.70
VGG16	88.56	87.77	87.93	87.53	87.77
ResNet50	90.63	90.55	90.79	90.23	89.83
Inceptionv3	92.06	90.87	91.26	92.14	91.90

Table 6. Accuracy [%] results with L2 regularization variations using SGDM as optimizer.

When ADAM is used, as shown in Figure 38, lower values of regularization give higher classification accuracy. On the contrary, with SGDM illustrated in Figure 39 some networks improve with medium values. Only VGG16 performs better with the lowest numbers tried in this analysis. With both optimizers, it is not possible to extract a clear trend as with the learning rate and drop. In this case, we can only state that the highest regularization value has never returned the best accuracy. This means that the regularization is beneficial when too high values are not used. AlexNet and GoogLeNet show the highest improvement with the regularization using ADAM, with a delta between the maximum and the minimum accuracy of 0.95% for the former and 0.66% for the latter. In all the other cases, the delta around 1%.

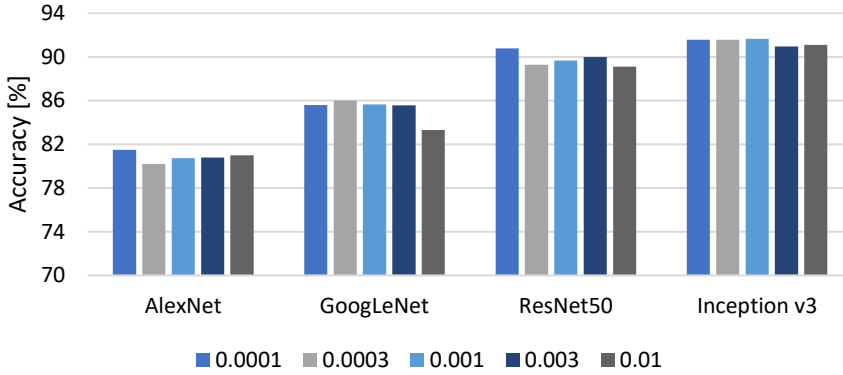


Figure 38. Accuracy with regularization variation using ADAM optimizer.

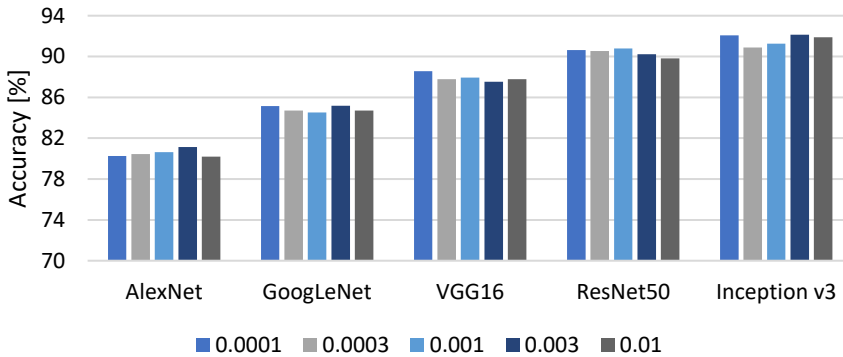


Figure 39. Accuracy with regularization variation using SGDM optimizer.

Optimization algorithms

A first analysis regarding the optimization algorithms can be carried out starting from the results shown in the previous Sections. ADAM performs better with lower learning rates with AlexNet, ResNet50 and Inception v3, while GoogLeNet shows higher accuracy with the medium value of α . Generally, ADAM works better with high drop periods for network with many layers and with low regularization terms for all of them. Regarding SGDM, it exhibits the best accuracy with a high α only for GoogLeNet. Low drop periods work better with AlexNet, GoogLeNet and ResNet50, high periods with the others. As far as the regularization is concerned, improvements can be noticed with high values, in contrast to what shown by ADAM.

The trainings performed in this study are based on two optimization algorithms that led to different results in terms of accuracy and training time. To compare the training time and to present a result independent of the iteration number, some metric must be introduced. First, the total training time is divided by the iteration number. The result is then divided by the ratio of batch number currently used to the minimum ever adopted in all trainings. In this way, the result is independent of the batch size and the iteration number. Classification accuracy and the average training time, normalized on batch size of the best performing network, are reported in Figure 40.

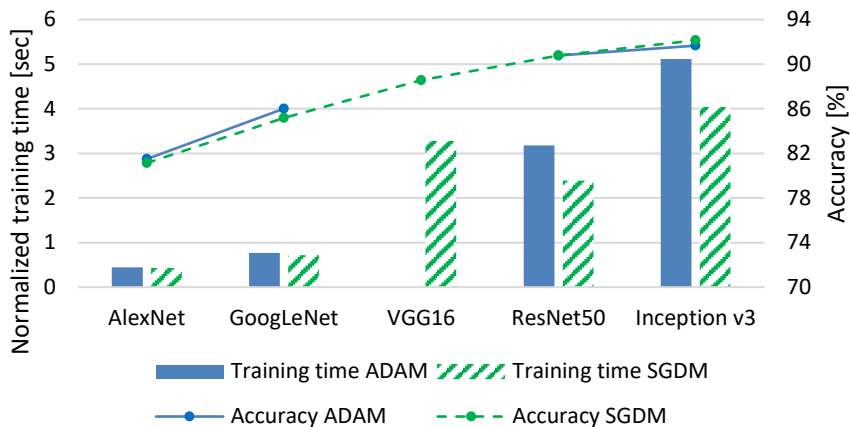


Figure 40. Accuracy and average training time normalized on batch for the best performing CNNs.

The training time, when ADAM is used, is always higher than when SGDM is utilized. The difference increases with the network complexity; in the worst case, ADAM takes 1.3 times SGDM for each batch to train the Inception v3 network. This difference is not offset by a performance increase for all the architectures. Inception v3 performs better using SGDM and ResNet50 has the same accuracy with both optimizers. In conclusion, it is convenient to use ADAM only for AlexNet and GoogLeNet because they both have a higher accuracy with a similar training time. On the contrary, ResNet50 and Inception v3 performs better with SGDM, both in terms of accuracy and training time.

Networks comparison

The framework designed for this study is suitable to compare the best performing architectures in terms of accuracy and prediction time. The steps considered in this study can also be seen as an optimization path to reach the best accuracy possible for each network. In Figure 41, the top accuracy achieved for every architecture is shown. AlexNet exhibits the worst performances while Inception v3 is the best one.

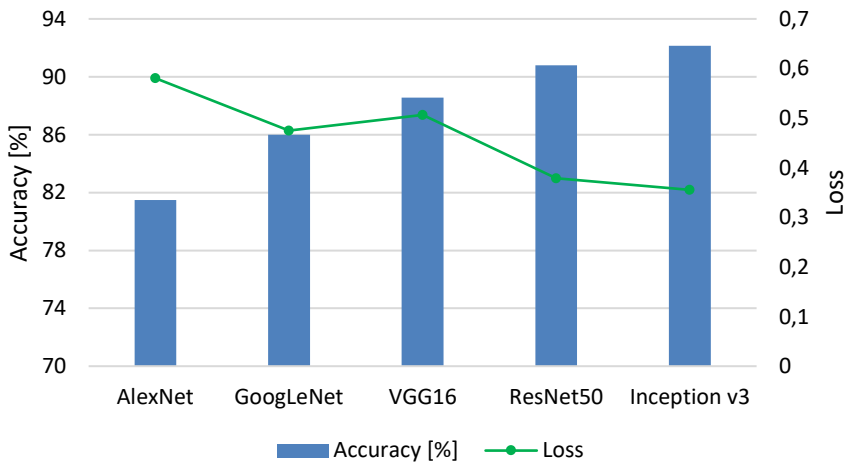


Figure 41. Accuracy and loss of the best performing architectures.

The accuracy gives only an indication about the correct class of the prediction without any information regarding how much the predicted output differs from the desired one. For this reason, another variable to consider is the loss. It is representative of the confidence of the network in its prediction since lower values correspond to higher precision in the classification. In Figure 41, the loss is shown with green segments. It is interesting to notice that, while the accuracy is increasing, the loss is not always decreasing. VGG16 has higher accuracy with respect to GoogLeNet.

Training time is an important parameter to consider when a network must be selected to solve a classification task. It is dependent both on the network complexity and on the optimization algorithm used, as shown previously in Optimization algorithms. Instead, prediction time is related to the layers and parameters number, which is representative of the network complexity. In Figure 42, the training time is represented by the

radius of the bubble for each architecture that has the best accuracy, independently from the optimizer. The prediction time, calculated on the validation set, is reported relative. Inception v3, the most accurate network, is also the slower one, in training as well as in prediction. It takes more than four times than AlexNet to provide the classification. From the chart, VGG16 is not a convenient network to use because ResNet50 is faster both in training and prediction time, with even a higher accuracy and lower loss. Residual modules are more efficient than the classical structure used by VGG16, which replicates AlexNet but with more convolutional layers. The best solution for a fast classification is AlexNet while, for an accurate prediction, the best network is Inception v3. A good balance is represented by ResNet50.

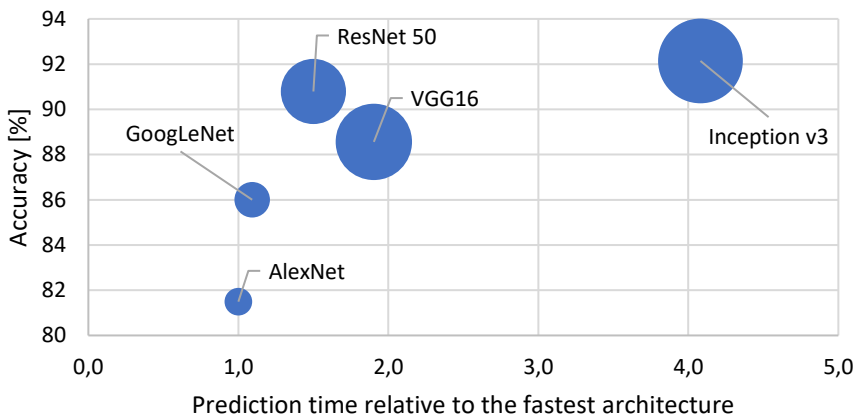


Figure 42. Accuracy and prediction time relative to the fastest network of each architecture.

Network selection

The comparison of the relative performance of these networks reveals that the best solution for a fast classification is AlexNet, for an accurate prediction is Inception v3 while a good balance is represented by ResNet50. VGG16 is not a convenient network to use because ResNet50 is faster in both training and prediction time, with even a higher accuracy and lower loss. Moreover, VGG network requires a lot of computational power for the training. For this reason, the best network to use for the garments classification system is **ResNet50**, trained using SGDM as

optimized as the final accuracy is the same as ADAM but with a lower training time and computational effort.

Prior to this study, there were no rules to follow to obtain the best accuracy possible because of the different impact the constants have on different network architectures. For this reason, a new framework has been presented to analyze the most important parameters, namely learning rate α , drop period, drop factor and regularization, and to provide an optimization path for the training process. The proposed streamline for the parameters optimization has demonstrated to work for all the network, in particular the selected ResNet50 with SGDM as optimizer showed an accuracy improvement delta of 1,67% comparing the best value obtained to the first trial on the learning rate definition. In Table 7 are summarized the transfer learning training parameters that results from the optimization streamline.

Training Parameters	
Learning rate	0.003
Drop period	1
Drop factor	0.8
Regularization	0.001
Final accuracy	90.79%

Table 7. Training parameters using Transfer Learning that results from the optimization using SGDM.

To evaluate the classification accuracy for each category, the confusion matrix is showed in Figure 43. The categories that achieve the best recognition rate are No garments and Denim. The former is different compared to the others, and consequently is easier for the model to recognize the pictures. Instead, the latter contains not only jeans but also shirts in denim, consequently it is surprising to see a so high accuracy and the ability of the network to recognize properly the images also with items that can be confused with the Shirt class. This is probably related to the high images number in the database, when compared to the other categories. At the contrary, Sports wear and Delicate wear achieve a relatively low accuracy, 74.6% and 77.6% respectively. The model

accuracy can be improved increasing the number of images numbers for the Sportswear that, as Denim class, contain items that can be confused with other categories. In fact, looking to the confusion matrix, the errors are distributed in several categories. Different is the reason for the low accuracy of the Delicate wear class, whose images are misclassified mostly with Woman wear. In Delicate category there are garments with lace, breads, paillettes, etc., that are details in the item which are difficult to notice when the original image is resized to the ResNet50 input, that is 224 x 224 pixels.

ResNet50 Confusion Matrix

Bathrobe	55	0	1	1	0	0	1	0	0	2	0	0	2	0	1	0	87,3	12,7
Bra	0	59	1	0	0	0	0	0	0	0	0	0	0	0	0	1	96,7	3,3
Delicate wear	1	2	52	0	0	0	0	1	0	0	2	0	0	0	1	8	77,6	22,4
Denim	0	0	0	118	0	0	1	0	0	0	0	0	0	0	0	0	99,2	0,8
Elegant Jacket	0	0	1	0	62	0	0	0	0	1	0	0	0	0	0	0	96,9	3,1
No garments	0	0	0	0	0	121	0	0	0	0	0	0	0	0	0	1	99,2	0,8
Shirt	0	0	0	1	1	0	66	0	0	1	1	0	0	0	0	0	94,3	5,7
Sock	0	0	0	0	0	0	0	63	0	0	0	0	1	0	0	0	98,4	1,6
Sports wear	0	0	0	0	0	0	0	0	47	0	2	4	1	4	0	5	74,6	25,4
Sweater	0	0	4	0	0	0	1	0	0	75	0	5	0	0	0	1	87,2	12,8
T Shirt	0	0	0	0	0	0	2	0	1	1	103	2	0	0	0	0	94,5	5,5
T Shirt Long Sleeve	2	0	1	0	0	0	3	0	2	1	3	51	0	0	0	2	78,5	21,5
Towel	0	0	0	0	0	0	0	0	1	0	0	0	106	1	0	0	98,1	1,9
Trousers	0	0	0	2	1	0	2	0	2	1	0	0	1	63	0	0	87,5	12,5
Undergarment	0	0	1	0	0	0	0	0	1	0	0	0	0	0	59	0	96,7	3,3
Woman cloth	0	0	3	0	0	0	2	0	0	1	2	0	0	1	0	56	86,2	13,8
																	90,8	9,2
	Bathrobe	Bra	Delicate wear	Denim	Elegant Jacket	No garments	Shirt	Sock	Sports wear	Sweater	T Shirt	T Shirt Long Sleeve	Towel	Trousers	Undergarment	Woman cloth		

Figure 43. Confusion Matrix of ResNet50 fine-tuned with Transfer Learning on the custom database.

In order to increase the accuracy of the low-performing classes, the faster solution is to increase the images database until the Denim class number, which showed a great accuracy. For the Delicate wear class, an analysis can be carried out after the recognition to check the presence of details that are typical of this category.

2.3.4.3 Bayesian Optimization

As described in 2.3.4.1 and then verified in 2.3.4.2, the internal parameters of the transfer learning learning process, called hyperparameters, has a great impact on the final accuracy and loss that results after a training

process of a Convolutional Neural Network. For this reason, the best parameters must be found in order to achieve the best network possible for the classification problem. The framework presented in Figure 32 is a good starting point to improve the overall accuracy, as demonstrated in 2.3.4.2, but requires the manual choice of the initial parameters to try for the training process and became long and time-consuming when many values must be tried. Moreover, as the hyperparameters selected for the optimization grow in number, the number of possibilities for the trials increase exponentially and the work of manual setting and following the training is hard and difficult.

An option to automatize the process of selection the hyperparameters, based on the final accuracy or loss of a CNN, is to use an optimization function. Optimization is the process of locating a point that minimizes a real-valued function called objective function. A possible way is the use of Bayesian optimization. The Bayesian algorithm attempts to minimize a scalar objective function $f(x)$ for x in a bounded domain. The function can be either deterministic or stochastic, with the consequence that it can output different results when evaluated at the same point x . This type of optimization maintains a Gaussian process model of the objective function and use its evaluation to train the model. One advantage of the Bayesian optimization is the acquisition function, that is used by the algorithm to select the next point for the evaluation. This function can balance sampling at points that have low modeled objective function, so that new areas that have not been modelled well yet are explored [93]. In order to perform the Bayesian Optimization, the MatLab function *bayesopt* is used, creating an objective function that trains the Convolutional Neural Network and returns the classification error on the validation set. The function performs the following steps:

- Import the values of the optimization variables in input
- Select the network architecture, that in this thesis is ResNet50, and impose the training options
- Train the CNN on the training set and verify the results on the validation set
- Save the trained network with the validation error and the training options.

The presented optimization technique has the clear advantage of trying a higher number of parameters compared to the framework proposed in 2.3.4.1, with a wider range of values. In order to compare the results with the framework, the choice is to use the previously selected network for the garments classification, ResNet50. The parameters tried, with the range, is reported in Table 8.

TL parameter	Range
Learning rate	0.008 ÷ 0.08
Drop period	1 ÷ 4
Drop factor	0.1 ÷ 0.9
Regularization	0.00001 ÷ 0.01
Momentum	0.7 ÷ 0.98

Table 8. Parameters selected for Bayesian Optimization, with the range for the values evaluation.

Compared to the evaluation previously proposed, a new parameter is here considered, the momentum, which is related to the SGDM optimizer. Moreover, the range are wider for all the other parameters, with the possibility also to use intermediate values in the drop period and factor, that were not considered before. The training options selected are the same as in the previous paragraph. The maximum number of evaluations set is 30, to avoid a too long optimization loop. The details of the parameters' values for each iteration are reported in Table 9, with the result of the objective function, that represents the error on the validation dataset. As it is possible to notice from the table, a wide range of values are tried for each hyperparameter from the optimization algorithm, so it increases the possibility to reach a maximum value of accuracy.

#	Objective	Accuracy [%]	Learning Rate	Drop factor	Drop period	L₂ Reg.	Momentum
1	0.21	79.00	0.052	0.6	2	1.41E-04	0.77
2	0.11	89.02	0.008	0.8	2	8.20E-05	0.71
3	0.11	88.62	0.010	0.1	2	2.39E-04	0.83

Autonomous Laundry Sorting

4	0.69	31.03	0.027	0.4	3	4.75E-03	0.97
5	0.11	89.10	0.002	0.7	1	5.50E-05	0.72
6	0.12	88.47	0.008	0.1	2	2.26E-05	0.78
7	0.14	86.48	0.061	0.2	4	3.30E-05	0.70
8	0.11	88.78	0.008	0.6	2	7.87E-05	0.81
9	0.79	20.92	0.027	0.7	3	1.01E-05	0.94
10	0.11	89.26	0.008	0.7	2	3.34E-05	0.74
11	0.70	29.67	0.080	0.2	2	6.44E-03	0.87
12	0.10	89.58	0.023	0.4	3	6.03E-05	0.70
13	0.11	89.34	0.023	0.4	4	5.72E-03	0.73
14	0.13	87.19	0.008	0.1	1	1.28E-05	0.83
15	0.11	88.54	0.015	0.5	4	2.07E-03	0.79
16	0.11	88.62	0.014	0.5	2	2.56E-04	0.75
17	0.11	89.18	0.013	0.3	1	7.16E-05	0.81
18	0.11	89.02	0.017	0.5	2	2.96E-03	0.71
19	0.11	89.02	0.031	0.2	3	4.47E-03	0.71
20	0.10	89.74	0.008	0.1	2	1.42E-04	0.70
21	0.11	89.42	0.013	0.8	3	1.83E-04	0.70
22	0.11	89.34	0.008	0.8	3	3.93E-03	0.70
23	0.10	89.66	0.011	0.1	3	1.06E-05	0.81
24	0.11	88.70	0.011	0.1	3	3.04E-04	0.82
25	0.11	89.10	0.020	0.2	2	3.09E-05	0.70
26	0.55	44.95	0.078	0.3	2	5.97E-04	0.82
27	0.11	88.70	0.030	0.6	2	1.01E-05	0.74
28	0.10	90.45	0.011	0.4	2	1.50E-05	0.80
29	0.13	86.79	0.010	0.8	3	6.34E-04	0.80
30	0.11	88.86	0.012	0.3	2	4.58E-04	0.10

Table 9. Iterations details of the Bayesian optimization with ResNet50. The objective function shows the error on the validation dataset. Learning rate, drop period and factor, regularization and momentum used for every training are reported.

The best accuracy is reached at iteration number 28, with a value of 90.45%. It is a lower value compared with the one reached in 2.3.4.2, probably the numbers of trials should be increased to reach higher accuracies. The results, considering the best results obtained for each iteration so far, are shown in Figure 44. In green there is also the estimated accuracy calculated by the Bayesian optimization for each trial. It is interesting to notice that an increase of accuracy is obtained every six trials.

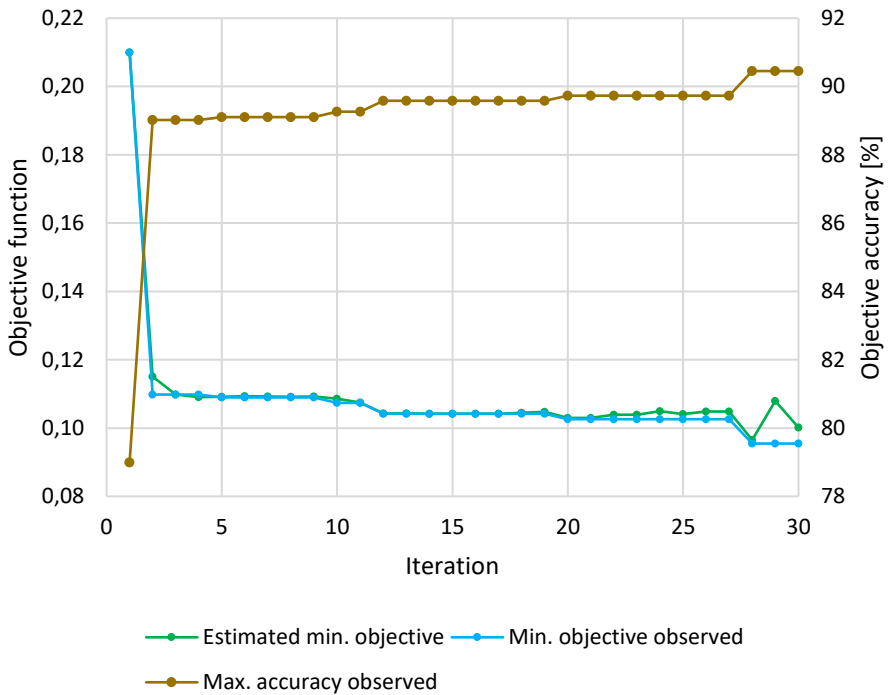


Figure 44. Results from Bayesian optimization. The blue line is the minimum value of the objective function obtained so far; the green line is the relative estimated value from the optimizer. The brown line is the best accuracy reached from the network so far.

Bayesian optimization has shown to be a reliable method to automatically optimize the hyperparameters for the CNNs training. The results are similar to the one achieved using the framework proposed, more parameters and a wider range can be explored for the optimization. The disadvantages are the high number of iterations required to reach a high accuracy, and the fact that, being a local optimizer, it can stack on a local minimum of the objective function instead of a global one.

2.4 Garments features extraction

When an image is captured by the camera, it is firstly classified into one of the 16 categories previously defined, using ResNet50 selected with the framework presented in 2.3.4.2. If the output is a garment category, the second step is to identify the correct color and to find a gripping point for the robot. To get this information, the location of the garment must be previously investigated. There are several methods investigated in literature to achieve for the detection of objects.

2.4.1 State of the art

2.4.1.1 Object Detection

A significant amount of research papers is focused on detection and identification of garments. It is aimed at solving two main problems: the detection of landmarks and reference points for the subsequent manipulation with a robot and the features extraction for further categorization or analysis. In robot operations, the first step is to localize the item in order to decide where to grasp. Then, the robot picks up the garment and, depending on the task, sort it into a defined place or perform preparatory actions for the next manipulation. Feature extraction is mostly used in fashion and e-commerce websites, for customers suggestions or for category division based on garments attributes. Despite the application, garment detection is often the first step to focus on the correct area of the image for the analysis.

Different techniques are used for the garments localization and most experimental scenarios assume that the cloth is the main part of the image in a complex background. The first operation that is usually done is a segmentation, to remove the background and isolate the item [94]. In [95], the authors use and RGB-D sensor to detect feature points on towels, pants and t-shirts. The background is subtracted applying Gaussian mixture model and then polygonal approximation acquire reference points.

Features can be also extracted using traditional CV techniques. Polo shirt are grasped based on a detection of their collar using Bag of Features, that are generated from a two-dimensional image and a histogram for

depth data [96]. Edges are detected by [97] using a depth camera to pick up a crumpled cloth. The contour is detected using the data collected by the depth image. Then, each point is compared to a training dataset to select the best grasp coordinates. Images taken by stereo cameras are used also by [34] to isolate shirts, socks and dresses from a pile, decomposing the problem into high, low and mid-level features. A double-filtering analysis is performed in [98] to localize the garments edges. First, a denoise and a Gauss filters are applied to the image, then the contour is detected using Canny automatic threshold. The method can locate the edges of soft fabrics of different colors and textures with a good robustness.

Most successful algorithms are based on deep learning techniques, that achieve good results in detecting grasping points and extracting features from images. [54] uses a hierarchical CNN with different levels of specialization. The first layer is to classify images while the other two are dedicated for the selection of the picking points. The spatial coordinates for grasping are selected with a neural network also by [38]. There are only three categories, and the database is custom, because the Kinect sensor is used for the images acquisition. Full-sleeved and sleeveless t-shirts show better performances in grasping point detection than jeans. A modified VGG16 network is proposed by [99] for landmark localization, starting from planar images divided into six categories. The model is able to generalize to robotic specific item configurations which differ from the training dataset. The deeper version VGG19 is used by [19] to both classify and extract features from RGB images of fashion products. A Single Shot Multibox Detector (SSD) is presented by [43] for detection of clothes from e-commerce images. The clothes network is trained on a dataset that contains box annotations with several attributes like color, pattern, sleeve, neckline and hemline. The average of correct labels is 83%. [40] uses YOLO, a well-known object detector, to find the landmarks and attributes in upper-body clothing images.

2.4.1.2 Object Detection using Class Activation Map

Class Activation Maps has been developed to explore the points where the CNNs focus to make their predictions and for a weakly-supervised localization. The former task is useful to verify the correct training of the

model and to understand why a network fails in wrong predictions. The latter gives an area where the object is located inside the image, without the needs of training an object detector, like YOLO or SSD in the previous section. This is a great advantage, as it provides a location starting from the same network used for the image classification. Only few papers based on CAM are available and have shown a good accuracy in the location. According to the literature, CAM has never been used for garments detection and for a subsequent feature extraction. In the medical field, this methodology is applied for femoral fractures on radiographs [100], in tooth-marked tongue recognition [101], for breast cancer [102] and pneumonia detection [103]. Moreover, CAM is used for face detection based on the Inception v3 network [104].

2.4.2 Methodology for garments features

When CNNs are selected to approach a classification or a location task, the usual way to detect the objects is to train the model with the coordinates of a bounding box around the items, along with the class name. The design of the boxes is a time-consuming step, as it must be performed for every image in the database. Since that it has been used a new custom dataset, adapted for the required needs, the information about the garment location is not available and the work of locate the items must be done manually. To avoid this lack of time, and to be more flexible when new images are added to enlarge the database, the Class Activation Map is tested to have an indication of the area where the garments are in the images.

Neural Networks are often considered to be “black boxes” that offer no way of figuring out how the architecture works and what has learned. With CAM, it is possible to have a visual explanation of the prediction, as it checks the area that is most responsible for the final result. The hypothesis is that, if the training is performed well, the network will focus on the garments details to predict the correct category and, consequently, the information of its location is available. CAM allows the identification of the image regions in a single forward-pass for a wide variety of tasks, even if the network was not originally trained for this goal. The first reports of CAM tested using AlexNet are sown by [105]. The final result in

their research was a 37.1% top-5 error for object detection on the ImageNet database, without training on any bounding box annotation.

To generate the CAM starting from ResNet50 fine-tuned in this study, it is used the activations available from the last Rectified Linear Units (ReLU) layer, that is able to retain the location before the fully-connected layer. The activation map can be generated for any output class, but in this study, it is interesting only in the predicted one to check for the location of garments. In the network architecture, the features coming from the ReLU layer are used by the fully-connected one to produce the classification output. It is possible to identify the importance of the image regions by projecting back the weights of the fully-connected layer to the activations, to check what are the most important. To obtain the activation map, a weighted sum of the image activations is computed. Firstly, after the image submission to the CNN, activations f of unit k at location (x, y) are extracted from the ReLU layers, the array has dimension $7 \times 7 \times 2048$, where 2048 is the number of the units fully-connected units. Then, the weights w_k^c corresponding to class c for unit k are taken out. Each spatial element (x, y) of the activation map for the class c is defined as:

$$MAP_c(x, y) = \sum_k w_k^c \cdot f_k(x, y) \quad (9)$$

Thus, $MAP_c(x, y)$ indicates the importance of the activations for the classification of an image to the class c . Then, in order to visualize the CAM over the original image, the map is resized to the original image size and then normalized between 0 and 1, to remove all the small activations smaller than 0.2. The values are shown using the jet color map, where the blue means small activations while red is the opposite. The map is overlapping the grayscale version of the classified image.

Once the area has been identified, it is used for two purposes: gripping point selection and color extraction.

Firstly, the area that CAM has normalized with values greater than 0.65 is selected. There are two possibilities to select the grip point for the robot: the highest CAM value or the centroid of the area. The two points does not overlap and are both good candidates for the selection. In order

to evaluate their performances, they are both tried in a random selection of the database with all the categories, and the results will be presented in the next Section.

Then, to extract the color, some preliminary operations must be done, in order to remove some eventual background areas inside the selected CAM. This activity is performed using Image Processing techniques, and the streamline is shown in Figure 45.

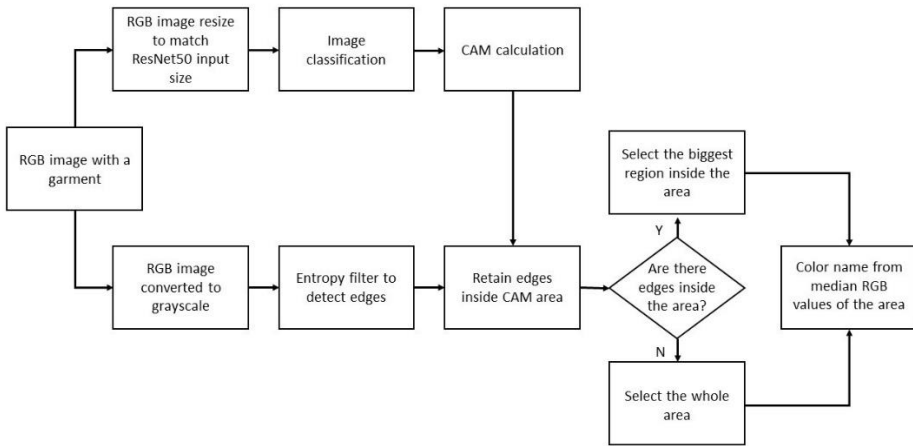


Figure 45. Streamline to extract the garments color from the original RGB image using Class Activation Map to localize the item.

The image is initially converted into grayscale, then a local entropy filter is applied [106]. Entropy is a statistical measure of randomness, which can be used to characterize texture in an image. An image with less variation in its intensities has lower entropy. It is calculated starting from the normalized histogram of the grayscale image:

$$e = - \sum_n p_n \cdot \log_2 p_n \quad (10)$$

where p is the normalized count of the histogram and n is the number of counts.

The hypothesis is that the entropy is higher in the contour of the garments because they have a different texture when compared to a

complex background. Applying a threshold, the edges are detected in all images, and then only the ones inside the CAM area are retained. If there are borders inside the area, the largest region is selected for color extraction, instead if there are no edges, the whole CAM area is chosen.

For the color extraction, the RGB values of the original images that are inside the selected region are used. The median value is calculated for each channel, to exclude some outliers' values given by shadows and wrinkles. To output a color name based on the RGB values, an appropriate color space must be used, with its associate color distance. The names depend on their mapping into the space used. In this study, the Natural color space is used, which contains six colors: white, black, green, red, yellow and blue. The metric to calculate the distance between the image input values and the ones of the color space is the *CIE94* which provides a good matching for various palettes and colors. The algorithms return the name of the nearest color of the Natural space.

2.4.3 Color extraction and gripping point selection

For color extraction and grip point selection, the starting point is the item localization based on the Class Activation Map. The application of this technique to three images randomly chosen by the database is presented in Figure 46.

On the left there are the three original images, while on the right the CAM is applied to the grayscale version, with the red color that indicates the highest activations. On the top of each image on the right, the top-3 class predictions are reported, with the percentage of confidence. In all the three cases, the CAM is able to locate the garment inside the image, and the area is suitable for the feature extraction.

Once that the image has been classified and the CAM calculated, this information is used to extract the garment color and the grip point. The streamline that was presented in Figure 45, is now applied to three images in Figure 47.



Figure 46. Class Activation Map applied to three images randomly chosen from the database. On the left the original image, on the right the CAM applied to the picture, with the top-3 class predicted by the network.

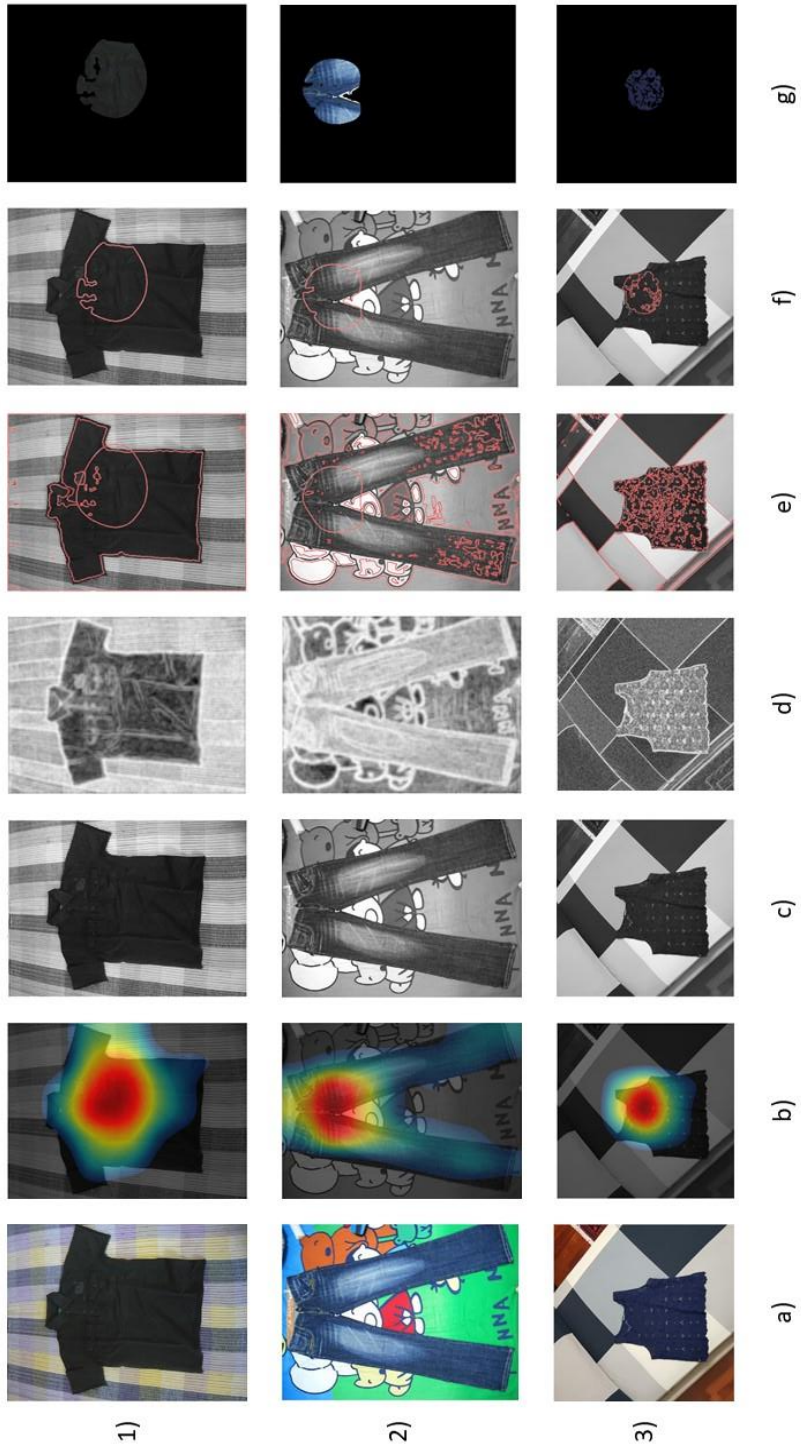


Figure 47. Streamline for color extraction applied to three database images. a) original image; b) CAM; c) grayscale image; d) entropy filter; e) entropy borders with CAM border; f) borders inside CAM area g) area for color extraction.

In column a) the original image is shown, all the three images have different dimensions; in b) the CAM is calculated and shown over the original image; c) is the grayscale picture; d) shows the entropy filter applied to c); e) are the edges obtained with a fixed threshold over the entropy filter, merged with the CAM border; in f) only the edges inside the CAM area are retained; finally in g) the biggest region from the previous area is extracted and applied to the original RGB image.

In the first row of images, it is interesting to notice that the entropy filter is able to remove the label over the t-shirt, that is inside the CAM area and can cause a wrong evaluation of the color. In the second row, the complex background has been totally removed and only the jeans remained inside the CAM area. In the third row, the filter removes also the small holes of the cloth, cleaning the area from the background disturbances. All the three garments here presented were finally categorized with the correct color.

To evaluate the accuracy of the color extraction, at least 190 images were randomly selected from the database for each category, then manually classified into one of the colors parts of the Natural color space and then compared with the result coming from the algorithm. The results are reported in Table 10. In the first column there is the number of analyzed images (N), in the second the white garments misclassified as colored (*White as Colored*), in the third the vice versa (*Colored as White*), in the fourth the misclassification of color, not considering the white (*Color with color*).

The final color accuracy for each category is showed in Figure 48. The values are between 89.2% for the bathrobe to the 98.0% of the trouser class, with an average of **91.5%**. It is interesting to notice that the accuracy obtained from the color extraction is also higher than the classification accuracy, which means that the activations are located in the correct areas and the misclassifications are due to the lack of details of images in the database, as for Delicate wear and Sport wear classes. The algorithm developed works well with all the types of images, independently by the size and the background, and can correctly remove the background from the CAM area, when it is part of that region. In Table 10, a division between color and white misclassifications is necessary because some images in the database are not correctly white-balanced,

resulting in a yellow color instead of white. In these cases, the algorithm fails to correctly identify the white color, as it relies on the RGB values. For this reason, in the Image acquisition module is fundamental to first calibrate the camera in order to avoid color errors due to a wrong white balance.

Category	N	White as Colored	Colored as White	Color with Color
Bathrobe	194	15	3	3
Bra	216	9	2	9
Delicate wear	242	6	6	12
Denim	214	0	0	16
Elegant jacket	232	3	5	14
Shirt	238	7	10	5
Sock	238	7	4	13
Sports wear	242	4	4	12
Sweater	241	5	8	10
T-Shirt	224	9	9	4
T-Shirt Long Sleeve	243	1	6	7
Towel	197	10	4	6
Trouser	203	2	2	0
Undergarment	225	6	6	7
Woman cloth	231	2	7	8

Table 10. Color misclassification for the category of garments. No garment class is not part of this table, because the category does not contain any item.

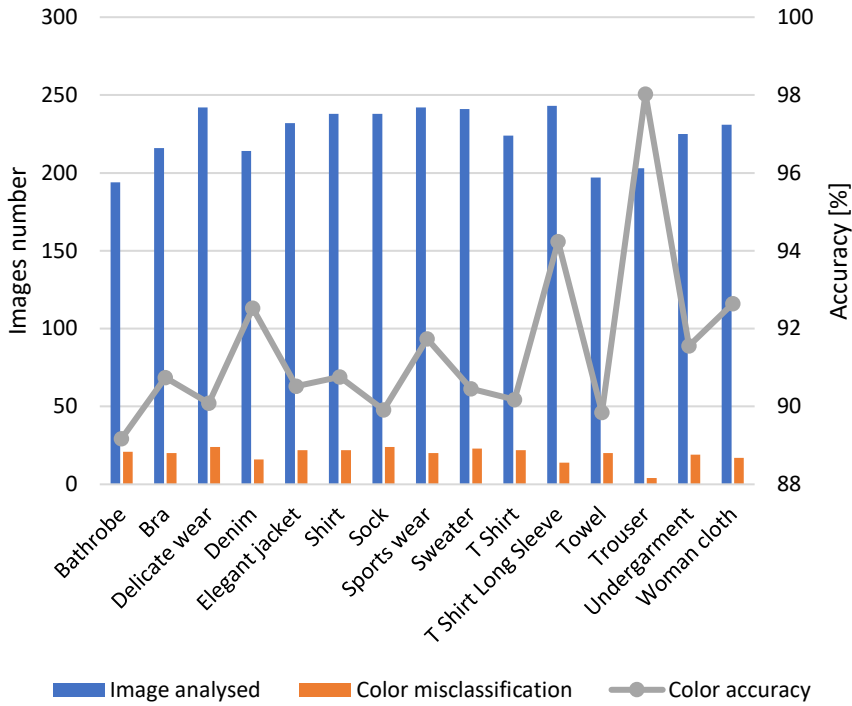


Figure 48. Color accuracy summary for each garment category. Blue bars are the image analyzed for each category, orange bars are the number of images with the wrong color extracted, the gray points are the color accuracy in percentage.

Regarding the gripping point, a comparison between the maximum activation point and the centroid of the CAM area is performed for all the categories. The results are reported in Table 11. In the first column there is the number of analyzed images (N), in the second the errors using the centroid of the area (*Centroid errors*), in the third the errors when the highest CAM value is used (*Max activation error*). For error, the meaning is that the grip point falls outside the garment.

Category	N	Centroid errors	Max activation errors
Bathrobe	194	2	1
Bra	216	19	15
Delicate wear	242	6	8
Denim	214	6	1

Elegant jacket	232	0	0
Shirt	238	0	0
Sock	238	21	13
Sports wear	242	1	6
Sweater	241	0	0
T Shirt	224	3	14
T Shirt Long Sleeve	243	0	3
Towel	197	0	0
Trouser	203	9	5
Undergarment	225	0	0
Woman cloth	231	0	3

Table 11. Gripping point errors for each category.

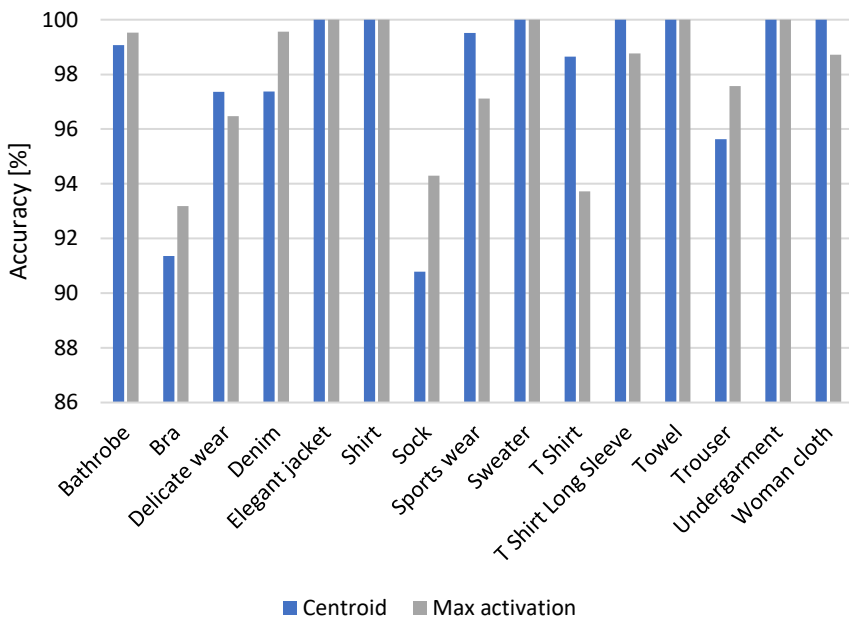


Figure 49. Gripping point accuracy for each category. Blue bars are the centroid of the CAM areas, gray bars are points of the maximum activation.

The points that are inside the garments area are the **98.0%** for the centroid and the **97.9%** for the maximum activation. These values seem similar in the final results, but large differences can be found based on the

categories. The biggest difference is in the T-shirt class, where the centroid accuracy is 4.9% higher than the maximum activation. On the contrary, in sock class the centroid is 3.5% less accurate than the maximum point. This means that, according to the class type, the use of the two alternative is not interchangeable, and the Figure 49 gives a clear indication of the best solution for each category. However, for some classes an accuracy of 100% is reached for both methodologies. After a selection of the best method for every class, **98.7%** of the gripping points are inside the garments area. This is a surprising result, considering that only a CNN dedicated to image classification is used to extrapolate the location, color, and gripping point information. Two examples of gripping point errors are showed in Figure 50.

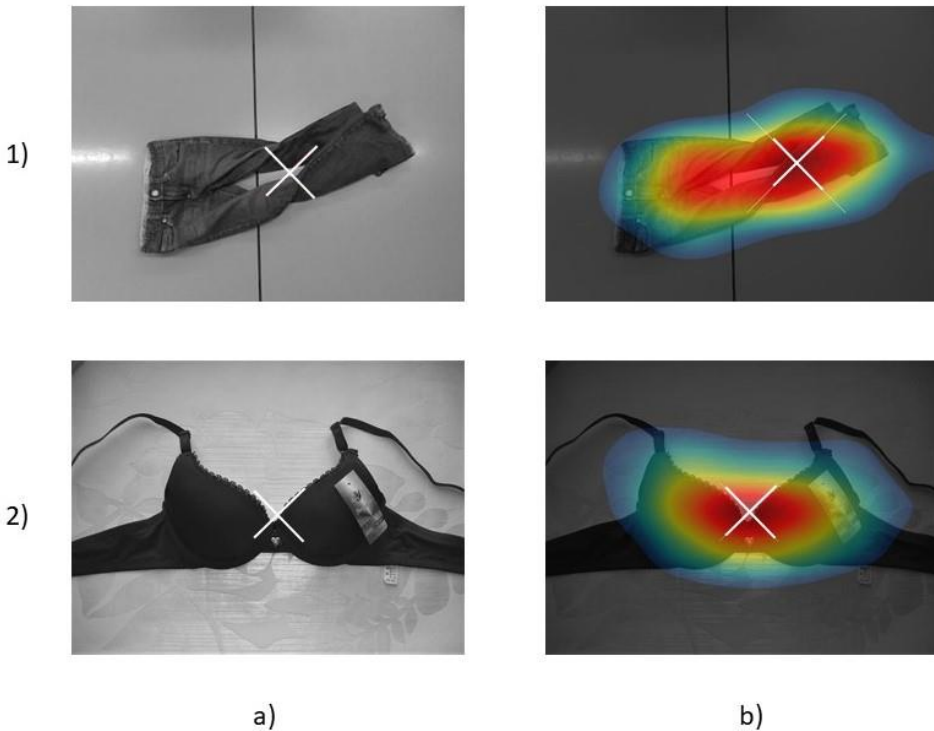


Figure 50. Two examples of gripping point errors. a) are the CAM centroids; b) are the maximum activation points.

In the first row, the centroid fails because of the geometry of the item, which is typical of trousers. For this class, is preferable to use the maximum point because is more probable that falls inside the garment. In

the second row, a case in which both solutions are failing. In this case, the centroid and the maximum points are close to each other, and both falls in the middle of the bra. According to these observations, some modifications of the gripping points can be done based on the class type if the grip of the robot is not successful. However, these cases are rare, given the high percentage obtained using the CAM methodology.

2.5 Washing program selection

When soiled garments has to be cleaned, it is important that the items are sorted based on the washing program to used. A cycle has generally two speeds: one for agitating and tumbling the load, the other to spin the water out of the garments. Moreover, the temperatures of different washing cycles are diverse, they are divided between cold and warm values. Selecting the wrong washing program means to damage or disrupt the garments, as certain fabrics cannot tolerate high temperatures and speeds, or the items can harm each other. For this reason, the assignation of the washing program to a garment is an important operation which must be done carefully based on the information that are available.

There are several guidelines available, each of which suggests a different way to perform the sorting. All the documentations can be divided into different categories. The sorting can be done based on:

- Colors
- Textiles
- Category
- Load weight
- Steins.

Color is an important information to know, as white items can be damaged if washed with colored ones. Usually colors are divided among whites, darks, lights and jeans. This is an important information to know for the temperature selection. The advantage of using hot water is that it sanitized and kills germs, dissolves detergents more efficiently, remove stains more efficiently. The disadvantages are that it causes shrinking and fading in some fabrics, it can set in some type of stains, as blood, and uses

more energy to heat the water. Cold water is used for dark colors while warm water for light and white colors.

Textile has an impact on the washing cycle, as different fabric can tolerate better the mechanical action that is consequence of the drum speed. Delicate textiles, for example, will damage if washed and extracted at the maximum speed allowed by the washing machine. Washing program can be divided into Normal, for cotton, Permanent, for synthetic and blended fabrics, Delicate, for silk, and Handwash, for wool.

Not only textile, but also the garments' category can be used for the washing program selection. This is due to the fact that some categories are related to the fabric type, and the manufactures are designing cycles dedicated to certain classes of clothes, as it is more comfortable for the customers to wash items together after an activity, like sport. This is particularly important also for the professional business, as in laundries a big amount of the same types of items has to be washed together. Some examples can be the cleaning service for hotels, which have to wash mainly towels and bed sheets, or special sectors as fire fighters (suits) or cleaning services (mops). Some companies, that provide domestic appliances as Samsung [107] and Miele [108], are today basing their suggestions on the categories type. In Figure 51 it is shown the user interface of the actual washing machines manufactured by Electrolux Professional, with some garments' categories.

The correlation between categories, color and washing program with the related temperature is illustrated in Table 12. This table is the result of the research on the manufactures website, as well as on laundry guidelines and company internal professional knowledge. Some programs, like "*Sport program*" and "*Denim*" has been dedicated to garments categories, as the washing programs already exist also in the domestic business. Other categories are independent by the color, either because the washing program allows only cold temperatures, or the category does not allow hot temperatures in the cycle they are assigned to. In any case, it is important to recognize the color also for these categories as it is not allowed the mix between colored and white.

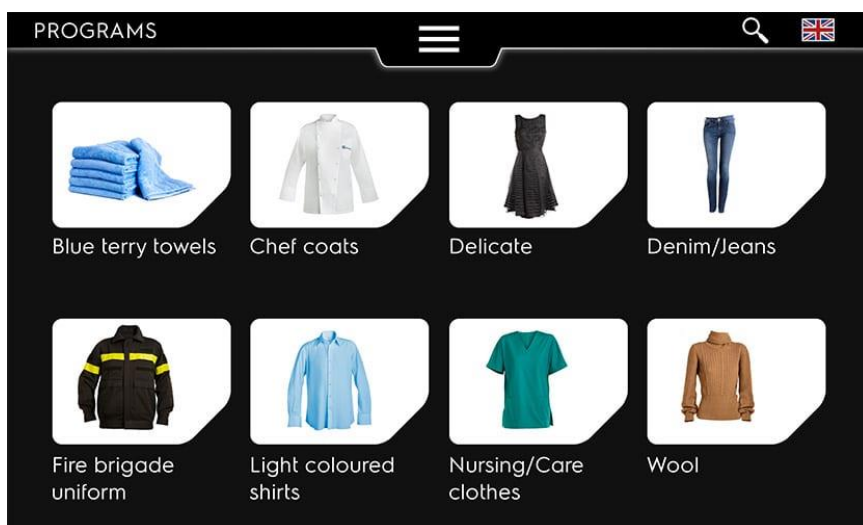


Figure 51. Touch user interface of Professional Washing Machine, line 6000. The washing programs are based on garments' categories.

Category	Color	Washing Program
Towel	White	NORMAL 60
	Colored	NORMAL 40
Sock	-	NORMAL 40
Undergarment	-	NORMAL 40
Bathrobe	-	NORMAL 40
T-Shirt	White	PERMANENT 40
	Colored	PERMANENT 30
Shirt	White	PERMANENT 40
	Colored	PERMANENT 30
Trouser	White	PERMANENT 40
	Colored	PERMANENT 30
T-Shirt Long Sleeve	White	PERMANENT 40
	Colored	PERMANENT 30
Woman cloth	White	PERMANENT 40

	Colored	PERMANENT 30
Sweater	-	DELICATE 30
Elegant jacket	-	DELICATE 30
Bra	-	HANDWASH
Delicate wear	-	HANDWASH
Sports wear	-	SPORT PROGRAM
Denim	-	DENIM PROGRAM

Table 12. Washing program assignation based on garment's category and color.

To evaluate the accuracy of the washing program, at least 190 images were randomly selected from the database for each category. These pictures have been classified using ResNet50 and the color of the garments has been identified using the CAM technique. Based on this information, the washing program has been assigned to each image and then compared to the ground truth, obtained starting from the true category and color of each garment in the images. The results, for each category, are shown in Figure 55. The blue bars represent the accuracy of the washing program on the ground truth. Removing the errors that led to a less aggressive cycle, which does not damage the garments, the results are shown with the gray bar. The final accuracy of the washing program is 97.1%, while removing the non-pejorative errors the values increases until 98.8%. This is an excellent result, considering the accuracy of the classifier and the color extraction on which the washing program selection is based on.

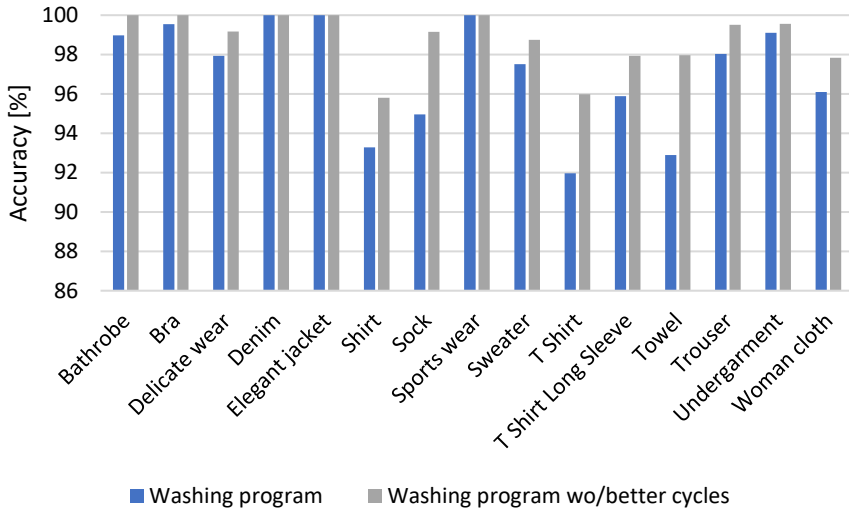


Figure 52. Washing program accuracy on random images taken from the database. The blue bars are the washing program final accuracy for each category, the gray bars remove the error that with a less aggressive cycle.

2.6 Automatic Sorting System

Garments category and color recognition has a wide range of potential applications, like sorting for laundry or recycling sites. In this study, the developed vision recognition system of a single garment, lying on a conveyor belt, has been included into an autonomous sorting platform with the use of a cobot. In this application, the garment category is first recognized, then the color and gripping point information are extracted to finally send to the cobot the correct instructions of the movement, to pick the garment and release it in the corresponding basket.

In order to send to the robot the correct coordinates, an algorithm perform an interpolation to convert the pixel values. The function depends on the robot and conveyor belt position, the height of the camera and its angle. If one of these parameters change, the interpolation function must be updated. Two reference frames are considered: the robot and the camera one. Three points are fixed in the conveyor belt, so that their coordinates are known in both reference frames: two of them are used for the conversion, the third one only to check the accuracy. The equations used are those of roto-translation:

$$\begin{cases} \frac{x_r}{c} = a + x_c \cdot \cos \alpha - y_c \cdot \sin \alpha \\ \frac{y_r}{c} = b + x_c \cdot \sin \alpha + y_c \cdot \cos \alpha \end{cases} \quad (11)$$

where (x_r, y_r) are the point coordinates in the robot reference frame, (x_c, y_c) the same coordinates in the camera reference frame, a and b two constants for the translation, α the rotation angle and c a constant for the different scale of the two reference frames. Since there are four constants to determine, four equations are needed to solve the problem, and therefore two known points. The situation is summarized in Figure 53.

The camera is not only used to acquire images but is also useful as a sensor to identify the presence of garments and stop the conveyor belt. In this study, a different technique has been used, compared to the one presented in other researches, as by [109], [110]. The common method is to compare two subsequent grayscale frames, looking for a difference to identify the presence of an object. This technique requires a stable light condition and the same image background, so that the camera acquire the images only in a restricted area where the objects can be located. In case of unstable light conditions, as in indoor environments lit with neon lights, the difference of the images is not zero even that there are no objects, because of the flickering effect. To avoid the light dependence, it has been developed a new simple method to overcome this problem, taking the advantage of having a uniform background of the conveyor belt.

Inside a single image, after a conversion into the HSV color space, a line of pixel is extracted near the end of the conveyor, that is the point where it is needed to stop the belt for the picture evaluation. In this line, the first derivative is calculated between subsequent pixels. Then, the maximum value is calculated and, if it is higher than a threshold, an object is detected, and the conveyor belt is stopped. This methodology is independent from the environmental light as only one images is needed for the analysis, and the derivative is near to zero if there is no object above the conveyor.

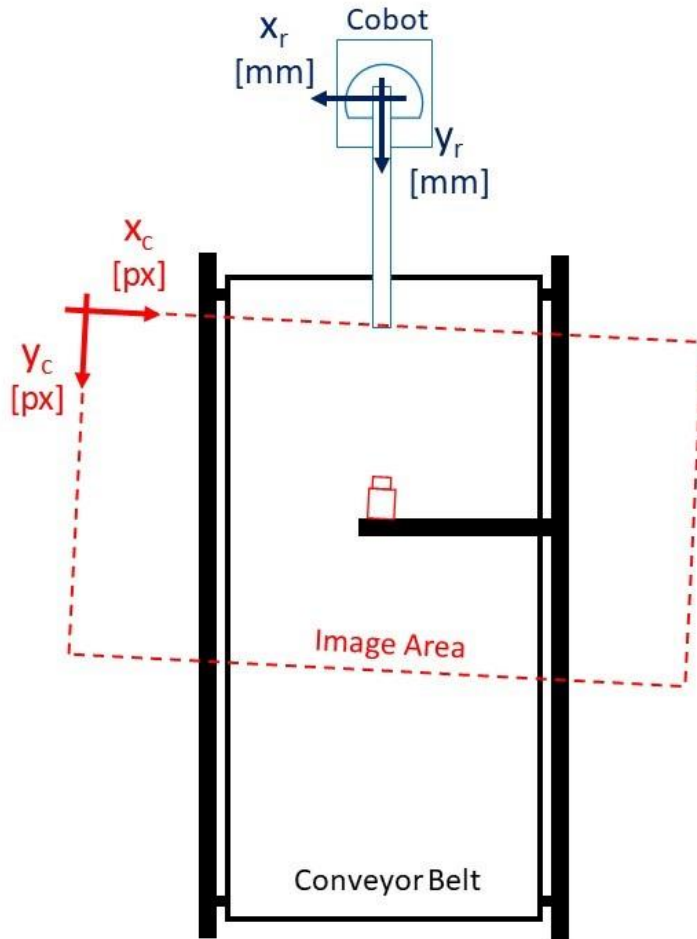


Figure 53. Coordinates conversion between camera and robot reference frames, from pixel to millimeters.

2.6.1 Robotic sorting prototype

The robotic sorting system is made up of a conveyor belt, a camera and a cobot, which has the advantage of sharing the same workspace with workers, without the needs of physical barriers. The cobot is placed at the end of the conveyor, to grab the garments and place them in one of the baskets around it, based on the category and the color. The conveyor is stopped when an item is detected, so that the next can be placed on the belt, in the meanwhile the cobot moves to place the current garment in the correct basket. This allows to have a completely automatic system, where a human or other system can place the items on the belt without putting

attention to the cobot status. The entire system is showed in Figure 54. The system has been tested in a closed room, with standard environmental conditions.



Figure 54. Robotic sorting system in an indoor environment. The baskets are placed around the cobot, that grabs the items onto a conveyor belt. There is one basket for every washing program presented in 2.5. The only sensor used is a camera.

The operation flowchart of the algorithms that connects all the modules presented until now is illustrated in Figure 55. Firstly, the variables and constants that are needed for the next operations are loaded, with the CNN fine-tuned for the classification. Then, a button is displayed to the user to stop the sorting cycle and the acquisition starts. When a garment is detected over the conveyor, the image is classified into one of the 16 categories and the garment color and grip point is extracted. The conveyor is stopped, then the basket and garment coordinates are communicated to the robot, that sort the item. Finally, if the user has not stopped the cycle, the conveyor is moved again, and the image acquisition restarts.

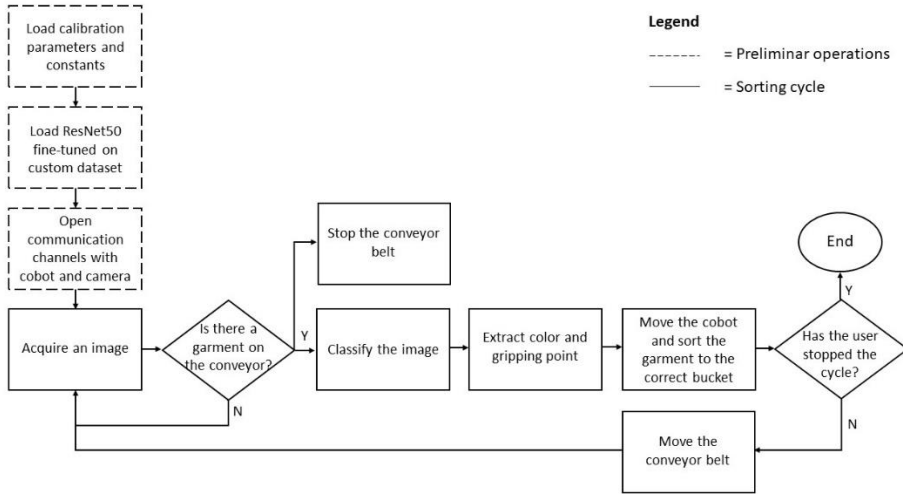


Figure 55. Automatic sorting system flowchart, which connects all the modules developed.

In order to pick the garments from the conveyor, the points obtained by the CAM are used, selecting the centroid or the maximum according to the class type. The pixel must be converted into robot coordinates and, for this reason, Equation (11) is used. The robot coordinates are collected manually, placing the center of the grip over each point and logging the data. The same is done for the pixels, looking to a reference image taken after the completion of the camera set-up. Three points are used, two for the calculation of the constants for the conversion and one as reference for the evaluation of the precision. All the points are taken at the borders of the conveyor, on opposite sides. The result for the check point, with reference to Figure 53 for the reference frames, is presented in Table 13. Pixel coordinates are input of the equations for the conversion, then the output result is compared with the values logged with the robot. The difference is 8 mm for the x coordinate, while is 4 mm for y. The precision is not high but still acceptable, and it can be explained with the camera distortion, given by the wide optic, the human error in the positioning of the robot over the points and in the robot tolerances.

	Point 1		Point 2		Check Point	
	x	y	x	y	x	y
Camera [px]	210	1931	432	621	784	1938
Robot [mm]	-177	549	477	702	-190	842
Result [mm]					-198	838

Table 13. Results of pixel to robot coordinates conversion. Points 1 and 2 are used for the constants determination, result is presented for the Check Point.

Finally, the entire system is tested into an indoor environment with new garments, not present at all in the custom database used for the training. 40 items belonging to all the categories have been used for the final test, with a random placement on the top of the conveyor. The final accuracy for classification, grip point selection and color are aligned with the ones obtained in each section evaluation, with 3, 1 and 2 errors respectively. The detection of the item, used for stopping the conveyor, has always worked with all the garments. This confirms the validity of the proposed new method to detect the presence of the garment, that can be used in indoor environments and is independent of the lighting conditions. Moreover, the accuracy values for classification and color give the confirmation that the system works also with new garments never seen before by the CNN.

A further test has been done with three garments in pile, belonging to different categories. The height of the gripping point on the z coordinate has been calibrated using different items, and the conveyor was held steady until all the garments were sorted. The results are satisfactory, even though the system was not originally intended for this use. The accuracy in recognizing the category is lower than that measured with a single garment, at 82.5%. The most frequent mistakes occur when the dress underneath is larger than the one on top, for example socks or undergarments over sweaters. The main cause is CNN training, which is based on a database containing individual items. However, the recognition rate is high considering the difficulty of the task, and the fact that the system is based on an RGB camera without a depth sensor.

Water Retention Model

This chapter presents an experimental study and model on residual water content of a cotton load during the extraction phase of professional washing machines. The dewatering process is an important part of the washing cycle, because it permits to short the post drying operations in tumble dryers and thus to save energy and time in the entire laundry process. As discussed in [12], the energy necessary for drying textiles strongly depends on the final residual moisture content. Moreover, to guarantee the best performance possible during the extraction, it is important that the washing machine can detect and predict the amount of water content in the load during the extraction cycle, based on the type of load, the dimension of the drum, the spinning time and speed.

Literature lacks data about spinning dewatering performances and thus a method is proposed to measure and predict water retention with respect to the main parameters that affect the washing process. This chapter first provides a survey about retention models that are developed for different applications. Then a new methodology is introduced to estimate residual moisture content as a function of time and centrifugal effects, avoiding time consuming and direct measurements. The model is derived with respect to a customised washing cycle that allows experimental validation with commercial washing machines. A scaling analysis is finally performed to verify the influence of the drum shape on retention performances. Results confirm the validity and versatility of the model on a wide range of professional washing machines.

3.1 Introduction

Washing machines are used both for domestic and industrial laundry. Their operations are normally characterised by the so-called washing, rise and spinning phases. The latter is an important step to extract water from garments placed in the drum before drying and it is normally called dewatering. Mechanical design of the appliance affects water extraction performances because the centrifugal force, that is responsible of the water removal from wet textiles, increases with the diameter of the rotating drum. Residual water content influences also the setup of the spinning phase in order to reduce successive dry process that are costly and time consuming. In fact, the energy spent in drying fabrics depends on the textile residual moisture [12]. For this reason, it is important to predict and control the water content during the extraction phase. Many parameters may influence this process, depending on textile types, appliance capacity, load and aging, quantity and chemical composition of detergents, principal fluid parameters (water temperature and hardness), spinning speed and washing programs [111]. To the best of the author's knowledge, literature lacks data on textiles water retention with no information related to washing machines whereas there are studies on soil and generic porous media. These researches are typically based on empirical models derived from numerical approaches, which are usually implemented with Computational Fluid Dynamics (CFD), either analytical or experimental. From the specialists' experience, only the latter can be effectively implemented for laundry applications due to the many parameters involved. For this reason, this study aims to define a standard methodology to analyse the extraction phase, which takes into account only the relevant physical effects that characterise the process. The tests were performed using three different professional washing machines with diverse washing capacity. The principal result of the research is an approximating surface that can be used to univocally derive the water retention value.

3.2 Water Retention models

Literature lacks studies on dewatering applied to washing machines, while in hydrology several water retention models are used to predict fluid flow through the media. Typically, they based on analytical, numerical or experimental models in which some parameters are established by empirical data due to the complexity of the physical phenomena.

3.2.1 Numerical models

Numerical analysis is based on multi-phase fluid flow on porous media and its implementation has grown during the last years thanks to the increasing computational power of new PCs [112]. In [113], a geometric reconstruction of a fabric has been made to calculate permeability and retention properties. Numerical simulations with a definition of macro, meso and microstructure and a determination of associated model parameters for the permeability was proposed using a fabric virtually generated. Two methods were applied: the first modelled woven textiles from a series of realistic input parameters while the second reconstructed the 3D geometry from sequences of 2D cross section images. The model was used to predict the mechanical flow properties solving the porous media equations of motion. The outcome was not satisfactory due to the complex stresses (mechanical, thermal and chemical) that occur in reality.

There are problems in applying CFD techniques on a washing machine because the gradient of pressure is unknown. To predict the transient state both the water and airflow conditions must be modelled through the media. Moreover, the equations of motion do not describe the textile's elastic behavior and the absorption limit due to capillary effects [114]. During the cycle, the physical and geometrical parameters of the textiles change in relation with the relative stretching. This complicates the model even more and makes the computing time unacceptable for laundry applications.

Water retention numerical analysis is applied on soil drainage simulations. [115] presented an Integrated Finite Difference Method (IFDM) to solve ground water flow problems. It is easier and faster to

apply respect to Finite Element Method (FEM) with similar accuracy, but it is difficult to implement on the textile field because of the parameters dependence on multiple factors related to washing and spinning phenomena.

For the reasons explained above, the numerical approach is not easily applicable to the water retention estimation when textiles are drained in a washing machine.

3.2.2 Analytical models

[116] and [117] described flow on porous media considering bi-phasic fluid composed by water and air. They presented some analytical solutions to model the effective permeability, like Corey's approximation, including also the capillarity pressure trend across the fluid interface. The use of Richard's equation is suggested to simplify the calculation considering the air-phase pressure constant. [116] proposed also a test rig to characterise the media features when air and water flow through it at steady-state condition. The models used cannot be implemented on washing machines because the hypothesis of constant pore size distribution is not respected due to the stretching and compressing phenomena that occur in the drum during the spinning. Moreover, the effective permeability estimation cannot be run under steady-state conditions. A similar experimental setup was built by [118] to study pressure drops of air and water through several different textile fabrics. Data were inserted into Belkacemi and Broadbent's model and the outcomes were used to train a Neural Network (NN) for successive statistical analysis. The study confirmed the influence of operating conditions and swelling phenomena on pressure drops effects.

[119] used Gurnham and Masson's soil hypothesis to describe water retention of cotton fabric. A step-by-step compressional load was used to reduce water content. The model showed limitation of its validity only for low pressure range. [120] analysed water retention in hollow fibres compared to solid assemblies with equal linear density. They discovered a relationship following a theoretical analysis that shows the water retention dependence by varying the hollow-fibre weight fractions.

A variety of different analytical models are used in hydrology. Darcy's law is commonly implemented to predict steady-state laminar water flow. [121] used a centrifugal technique to vary the gradient of pressure and extend the validity of the Darcy's equation also to transient condition, while [122] introduced Forchheimer's coefficient to consider non-Darcy inertial effects. [123] presented a pore-size distribution analysis incorporating porosity and particles of different sizes, shapes and separation distances to predict water retention properties. This geometric approach is time consuming and needs the knowledge of micro and macro structure of every media. Other techniques were explained by [124] using three different Beerkan Estimation of Soil Transfer (BEST) procedures in such a way to obtain a complete hydraulic characterization which was compared to the reference evaporation method. Two important constants of the soil must be determined: β , related to the shape of the grains and γ , a geometric correction factor. The results underestimate the flow because a finer tuning is needed.

The mathematical models described above used many parameters connected to the physical characteristics of soil and textiles. For the determination of such parameters an algorithm was explained by [125] that used an heuristic global optimization method (well suited to solve multidimensional problems involving continuous variables), which achieved significant results. Furthermore neural networks can be exploited to carry out the coefficients of the models. [126] applied a NN on ten soil water retention curve models with fitting accuracy that depends on the functions used in the hidden layer. [127] implemented two NNs to estimate volumetric water content of soil and matric head as input for Van Genuchten model with an accuracy strongly dependent on the equation used.

3.2.3 Experimental models

Water retention trends can be described without the use of theoretical models that must include several physical parameters estimated by empirical approach. In literature some experimental techniques estimate the water retained by different porous media under controlled conditions. One of these is the spinning technique, which is similar to what happens

to cloths in the drum of a washing machine. [12] studied the water surface tension on cotton, which is related to the residual water content in fabrics, by using a centrifugal system. The setup was made by a centrifuge tube with a drilled copper insert on it, in such a way to allow water to flow out. The relationship between the Residual Moisture Content (RMC) and the water surface tension was demonstrated. They showed that the RMC tends to lower exponentially by increasing the ejection force. Similar techniques are also used for soil, clay and cellulose as proved by [128] who obtained positive results and compared the centrifuged method in respect to the standard one. Saboya [129] exploited a small centrifuge system to confirm the Van Genuchten model. Caputo & Nimmo [130] compared Steady-State Centrifuge (SSC) and Quasi Steady-State (QSC) methods to establish water flow in unsaturated porous rock samples. Spinning tests increase driving force, yielding more accurate values of water retention and hydraulic conductivity. They reported the SSC approach in the best condition has an uncertainty of about $\pm 8\%$ for compressible media. Cheng [131] demonstrated that for cellulosic material the main parameters which affect water retention value under centrifugal force are time, speed, and the type of filter used in the machine.

The water absorption of terry towels was investigated by Petrulyte & Baltakyte [132] using stereoscopic zoom microscope and a digital camera. They studied the impact of water, heat, mechanical action and industrial washing on absorption performance. The wetting process was faster in fabrics affected by laundry and the experimental results were best described by polynomial and exponential equations. Furthermore adding detergent at the washing of terry woven fabrics increase water absorption up to 1.8 – 2.2 times compared to grey samples [133].

The aim of the present work is to univocally predict water retention in cotton towels as a function of time and spinning acceleration using professional washing machines. An approximating surface is derived by the collection of water extraction data following the spinning experimental approach. This method includes complex phenomena acting on the drum and allows to save computing time.

3.3 Water retention in washing machines

When washing machines are used to certificate water Retention (R) performances, textile samples are subjected to a centrifugal force at specifically conditions of time, temperature, spinning cycle and apparatus. The International Standard [13] defines R as the percentage ratio of water content in the sample and the condition dry mass m_{cd} :

$$R = \frac{m_{wet} - m_{cd}}{m_{cd}} \cdot 100 \quad (12)$$

Here m_{cd} is defined as the textile moisture content when the cloth is conditioned into a standard environment at the temperature of $(20 \pm 2)^\circ\text{C}$ and relative humidity of $(65 \pm 5)\%$ for sufficient time. Instead m_{bd} is the bone-dry mass of the textile where the remaining moisture content has been reduced to low level and the mass variation must be less than 1% or 20g compared to the previous measurement taken after a specific drying cycle. Moreover m_{wet} represents the total mass of the wet textiles.

The spinning cycle aims to remove the water content from cloths thanks to the centrifugal force which acts according to Newton's second law; these phenomena is called dewatering. The infinitesimal centrifugal force dF is described as follow:

$$dF = dm_{wet} \omega^2 r \quad (13)$$

where ω is the angular speed of the drum and r is its radius.

To compare the performance of the spinning cycle regardless of the machine used, the dimensionless acceleration G is defined as:

$$G = \frac{\omega^2 r}{g} \quad (14)$$

It is the ratio between the centrifugal acceleration ($a_c = \omega^2 r$) to which the washing load is subject and the gravitational one g . This

parameter allows to characterize the spinning cycle only in terms of machine features (speed and radius) and to avoid the effects of uneven load distribution.

The garments placed inside the drum stuck on the internal surface of the tub during the water extraction cycle and form a layer with non-constant thickness along the circumference. To take into account this phenomenon the Fill Factor (FF) parameter is commonly used to describe the quantity of textile in relation with the washing capacity of the machine and it is defined as:

$$FF = \frac{m_{cd}}{V} \quad (15)$$

where V is the drum volume.

3.4 Experimental method

3.4.1 Experimental setup

Three professional washing machines of different washing capacity (6.5 kg, 7.5 kg and 13 kg) were tested to investigate their water retention performances during the spinning phase. The appliances used in this experiment are shown in Figure 56. In Figure 57 a picture and a sketch of the experimental setup used to produce the measures presented in this chapter. The machines are individually tested to replicate the same conditions of use and their washing cycles were customized in such a way to impose the same spinning sequences at specifically value of G . During this phase the water ejected from the drainage pipe of the appliance was gathered into a basin which laid on two load beam cells equipped with Tedeahuntleigh 3410 sensors, in order to measure the liquid mass discharged in time. The drum temperature and speed time history were respectively recorded using a thermocouple type K and a tachometer dynamo by Servo-Tek SB-757A-2. All the signals were logged by an Ahlborn Almemo 2590-9 V5 data acquisition system (DAQ) connected to a Windows PC.



Figure 56. Professional washing machines used for the experimental testing of water retention during the extraction phase. a) is WH6-6 with 6 Kg of capacity; b) is WH6-7 with 7 kg of capacity; c) is WH6-13 with 13 kg of capacity.

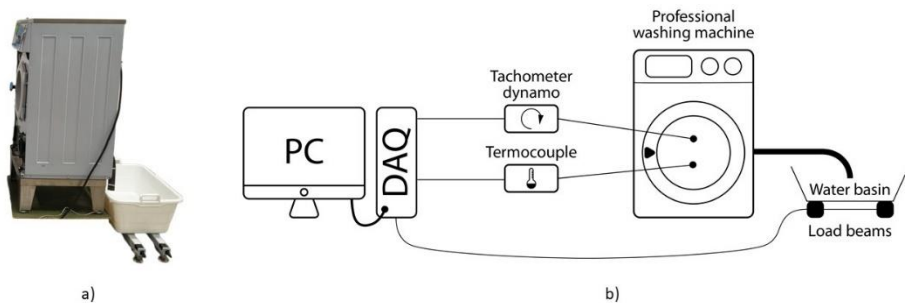


Figure 57. Picture (a) and sketch (b) of the experimental setup used to perform the water retention tests.

A dedicated sample load composed by a controlled weight and amount of new standard cotton towels was prepared for each of the appliances taken into account in accordance with the International Standard. Table 14 reports the properties of the cotton towels used for the experiments.

All the samples must be conditioned before proceeding the tests in order to establish the dry conditioned mass which is representative of the

dry status of the garments. Thus, all the cotton towels were placed in a controlled climatic chamber at imposed temperature and humidity.

To measure m_{cd} , m_{wet} , and m_{bd} masses a digital scale of Carl Liden DIGI DI-10 was used. After each spinning test every group of samples were dry until condition dry mass by using a professional tumble dryer.

Material	Terry
Quality	100% cotton
Color	White
Dimension (cm)	70 x 140
Density (g/m ²)	460

Table 14. Sample features.

3.4.2 Experimental procedure

Many conditions may affect water retention measurement in a washing machine. In order to obtain repeatable tests an own standard procedure was defined following the normative recommendations in such a way to compare the water retention history and washing machine performances. Figure 58 and Figure 59 show the procedure followed for each of the three different cotton loads prepared for the appliances. The results of this study were obtained at specifically water temperature, FF and no detergent. Thus, all the three cluster of cotton towels were conditioned and selected in such a way to respect the filling coefficient. In order to realize the correct weight of condition dry towels some stabilization washing cycle were initially performed using a secondary big washing machine. These pre-treatments were done for a larger amount of towels respect to what is request by FF, in order to guarantee the achievement of the correct quantity.

Starting from a selection of new towels, during the stabilisation phase all the samples were washed in a washing machine five times using a reference detergent and a standard 60°C cotton program, without intermediate drying. Pre-treatment is followed by a normalization phase in which the towels were washed without detergent using a standard 60°C cotton program and then dried until bone dry. The loads were later hung

to a drying rack and placed in a conditioning chamber under controlled temperature of (20 ± 2) °C and relative humidity of (65 ± 5) % for at least 15 hours. This procedure was done to moisten the towels in such a way to obtain the condition mass. From the entire amount of the conditioned load only the right quantity of samples was selected to equal the m_{cd} value in respect with the fill factor chosen for the experiments. The sample load cannot be used for more than 80 tests to avoid a performance decay due to extreme aging.

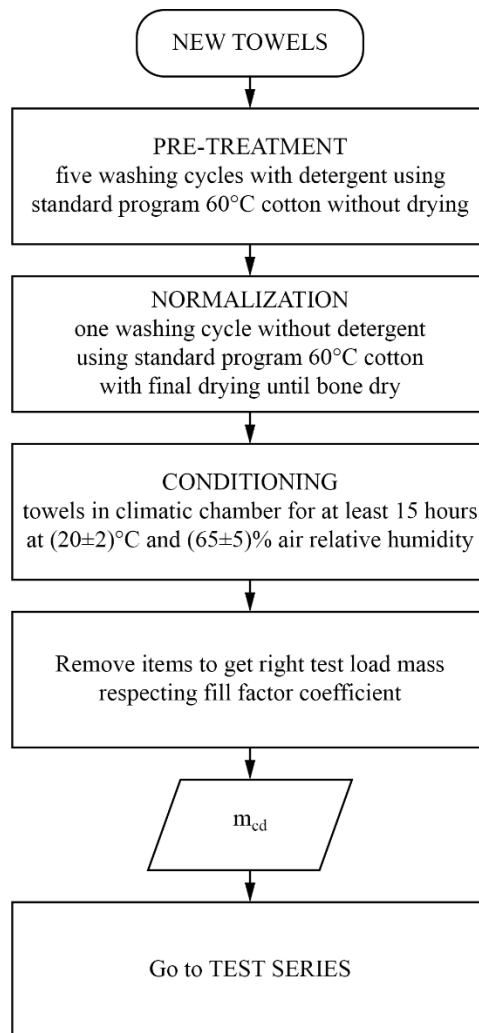


Figure 58. Flow chart to prepare the load before the test series through a stabilization, normalization, conditioning and weight process.

The test series to measure the dewatering performances of the machines started with drying the cotton load until m_{bd} condition. Experience has shown that the way in which a washing machine is loaded could slightly influence the results obtained; it is therefore necessary to specify the loading sequence in such a way to achieve reproducible outcomes. First grasp the towels in the center, shake it to hang loosely, fold it twice to a third of its total size and then place them in the drum.

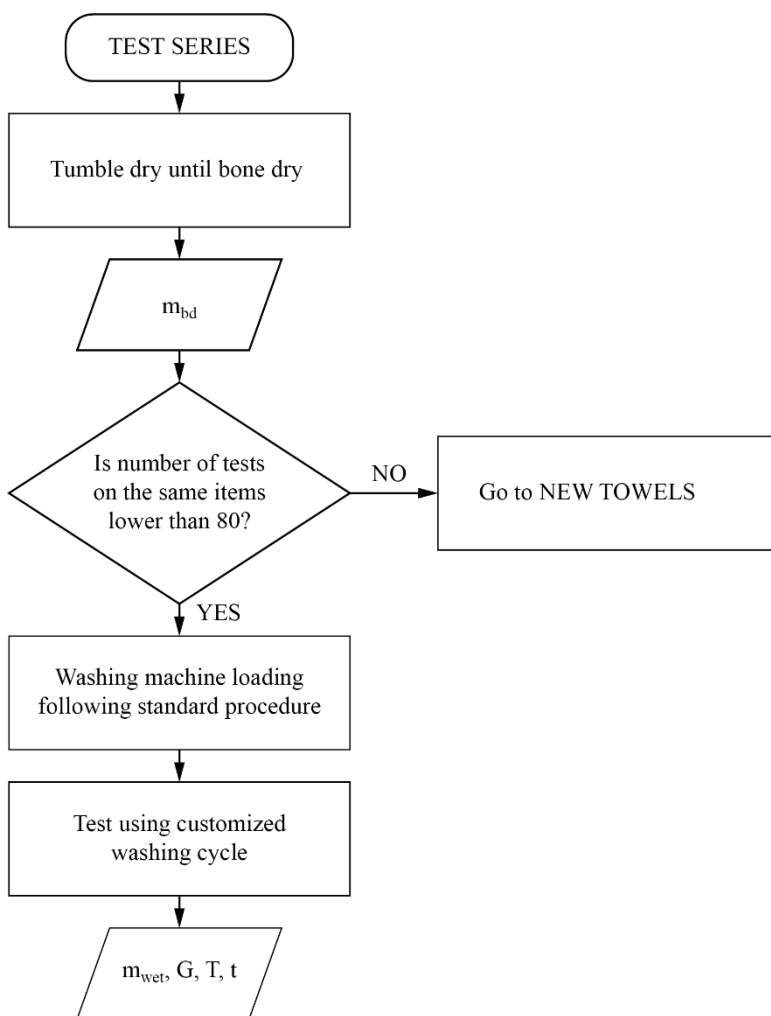


Figure 59. Flow chart describing the test procedure followed to test the dewatering performances of washing machines.

Starting from a real washing program, a customized washing cycle was designed to perform these series of experiments once the machine was loaded. It is composed of four different parts: water filling, clockwise and counterclockwise washing, drain and final long spinning, as shown in Figure 60. The extraction phase is the one of interest for this study and it is reached as fast as possible setting the same maximum drum acceleration for all the appliances considered. The spinning cycle last 10 minutes in the meanwhile the angular speed of the drum is maintained constant compatibly with the inertial dynamic unbalance effects in such a way to replicate real working conditions. In order to analyze the influence of the G parameter, the test series is performed for different values of extraction speed for each appliance.

At the end of the procedure, the wet mass of the sample, m_{wet} , was recorded as a reference point for the further analysis. Water extraction performance is expressed as the amount of remaining moisture content in the load at the end of the program relative to the conditioned mass after the final spinning operation.

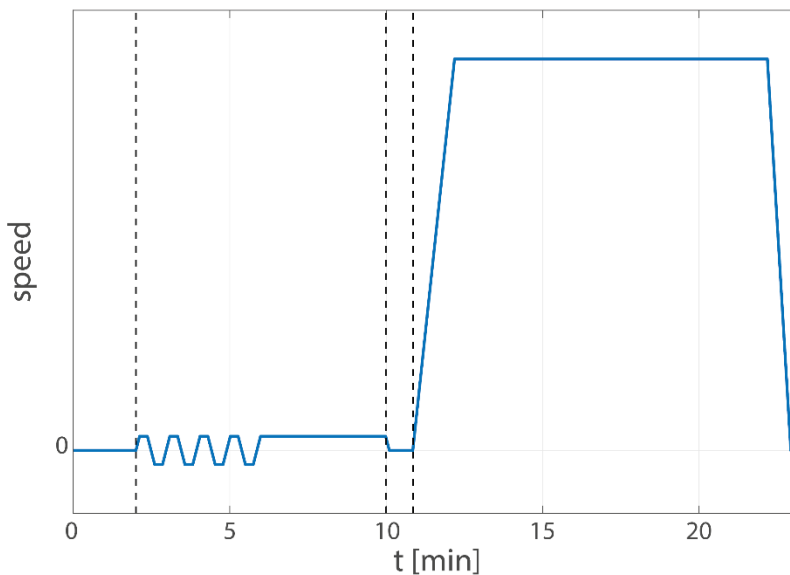


Figure 60. Customized washing cycle used to perform water retention tests.

3.5 Experimental model results

Experimental results are first provided with reference to water retention time history in order to evaluate the repeatability of the tests performed with the three different washing machines. Three relevant G acceleration factors were chosen for this analysis in such a way to cover all the working range of the appliances. Furthermore, a three-dimensional analysis is performed to include the geometrical features of the drum and spinning cycle set up. A fitting surface is sought to approximate the retention value as a function of time and G -acceleration. This has the advantage to predict the residual moisture content at required time and spinning speed, regardless of the washing machine used. The model is made up by a fifth order polynomial equation to obtain the fitting on the working range necessary for laundry applications. Data dispersion analysis and matching performances are reported to emphasise the validity of the model. Finally, a scaling analysis is carried out to evaluate the influence of the washing machines shape and capacity on residual moisture performances.

3.5.1 Time-analysis repeatability

Data acquired has to be processed to calculate retention value using Equation (12). In fact, the water extracted during the spinning $m_{w,ext}$ and weighted by the load cells, does not appear explicitly in the R definition that refers to the total amount of water in the textiles. For this reason, the numerator of Equation (12) can be rewritten as:

$$m_{wet}(t) - m_{cd} = m_{H_2O}(t) \quad (16)$$

where m_{H_2O} is the residual mass of water in the towels at specific time. Due to the water mass conservation of the system:

$$m_{w,ext}(t) + m_{H_2O}(t) = C \quad (17)$$

the sum of the water ejected during the spinning and the residual water in the textile must be equal to a constant C , which is calculated referring to a known point at the end of the extraction cycle:

$$C = m_{wet}(t = t_{fin}) - m_{cd} + m_{w,ext}(t = t_{fin}) \quad (18)$$

where $m_{wet}(t = t_{fin})$ is the entire wet cotton load weighted at the end of the tests.

Substituting the formulas above to Equation (12), the percentage of residual moisture content as a function of time can be derived with the following expression:

$$R(t) = \frac{m_{wet}(t = t_{fin}) - m_{cd} + m_{w,ext}(t = t_{fin}) - m_{w,ext}(t)}{m_{cd}} \quad (19)$$

Figure 61 shows the water retention time history of the cotton towels during a spinning phase at fixed speed, temperature and fill factor in a professional appliance. As expected by the investigation on hydrology and soil retention, the residual moisture decreases rapidly during the beginning of the extraction cycle that starts at saturation condition. As the fabric samples continues to drain water, the capillary force on them tends to equal the centrifugal one induced over the water molecules reducing the extraction performance as shown on the right-hand side of the graph.

To verify the validity of the methodology described in Section 3.4, some tests were repeated at three different speeds in order to cover low, medium and high revolution frequency range, for all the washing machines considered. For this purpose, Figure 62 shows an example of the repeatability tests performed at controlled drum speed for one of the three washing machines tested. The blue, red dashed and black dotted lines display the water retention time history for the same load composition and G at three different tests.

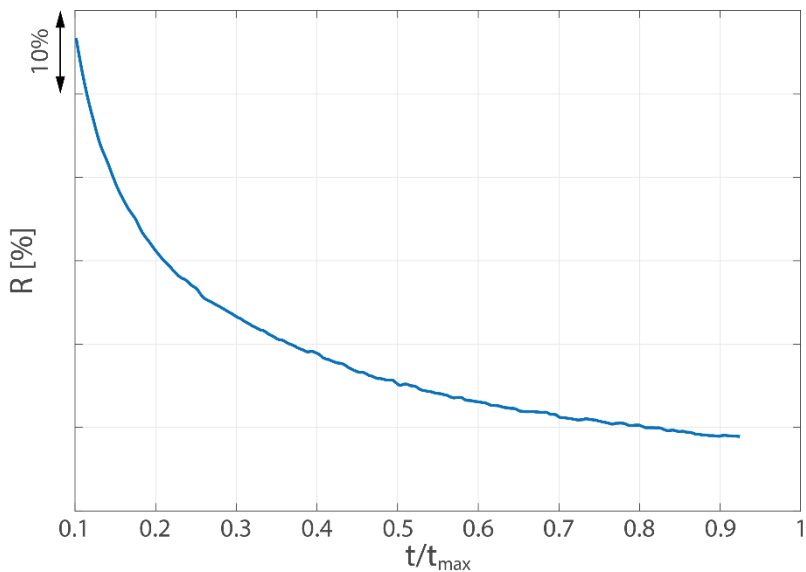


Figure 61. Water retention time history of the towels inside the drum during a spinning cycle considering a specified extraction speed, fill factor coefficient and drum dimension and shape.

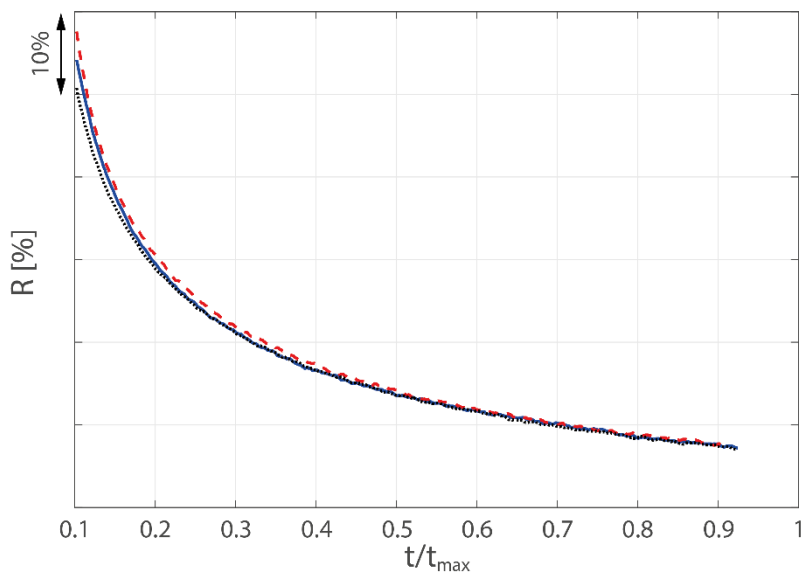


Figure 62. Repeatability of water retention tests at fixed spinning speed and washing machine. The blue line is the repeatability test number 1, the dashed red line represents test number 2 and the black dotted line the number 3.

The discrepancy between the trends is higher at the beginning of the extraction cycle and it gets closer at the end of the phase. These results validate the experimental methodology defined and point out that the

cloths distribution less influence the time history dewatering performance of the appliance for the fill factor chosen. Moreover, the comparison of the maximum difference between the final residual moisture values $\Delta R_{max}\%$ is collected in Table 15 for all the machines with the extraction speeds considered for this analysis. The final water content in the towels differs less than 1.6% after the spinning cycle and the variation gets lower as the revolution speed gets higher. In fact, at maximum G the difference on the final water content is lower than 0.3% regardless of the washing machine used to perform the test series.

	$\Delta R_{max}\%$		
	WM 1	WM 2	WM 3
Low speed [50G]	1.6%	1.2%	0.4 %
Medium speed [250G]	0.8%	0.8%	0.3%
High speed [450G]	0.3%	0.3%	0.2%

Table 15. Comparison of water retention repeatability results at three different speeds for all the washing machines (WMs) considered.

3.5.2 Proposed empirical model

The experiments presented in the previous section are time consuming and referred to specific and constant G -acceleration value. In order to extend the study to the whole possible working range of the machine a 3D model is provided at fixed temperature (20°C), textile type (Cotton Towels as in Table 14), fill factor (1/10 kg/l) and no detergent. In this way, it is therefore possible to predict the residual moisture content of 100% cotton at the time and speed desired. Literature lacks mathematical models that describe retention phenomena using washing machines, so the challenge is to define a general equation able to fit, with a good accuracy, all the experimental data. For this purpose, the water retention time history analysis described before was performed for a set of 11 G -acceleration factors for each of the three washing machines. The G value chosen in this activity are: 50, 90, 130, 170, 210, 250, 290, 330, 370, 410, 450 in such a way to distribute the data overall the common working frequency range of professional washing machines.

As reported in the introduction, the experimental results are best described by polynomial equations. The best approximation carried out with the data available consists in the following fifth order polynomial expression:

$$R\%(t, G) = \sum_{i=0}^5 \sum_{j=0}^{5-i} a_{ij} \cdot t^i \cdot G^j \tag{20}$$

where a_{ij} are the coefficients of the polynomial reported in Table 16 while Figure 63 shows the water retention fitting surface parametrized by t and G as described in Equation (20) using the test data from a professional washing machine.

Coefficient	Value	Coefficient	Value
a_{00}	55.75	a_{20}	0.96
a_{01}	-9.60	a_{21}	-0.23
a_{02}	0.93	a_{22}	-0.08
a_{03}	-3.04	a_{23}	-0.03
a_{04}	3.55	a_{30}	-0.13
a_{05}	-0.70	a_{31}	0.03
a_{10}	-6.11	a_{32}	0.04
a_{11}	0.90	a_{40}	1.33
a_{12}	0.79	a_{41}	0.01
a_{13}	0.14	a_{50}	-0.67
a_{14}	-0.39		

Table 16. Value of the coefficients of fifth order fitting polynomial expression.

High water residual content occurs for low value of G because the mechanical action is too weak to evince the flow resistances inside the textile even for long spinning time. Moreover, a significant amount of water content appears for short extraction cycles even if the revolution speed increases up to the maximum value. A fast dewatering effect can be observed when both parameters are low, whereas a flattening behavior

occurs when they become higher. Best dewatering performances are reached for highest values of G and t , where the retention decreases until about 120% compared to the initial point. The surface shows that G has a greater impact on water ejection compared to time. This is because the water extraction limit is reached faster and the capillary force on the fabrics equals the centrifugal one.

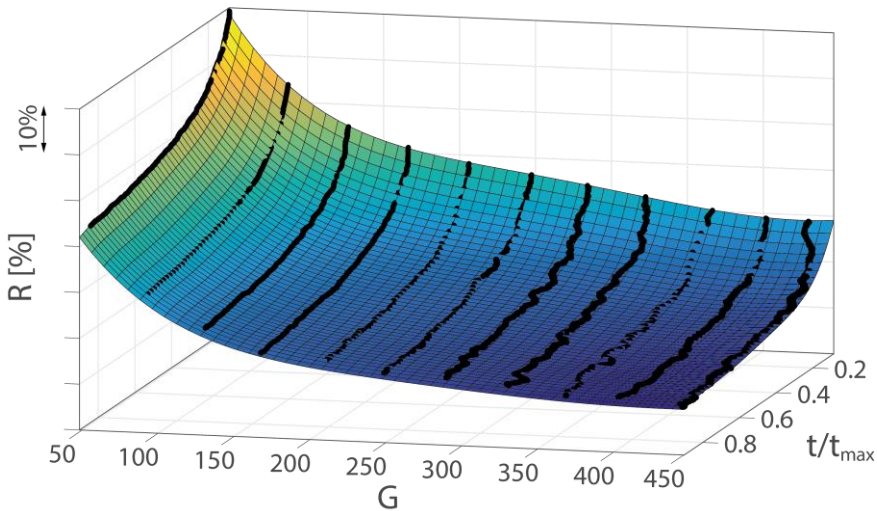


Figure 63. Water retention surface fitted on experimental data by a fifth order polynomial equation for a professional washing machine.

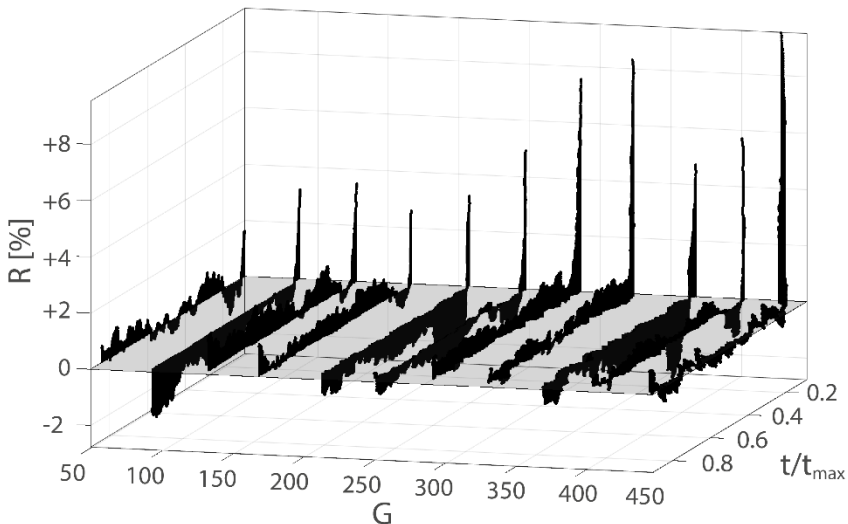


Figure 64. Data residual of the fitting polynomial equation respect to the experimental data for a professional washing machine.

To evaluate the accuracy of the predictive surface, residuals are calculated as the difference between the experimental data values and the estimated ones by using the polynomial equation. Figure 64 shows the residuals which are lower than $\pm 2\%$ of variation when the extraction time is higher than 2 minutes while they reach peaks up to 10% of variation for spinning time lower than 1 minute. Short extraction time could be affected by different ramp up behaviors of the machine due to dissimilar unbalance excitations.

The study described above was repeated for all the three professional washing machines considered using the same fitting equation. Additional parameters were considered to compare the model reliability and accuracy. A summary of R-square (R^2) and Root Mean Square Error (RMSE) is reported in Table 17. For each of the three machines, the R^2 parameters are close to one, meaning that the models replicate well the observed data. The RMSEs indicate that the washing machine with the biggest washing capacity (WM3) is best approximated by the equation proposed. Any way the RMSE values are similar for all the appliances and low enough to guarantee the validity of the model.

	WM 1	WM 2	WM 3
R^2	0.9991	0.9991	0.9992
RMSE	0.7359	0.6692	0.6080

Table 17. Statistical parameters to evaluate the accuracy of the model for the three washing machines.

3.5.3 Model scaling

The washing machines used in this study have different drum dimensions and washing capacity. An investigation to understand the impact of the tub shape geometry on water retention performances was thus carried out. All the experiments were performed under the hypothesis of the same FF coefficient (1/10 kg/l) to guarantee a constant relation between the amounts of cloths and drum volume. This FF value allows a distribution of the garments over the entire internal surface of the tub so that empty regions are almost absent. Nevertheless, different geometries imply

different thickness of the cloth layers during spinning, with possible consequences on the dewatering process. An analysis of the effects caused by the different thickness is therefore needed. Indeed, as described by Equation (15), under the hypothesis of constant and full filled distribution of textiles along the longitudinal axis of the drum, the fill factor coefficient can be rewritten as:

$$FF = \rho_t \cdot \left[1 - \frac{(r_{wm} - s)^2}{r_{wm}^2} \right] \quad (21)$$

where ρ_t is the towels volume density, r_{wm} is the drum radius and s is the average thickness of the textile layer stacked on the drum during the extraction. These hypotheses are reasonable because as the speed of the rotating drum rise up, the garments tend to evenly distribute on its internal cylindrical surface along the circumference and the depth of the tub.

Therefore, from Equation (21) it is possible to derive that different washing machines have different thickness of the washed layer when they are loaded with the same fill factor:

$$\frac{s_1}{s_2} = \frac{r_{wm_1}}{r_{wm_2}} \quad (22)$$

where subscript 1 and 2 indicate two washing machines with dissimilar shape of the drum. For this reason, an experimental scaling analysis was performed to understand the impact of the different dimensions of the drum and thickness of cloth layer on dewatering performances.

To classify the drum shape of the three different washing machines considered, the shape factor S_f is defined as the ratio between the drum depth d and its diameter D .

$$S_f = \frac{d}{D} \quad (23)$$

Table 18 contains the shape factor classification of all the machines considered. Two appliances have the same shape factor but different washing capacity, while the third one differs by 16.7% compared to the others. This range is representative of the professional washing machines portfolio available on the market.

	WM 1	WM 2	WM 3
S_f	0.6	0.6	0.7

Table 18. Shape factor coefficient of the washing machine considered.

To evaluate the impact of the shape factor on dewatering performances, the absolute difference in terms of residual moisture content is carried out among all the possible pairings of washing machines and then represented in Figure 65. The content of water is shown as a function of G-acceleration at the beginning (a) and close to the end (b) of the spinning time.

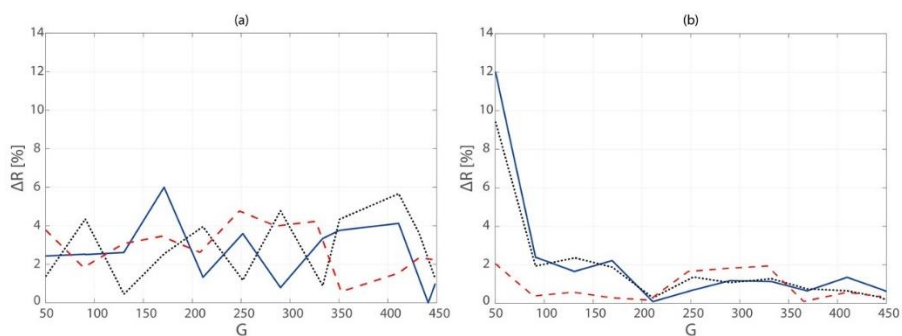


Figure 65. Comparison of water retention variation among the machines as a function of G-acceleration after one minute (a) and eight minutes (b) of spinning time. Each line denotes the absolute difference of water retention between two washing machines. The blue line shows the absolute variation between WM₁ and WM₃, the black dotted line between WM₂ and WM₃, and the red dashed line between WM₁ and WM₂.

At the beginning of the extraction phase, the variation of water retention among the machines fluctuates up to 6% overall the G range studied without any visible influence related to the drum shape. For longer extraction time there is a great variation of dewatering performances that reaches a ΔR of 10÷12% at low speeds when appliances of different shape factor are compared. Over 100G, all the

trends are close to each other within the 2% of residual moisture content variation, compatibly with the accuracy of the measurement system. Therefore, the shape factor impacts the performances only at low G-acceleration factors while no relevant correlation can be observed for extraction cycle shorter than two minutes. Low values of G generate lower centrifugal forces that mitigate the dewatering performances and makes the thickness of the layer of cloths and their distribution inside the drum, relevant for the process.

A standard spinning cycle for cotton garments is typically set at high angular speed for long periods; for this reason, the influence of shape factor on professional laundry is not relevant under the hypothesis of this study. Indeed, a unique polynomial model to predict water retention performances is valid for the professional washing machine within an accuracy lower than 2%.

Advanced Moisture Measurement

The moisture measurement, during a drying cycle, is important for knowing the trend of the water evaporation and to stop the appliance at the right point, based on the program selected by the customer. The sensors that are today used in the professional appliances are not accurate in the range between the condition and bone dry, so an improvement is necessary especially in this area. It is fundamental to have a sensor accurate in the entire range of the drying cycle, as it let to reduce the energy consumption, by avoiding the over drying, and a device that can be easily mounted on every model of tumble dryer. For this reason, a textile moisture content sensor based on self-capacitance technology is proposed, with an experimental evaluation on four different fabric types.

Initially, a brief review on capacitance-based sensors for moisture measurements is provided. Then, the strategy for the sensor development is presented, with the system that comprises an electrode on a printed circuit board (PCB) connected to a capacitance-to-digital conversion electronic circuit. The challenge is to adapt a board made for proximity and touch applications to moisture measurements, applied for the first time to textiles. The advantage is given by the low-cost and easy design of these configurations. Three sensor layouts with different configurations of the electrodes are tested, coupled with diverse overlays and cables. Once the best configuration is selected, an experimental evaluation is carried out using four textiles: cotton, polycotton, wool and polyester. The results show good repeatability and resolution in the entire moisture range tested, from 5% till 70% using bone dry weight as reference point.

The presented regression models, quadratic for cotton and polycotton while linear for wool and polyester, approximate well all the behaviors. Finally, an analysis of both temperature and humidity effects on the sensor measurement is discussed. The response is linear at low and high humidity, with the temperature effect that is predominant. This allows the usage of the sensor also in harsh environments, modifying accordingly the baseline of the measurement.

4.1 Introduction

Moisture content is one of textiles properties that is important to know for industrial and domestic applications, to regulate drying processes or machine parameters during manufacturing of fabric and yarns. In textile dyeing and finishing processes, is essential to measure continuously the water content, not only to guarantee the quality of products, but also to save energy [134].

In general, moisture content can be measured using many different methods with varying complexity and accuracy and are generally divided into direct and indirect approaches. The former is according to the definition, it measures the weight of the textile in dry and wet conditions, calculating the moisture content using a formula. The latter uses certain physical properties such as dielectric constants, resistance, absorption of external radiations, and a method is used to find out the moisture content based on those measured quantities [135]. In industrial applications, it is important to have a quick measurement of the moisture content in real time and, for this reason, many sensors have been developed using the indirect approach.

For moisture measurements, many authors have reported several methods to quantify the capacitance values. Capacitors are generally composed of two conducting plates separated by a non-conducting element, that is called dielectric. When a voltage is applied across the two terminals of the capacitor, the plates store electrical energy until the potential difference is equal to the source voltage. Capacitance is the measure of the amount of charge that a capacitor can hold at a specified voltage [136]. Once the sensor layout is fixed, the capacitance value is

determined by the dielectric material that fills the terminals of the capacitor and it can be measured using either mutual capacitance or self-capacitance. The difference is shown in Figure 66.

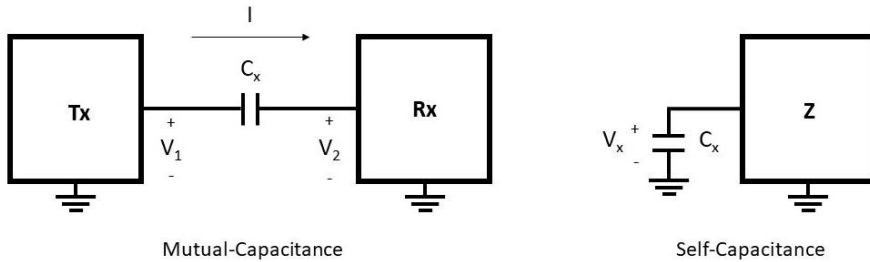


Figure 66. Difference between mutual capacitance and self-capacitance.

Mutual capacitance uses two electrodes, one is the transmitter (Tx) and the other is the receiver (Rx). However, self-capacitance uses a single electrode and measures the capacitance between that electrode and the ground. A sensing system based on self-capacitance operates by applying current to the sensor and measuring the voltage [137].

These type of sensors have been widely used for many years in several fields due to their low production cost and large range of applications [138]. Among the most popular, implemented solutions for these sensor types is to measure flow [139], pressure [140], linear and angular position [141], accelerations [142] and proximity [143]. The sensor reacts to changes of the physical parameter to be measured in the process, giving capacitance values between two electrodes or one electrode and the surrounding earth. The variation may be caused either by geometric variations or by the dielectric properties of the material in the field of the capacitor [138]. The usage of capacitance sensors is also spread in several fields to measure the moisture content of porous media. As example, they are used in textiles [144], soil [145], wood pellets [146] and grain [147].

The main advantage of capacitive sensors is their reliability and accuracy compared to mechanical technologies, because there are no moving parts. Other advantages of using capacitive sensing are the low power consumption of these sensor, and their good resolution, stability,

and fast response [148]. Finally, they can also provide a high Signal-to-Noise ratio (SNR) [149].

During the last years, sensors based on self-capacitance measurement system are becoming more popular. The main reasons are both that the sensor design is simpler when compared to mutual sensors and that the acquiring circuits are cheap, due to their widespread use as touch and proximity sensing [150]. Some examples are the measurement of soil [151] and wheat [152] moisture content and the estimation of water level [153]. To the best of author's knowledge, it is missing a sensor, based on self-capacitance, for the estimation of moisture content in textiles.

In this thesis, an innovative design and the validation of a sensor, based on a self-capacitance acquiring circuit, is presented. It is able to estimate the moisture content in four different types of textiles: cotton, polycotton, wool and pure polyester. According to literature research, such a sensor, which is based on the measurement of self-capacitance, has not been presented in previous studies. The main advantages are both the simple design, that is possible to manufacture on a large-scale, and the low-cost acquiring circuit, already tested on touch and proximity applications.

The key contributions of this chapter are:

- The design of the sensing components and the choice of a low-cost acquiring circuit for the measurement of the capacitance
- The definition of a standard procedure to validate the performance of the sensor with different textiles
- The experimental validation of the sensor using four different textiles with five repetition each, under steady conditions. The textile moisture content varies between 5% and a maximum of 70%, with environmental standard conditions, that is in the range for professional laundry appliances
- A reliable design of the sensor under harsh conditions, with a trial in a climatic chamber, varying both temperature and humidity.

4.2 Textile moisture sensors

Textile material and fibres have been the subject of study since many years. In particular, research on the moisture content of such material have been carried out in many directions, resulting in several sensor types that measure different physical properties.

One of the technologies used to sense the moisture content is microwaves, which is based on water molecules absorption of energy. It has been demonstrated that it is few hundred times higher than common textiles materials [134]. During the measurement, the microwave probe launches certain energy to the textiles and the sensor detects the difference of energy absorbed by the specimen. The fabric moisture can be measured real time without a direct contact [154] but the sensor is sensitive to temperature and requires expensive instrumentations, as a PLC [135]. Another method is proposed by [155], where a radio-frequency sensor with a PID negative feedback control system is used, with an infrared oven containing four modules of radiant elements. This technique was successful only using the same fabric at uniform tension and was not applicable under industrial conditions. It was found that the measured change of the dielectric is influenced by other factors, such as the type and construction of fabric and the presence of ionic substances in water. In [156], near infra-red (NIR) spectroscopy has been used to measure the amount of water in textiles, recorded with a diode indium gallium arsenide array spectrometer with a spectral range between 1200 and 2200 nm. Water content above 50% does not deliver good results and the instrumentation is expensive. The advantage is the possibility of analysing and identifying seven various textiles fibres. More recently, a coaxial resonator has been proposed to perform contactless measurements of moisture on surfaces of thin materials such as webs. The circuitry is low-cost, but the sensor is bulky. It is suitable for industrial analysis where an high precision is required [157].

Capacitive sensing, in the field of moisture quantification, features the advantage that the dielectric constant of the media to be examined is typically lower than the water dielectric. When compared to microwave technology, lower frequencies are employed, and the electrical field is evaluated instead of waves propagation. The penetration depth and

sensing volume can be designed according to needs, and multi-path propagation problems are avoided [138]. Moisture measurements by means of capacitive sensing have been reported for various porous media. This technique has shown great results for measurements in oil [158], [159], where the sensor is driven by a sinusoidal signal which is frequency stabilized and controlled. A similar system, with high frequencies, has been used as a moisture meter for mining and production of oil and gas bulk [160]. Capacitance is measured also in soil due to its importance in agriculture, for optimal plant growth [161]. Changes in the percentage of soil moisture during irrigation can be automatically controlled.

Many sensors have been developed based on mutual capacitance, because of several advantages over other common techniques. For instance, manufacturing and operating capacitive sensors are relatively simple compared to RF-based methods and the avoidance of potential health risks of radiation-based methods [145]. In [162], the electrodes were built of copper foils in cylindrical shape, with different sizes of plate diameters, to be used with pumice stones and soil samples. [163] have proposed a reliable unilateral capacitive soil moisture sensor, with a two-step calibration method that guarantees a high accuracy. A polymer capacitance sensor was also assessed for measuring soil gas relative humidity, with a precision of approximately $\pm 3\%$ [164]. A similar application can be found for wood pellets, with two different sensor topologies: one based on parallel plates; the other on planar structure. The electrodes are thin copper layers printed on FR-4 printed circuit board (PCB) material [146]. Capacitive sensors can also be controlled by neural networks (NN). For instance, in grain moisture measurements the temperature and the degree of compaction of grains have a strong non-linear relationship that can be solved with the NN models [165].

The change of capacitance in relation to moisture content has been observed also in textiles since many years [166]. Dielectric properties generally depend on the frequency of the applied electromagnetic field, but the amount of water is a dominant factor when compared to textiles, that behave mostly as insulators [167]. The permittivity of different textiles ($\epsilon_r \sim 3$) has been found to be dozens of times smaller than the permittivity of water ($\epsilon_r \sim 80$). Based on this principle, many sensors were developed for the measurements of the capacitance, related to the textile

moisture content. This technology offers the advantage of a volumetric measurement principle, compared to a sensor that measures only in the contact point. The use of capacitance sensors is a well-known concept in this field. A Burton-Pitt apparatus has been used by [166] to measure the capacitance of cotton fibers, wool yarn, cotton, rayon, linen, and silk fabrics. The use of capacitance requires the control of environmental parameters, like humidity and temperature, to know the previous history of textiles. [168] have proved that, if the distance of the electrodes is large in comparison with the fabric thickness, the increase of capacitance is proportional to the textile weight. The trend of the capacitance curve versus moisture content is constant, so the values can be adjusted based on the textile weight multiplying the result by the appropriate factor. In [169], a new device has been designed, with the measurement of the capacitance at low (8.6 kHz) and high (10 MHz) frequencies. The contribution of the absorbed water is the same, but the dry value differs considerably due to the different frequency. This led to the measurement of the textile capacitance, tested with wool, cotton and rayon. [170] have described a high-speed moisture meter to measure capacitance using a plane-parallel capacitor during production process. This method is coupled with the absorption of radioactive radiations, to eliminate the effect of changes in thickness. The use of these two technologies allows contactless measurement of moisture content for wool and staple fiber in layers of variable thickness. [171] have evaluated the dielectric properties of some woven fabrics at air temperature of 21°C and at relative humidity of 40%, 60% and 80%, with frequency ranging from 80 kHz to 5 MHz. The measurements were done using two different capacitance cells. More recently, the moisture content has been measured using a sensor connected to an integrated circuit that converts the capacitance to a voltage signal. The designed circuit has high sensitivity, rapid detection and high precision [172].

The main advantage of a capacitive sensor connected to an integrated circuit compared to a discrete one are low power consumption, reduced stray field, low-cost for volume products and more versatile application [138]. In addition, when self-capacitance is used, the possibility to use a single electrode gives more flexibility in the sensor design [173]. Another reason to use self-capacitance, is the availability of small, reliable and low-

cost electronic components usually dedicated to touch applications, that can be connected to a single or multi-plate sensor [150].

Capacitive proximity sensors are already employed in industrial applications for non-contact detection of conductive or non-conductive objects. [151] have presented a sensor manufactured by etching copper on a polyethylene terephthalate (PET) film. It has been connected to a capacitive touch IC sensor to measure the electrical capacitance, that have the possibility to be operated with a microcomputer. The developed sensor can capture the dynamic change in soil moisture at 10, 20 and 30 cm depth. [152] have developed a fringing field capacitive sensor for moisture content measurements in grain. The sensor accuracy is close to that of laboratory instruments and is appropriate for monitoring stored grain in bulk containers. Finally, [153] have discussed a sensor with electrodes on a PCB to measure water level. Experimental results have shown good repeatability and linear sensitivity.

4.3 Capacitance on lifter

The lifter is a metallic component connected to the drum of the tumble dryer which helps the garments to rotate and fall at the angle indicated by Figure 11. It is the place that is most in the vicinity to the garment and, for this reason, it is a good candidate for the placement of the sensor. As it is insulated from the drum by a polycarbonate base, the entire lifter can become the sensor for the moisture measurement. The drum is already grounded for the user electrical protection, and this is an advantage for the use of self-capacitance as the lines of electrical fields can close from the lifter to the tub. Moreover, it is painted with a varnish that guarantees electrical insulation with the garments to be dried. The situation is shown in Figure 67.

In order to calculate the capacity using the lifter, both with an empty drum and with a real load, a capacitive meter has been used. The model is Agilent U1733C and has been connected to the drum and to the lifter, as can be seen in Figure 68.

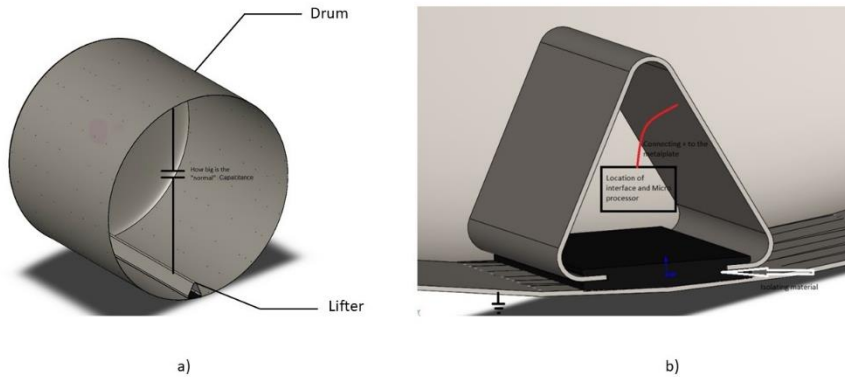


Figure 67. Lifter used as a capacitance sensor. In a) the positioning of the lifter in respect to the drum, which is grounded, in b) a focus on the lifter, which is hollow and have the space for the capacitance measurement circuit.



Figure 68. Capacitive meter Agilent U1733C connected to the lifter and to the drum.

Using the capacitive meter, the range and the accuracy needed for the capacitance measurements can be calculated. The range of measurement is defined between a small load, with a bone-dry moisture content, and a full load, with wet garments. The accuracy needed for the sensor to be developed is defined between bone-dry and condition-dry, which is the area where an improvement is needed compared to the actual sensors, with a small load. Considering the volume of the drum, the full load is defined as 1:22 of the entire drum volume, while the small load is 1:360. The load is composed by cotton towels of different dimensions. The

results, at a fixed frequency of 1 kHz, are shown for the range and the accuracy respectively in Figure 69 and in Figure 70.

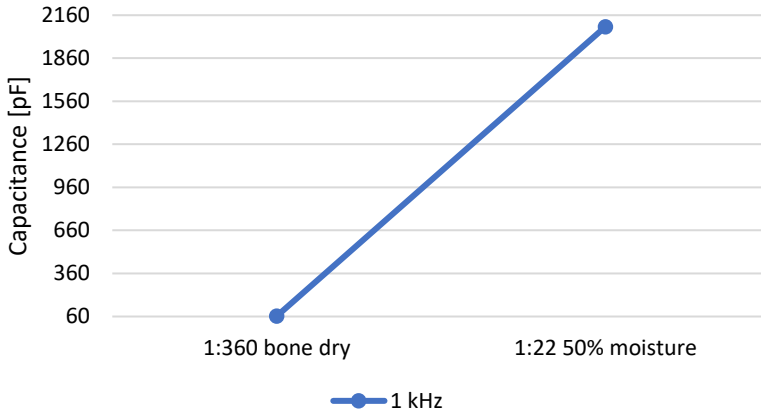


Figure 69. Range for capacitance measurement using the lifter as sensor.

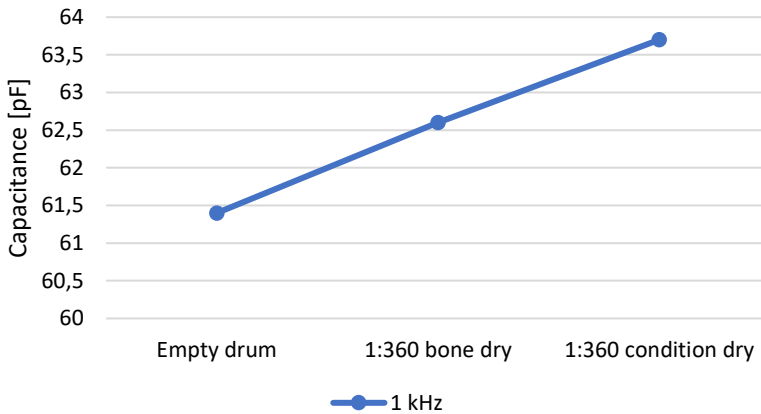


Figure 70. Accuracy for capacitance measurement using the lifter as sensor.

From both plots, it is possible to notice that the range is wide in comparison to the accuracy, which made very challenging the application of the capacitive measurement to the entire lifter as sensor. The range required is 2017.4 pF, while the accuracy between condition and bone dry is only 1.1 pF. This have driven the development of a new sensor, to be mounted on the lifter, that is smaller and standardizable. The difference of the lifter dimensions among the different tumble dryers' models brings

also the disadvantage to calibrate the measurement system for every model in Electrolux Professional's portfolio. On the contrary, the use of a sensor to be mounted in a lifter would simplify the development, focusing on only one design and a standardized dimension. For this reason, the focus has been moved to the development of a sensor to be connected to a self-capacitance circuit board.

4.4 Sensor development

The system developed in this study to estimate textile moisture content is composed by a sensory part, made up of a copper trace printed on a PCB, connected to an integrated circuit board through a cable. The communication to a PC, to collect and analyze data, is done using a wireless device, connected to the board. This allows the use of the sensor away from the PC, to position it flexibly at the measurement site. The development of the prototype for the moisture measurement has been prevented by the expensive and complicated circuits for the measurement of capacitance and it is possible to obtain a sensor much less expensive than currently commercialized ones. Thus, a trade-off between cost and accuracy is found, and the sensor presented can be a good solution where a low price is preferred.

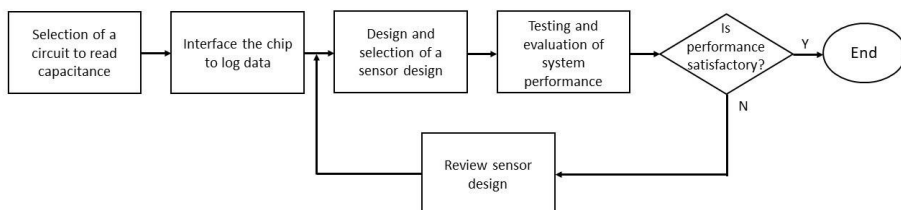


Figure 71. Design flow of the measurement system for moisture sensing.

The development flow for the system presented in this study is shown in Figure 71. Firstly, a measurement circuit is selected to read capacitance values. Then, the chip is interfaced with a communication system to send data to a PC for the subsequent analysis. Different sensor designs are developed and tested to evaluate their performance and select the best one. Finally, the entire system is tested with diverse textiles having

different moisture content, ranging from 5% to a maximum of 70% with respect to the dry mass.

4.4.1 Measuring circuit board

Different electronic circuits and software programs can be used to measure capacitance. Traditional methods are based either on the measurement of the capacitance charging time or on the resonating frequency in an RC circuit. These approaches are generally good but cannot be used directly when the change in capacitance is in the range of few pF. To measure a small capacitance, a high frequency clock is needed to obtain a good measurement, resulting in high noise. For capacitance to digital conversion, in this study a measurement system implemented in an Integrated Circuit, based on Sigma-Delta, has been selected [174]. This type of technology is currently used for proximity and touch sensing, due to the possibility of reducing the complexity, cost and power consumption. In addition, proximity sensing can give the advantage of measuring in depth.

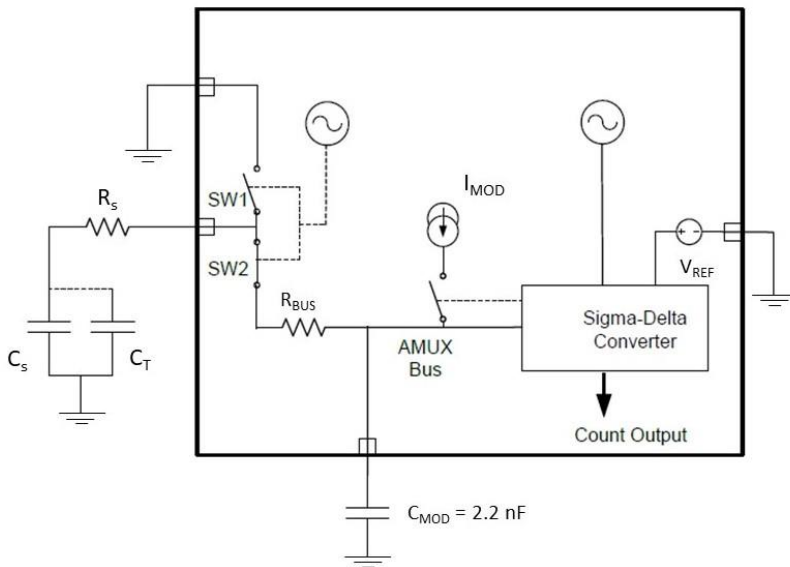


Figure 72. Sigma-Delta modulator.

In this thesis, a chip based on self-capacitance is selected. The model is CY8CKIT-145-40XX by Cypress Semiconductor shown in Figure 73 and the measure is taken between one board pin and the ground. A current is driven to the pin connected to the sensor and the voltage is measured, with a comparison to a reference value. The micro controller of this board converts in this way the sensor capacitance into a digital count, based on Sigma-Delta modulator as shown in Figure 72.

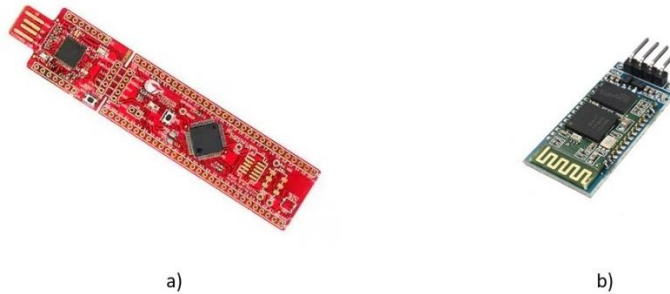


Figure 73. In a) the Cypress measurement circuit board, in b) the Bluetooth module to communicate with an external device far from the sensor.

When the capacitor voltage reaches the reference, a comparator triggers a bleed resistor discharging the capacitor. The comparator output becomes a bit-stream and the number of counts in each frame is analyzed to determine if the capacitive sensor was activated. The value of the count is the digital counterpart of the capacitance and is directly proportional to the current drawn out by the sensor capacitance [175].

Two switchers SW_1 and SW_2 , independently controlled by out-of-phase clocks of frequency F_{SW} , are used to convert the sensor capacitance C_S into an equivalent resistor R_{eq} . The equivalent resistor model is shown in Figure 74.

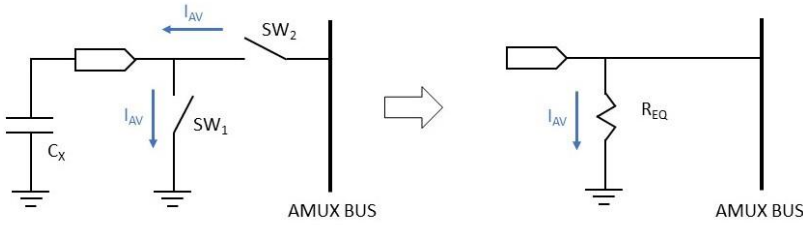


Figure 74. Equivalent resistor model.

Then, a Sigma-Delta modulator converts the current measured through the equivalent resistor into the digital count. When a wet textile is on the sensor, a capacitance C_T is in parallel with C_S and the total value C_X increase. The consequence is that the equivalent resistance decreases, with an increasing of the current through the resistor, which is balanced by the system that uses a modulation current I_{MOD} . The value of the equivalent resistance is:

$$R_{eq} = \frac{1}{C_X \cdot F_{SW}} \quad (24)$$

The Sigma-Delta converter maintains the voltage of the Analog Mux Bus (AMUX bus) at a constant voltage value V_{REF} . To reduce the noise, a R_{BUS} is inserted in the AMUX bus, that sends the signal to all the pins selected for the sensor. The average current taken by the sensor capacitor is:

$$I_{AV} = C_X \cdot F_{SW} \cdot V_{REF} \quad (25)$$

Finally, a comparator converts the voltage into a square wave and a counter counts the number of peaks in a pre-determined period. The digital count value, given N the scan resolution of the modulator in bits, is:

$$Count = (2^N - 1) \cdot \frac{V_{REF} \cdot F_{SW}}{I_{MOD}} \cdot C_X \quad (26)$$

The current driven to the sensor and the switchers clock are controlled by a micro controller on the board. Firstly, the switcher SW_2 is closed and the total capacitance C_X is connected to the bus, and then grounded, in alternating phases. The charge of C_X is shared with C_{MOD} until the bus settles to V_{START} , that is lower than V_{REF} . In the second phase, SW_2 is opened and SW_1 is closed. C_X discharges because it is connected to the ground and it is seen as an effective resistance to ground. After V_{START} is reached by the internal capacitance, the measurement starts. A counter clock is enabled and counts the charging time of the internal capacitance until V_{REF} . More counts are measured when the capacitance on the sensor is higher, because the equivalent resistance is smaller. The consequence is a lower voltage on the internal capacitor, with the current driven by the board that takes more time to charge the bus from V_{START} to V_{REF} . A low-pass filter removes high frequencies disturbances from the internal capacitor and discharge it when the voltage is higher than V_{REF} . This circuit lets to measure the capacitance at low pF values, that is in the range for the textile moisture measurement. The goal of the sensor design is to obtain a low parasitic capacitance, in order to have more range of measurement available.

A wireless module is than connected to the board to send the count number to a PC or to a control system for the analysis. This has the advantages of removing disturbances coming from other cables and giving more flexibility in the sensor positioning. The module selected is a low-cost HC-06 that communicate with the board using the UART (Universal Asynchronous Receiver Transmitter) protocol. The Bluetooth range is up to 10 meters and the baud rate is set at 9600 ms. A Python script have been developed to connect the module to a PC, to send the trigger for the data logging and to save the counts number into an Excel .csv file. It is possible to send also the configuration parameters and to read the internal variables.

4.4.2 Sensor design

The change in the electric field is mainly depending on the sensor design. In a typical sensor construction, a conductive surface is connected to the

capacitive measurement system using a conductive trace or a cable. Then, a non-conductive overlay is placed over the surface to avoid direct touch and interferences with the electric field pattern. In this study, a planar construction is proposed, where both the electrodes and the traces of the sensor are fabricated on the same plane of an insulating substrate, a printed circuit board. This choice has been taken to maintain the structure as simple as possible and to reduce the manufacturing cost.

The recent development of printed circuits on film is attracting attention because of both the lower cost and the possibility for easy, inexpensive and rapid prototyping, so that the cost and time of development can be reduced [176]. The PCB-based capacitor is formed between the copper pad or trace and the ground surrounding it. This topology works under the principle of the fringing capacitance. The electric field is allowed to straggle out in the area above the capacitor, with the lines that are more dominant near the edges between the two traces. When an object, that in this case is a wet textile, comes into the area above the sensor, the electric field is interfered causing a change into the capacitance value, proportional to the water content. The total capacitance increases beyond the base value, consisting of the parasitic capacitance of the cable and of the sensor itself. By continuously measuring the output coming out from the microprocessor, the system can determine the amount of water knowing the type of the textile sample. The presence of the ground is optional to adjust the sensor sensitivity, that is related to the gap with the sender pad. Moreover, the ground trace aids in shielding the sensor from interferences generated by surrounding electronics and helps to maintain a more constant base capacitance value.

A variety of sensors layouts can be examined using the PCB-based design. There are several shapes of the electrodes that can be used like discs, squares, rectangles, or simple round traces of diverse dimensions. It is also possible to use a hatched pattern for the electrode, that bring the benefit of reducing the base capacitance of the sensor but the disadvantage of reducing the area and the sensitivity. To the best of author's knowledge, it is missing in literature an analysis of the possible design for the sensors based on capacitance. For this reason, three different designs have been evaluated and tested:

- A round pad for the electrodes surrounded by a hatch ground

- A trace loop for the electrode surrounded by a hatch ground
- A trace loop for both the electrode and the ground.

The trace loops have the advantage of having higher sensing distance when compared to pads while the latter lets to be more flexible in controlling the signal coming from different electrodes. Shapes with right angles as squares were not considered as the electrical charge tends to concentrate near the corners. The PCB chosen material is FR4, and the traces were designed using Eagle. The layouts analyzed are shown in Figure 75.

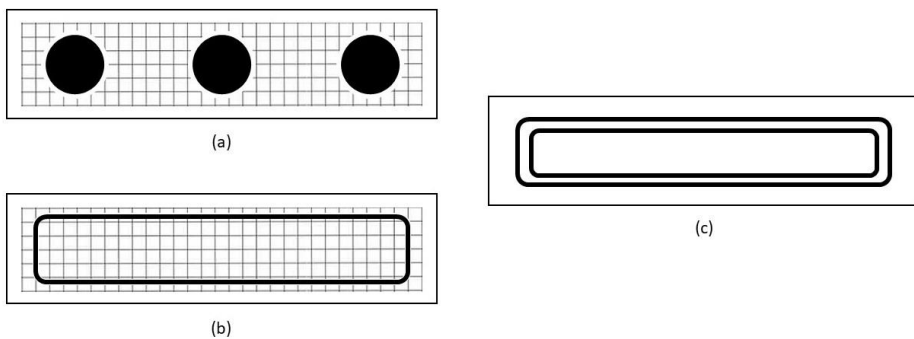


Figure 75. Sensor layouts for analysis. a) pad electrodes and hatch ground; b) trace electrode and hatch ground; c) trace electrode and ground.

The analysis is performed using an impedance analyzer Agilent Technologies model E4990A, with maximum frequency of 20 MHz. The signal coming from the instrument is connected to the electrode pads or traces while the ground is connected to the sensor ground. Along with the PCBs, two different cables and three overlays are tested. The cables are:

- Black cable with bare stranded copper wire, dimension 4x0.05 mm, length 30 cm
- Gray cable with bare stranded copper wire, dimension 3x0.14 mm, length 30 cm and 200 cm

while the overlays are air (no overlay), glass with 5 mm thickness and polycarbonate with 3 mm thickness. Over the glass, a layer of both dry and wet textiles is tested. These materials were chosen because of their low dielectric constant, as close as possible to air. The entire frequency sweep from 1 KHz to 20 MHz is saved, with 501 points for each trial. In order to

simplify the comparison, the values of the resistance [Ohm] and capacitance [F] are also saved at a fixed frequency of 750 KHz, the same used by the clock of the measurement circuit chosen in 4.4.1. An example of the entire frequency sweep of the PCB c) without overlay is shown in Figure 76. The resonance frequency is visible at around 2.5 MHz.

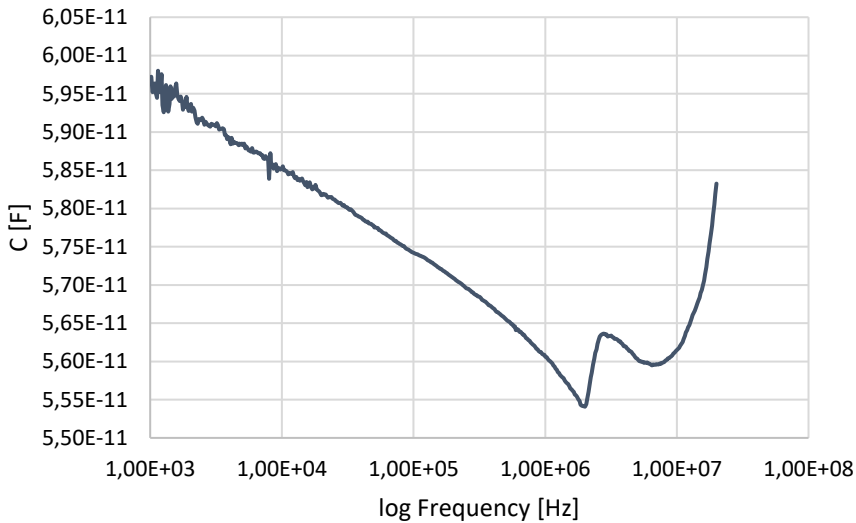


Figure 76. Frequency sweep of the sensor PCB c) without overlay.

In the first test the cables are compared using the sensor a) with no overlay, glass, and the dry and wet textiles over the glass, to check the resolution needed for the measurement. The graph is reported in Figure 77, with the limit of capacitance set to 200 pF, the maximum allowed by the measurement system selected for the sensor. It is interesting to notice the big difference in capacitance with the same cable at different length. The gray cable with 200 cm length has a capacitance approximately 6 times higher than the same cable with 30 cm length, that makes the first solution out of scale and unusable with the electronic circuit. In general, as expected, the shorter cable the lower capacitance measured. It is surprising to see that, with the same length, there is no difference measuring the dry and wet textiles with the black cable. On the contrary, the behavior with the gray cable is in line with the expectations, showing a small increase of capacitance moving out of air into glass with a layer of

wet textile. Different cables, of the same length, have a different influence on the measurement.

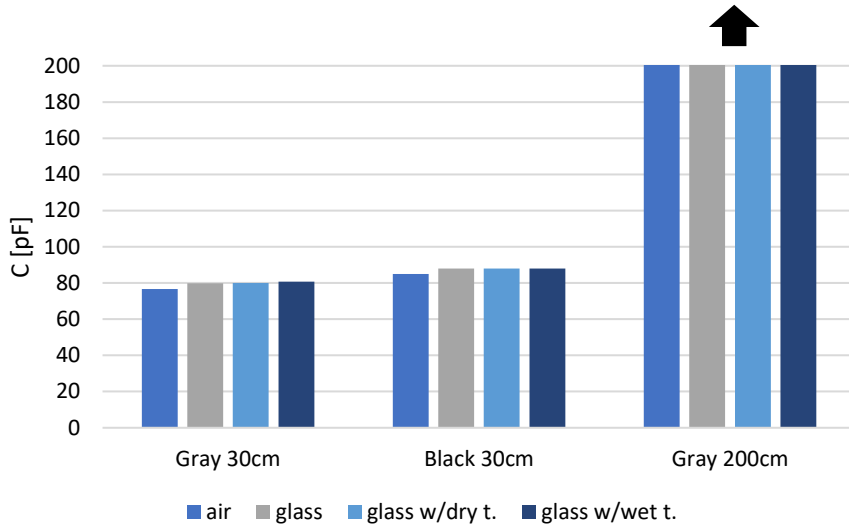


Figure 77. Cables comparison using sensor a) coupled with both no overlay and quartz glass overlay.

Another test is performed to compare the overlays, using the same sensor with the gray and black cables at 30 cm lengths. The results are reported in Figure 78. As before, the difference between the gray and black cables is significant. The addition of the overlay increased the capacitance as expected and the glass performed better than the polycarbonate, even if its thickness was 2 mm higher. The difference among the two is 6.9 pF.

Finally, the three layouts are tested using the best performing gray cable and glass. The results are showed in Figure 79. The sensor c) shows the lowest capacity compared to the others and the pads has a higher capacitance compared to the traces. Also, the hatched pattern for the ground has a negative influence, so the final design is the simplest with only two traces, that lets to have more range of measurement for the moisture content.

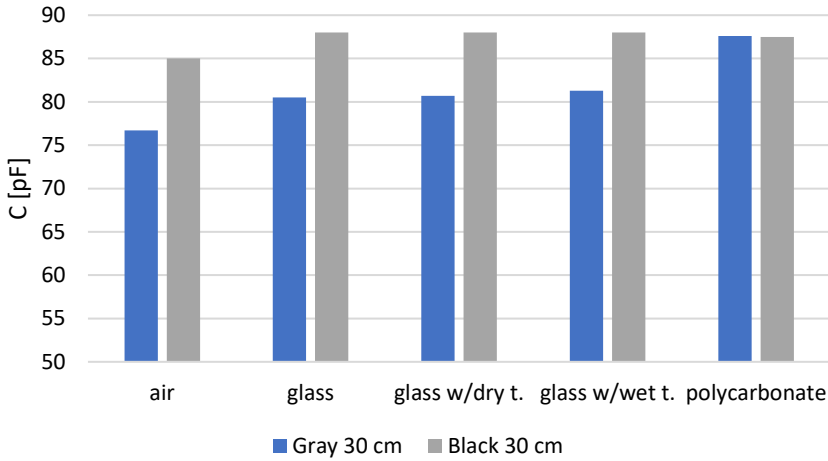


Figure 78. Overlay comparison using sensor a) connected with both gray and black cable.

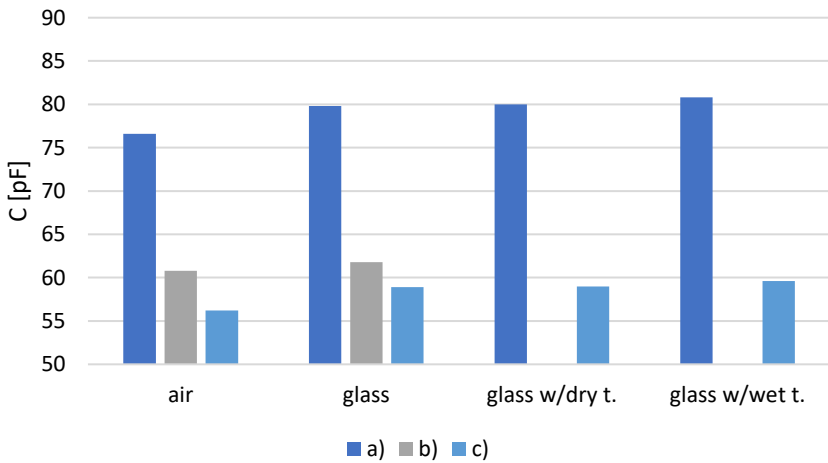


Figure 79. Sensor layouts comparison using gray cable with 30 cm length.

4.4.3 Shield

Capacitive sensing has a lot of advantages in proximity and gesture detection, material analysis and liquid-level sensing. This technology has several benefits, that includes very low power consumption, wide sensing range and high accuracy. Despite these advantages, there are some other points that requires attention. This measurement equipment is subjected to external disturbances and temperature and humidity changes that has

to be controlled. One way to mitigate these factors it to use the active shielding [177]. The shield driver in an active signal output that is driven at the same voltage potential of the sensor input, so that there is no potential difference between the shield and the sensor signals. In this way, any external interference will couple to the shield electrode with a minimal interaction with the sensor. Moreover, the use of the shield can direct and focus the electrical fields to a particular sensing area [178]. In Figure 80 the shield effect is displayed.

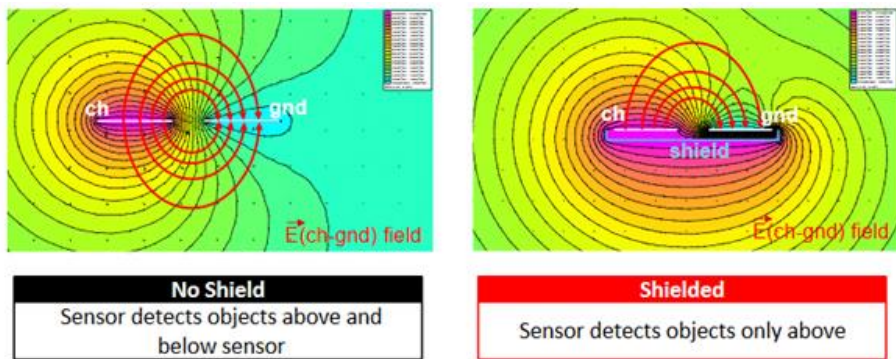


Figure 80. Electric field lines between the sensor (ch) and the ground (gnd) without (left) and with (right) the shield [178].

Ch is the sensor, which is excited with a voltage waveform, while gnd is the ground reference. The electric field lines (red lines) start from the higher voltage potential electrode (ch) and end at the lower voltage potential electrode (gnd) and, without the shield, they are symmetric above and below the sensor. In this configuration, the sensor detects objects both above and below the plane and depending on the application, detection above and below may not be acceptable and external disturbance coming from non-measurements areas can be detected. By using a shield sensor underneath the ch and gnd electrodes, only the top field lines can close throughout the ground [178].

The shield wrapped around the signal path between the sensor and the input pin to the measuring electronic board blocks environmental interferers from affecting the capacitance measurements. Environmental interferers include the human presence, radiated electromagnetic signals, and noise from other electronic devices. Since the shield has the same drive signal as the sensor, any interference is picked up along the shield

line, while the sensor line is unaffected. The electronic board selected for the capacitance measurement provide also a shield pin to be connected to the sensor electrode. It is important to use this protection not only in the sensor, but also in the cable that connects it to the measurement board, as it can become an amplifier for the disturbances coming from the environment. The shielding configurations for cables are illustrated in Figure 81.

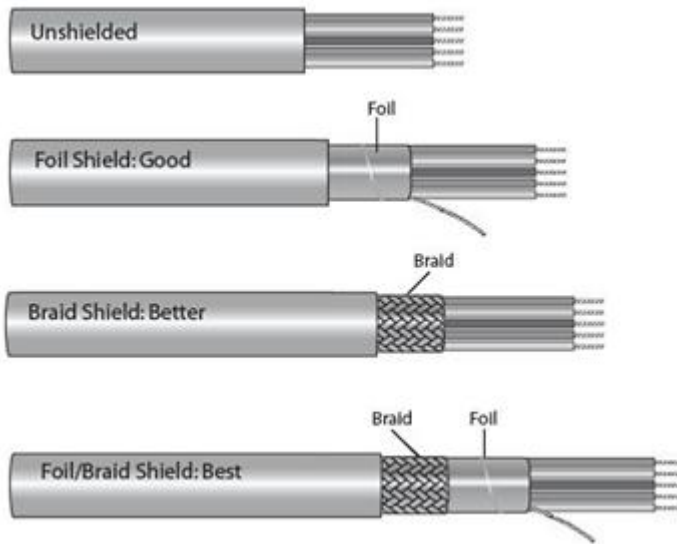


Figure 81. Shielding configurations for cables.

The driven-shield signal used by the electronic board and the shield electrode is a buffered version of the sensor-switching signal from the sigma delta converter, as shown in Figure 82. It has the same amplitude, frequency, and phase. Furthermore, the buffer provides current enough to drive the shield on the electrode of the sensor with a high parasitic capacitance, until 200 pF. It is also reducing this parasitic capacitance but, on the other hand, it is increasing the radiated emissions because it is a high frequency switching signal. To reduce it, the shield should be driven only when the sensor is scanned. Moreover, a passive low pass filter can also be implemented to filter the shield signal.

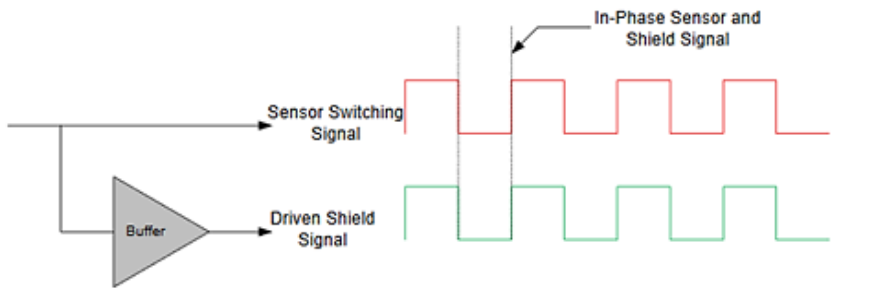


Figure 82. Shield signal compared to the switching signal driven by the Sigma-Delta modulator.

In order to apply the shield to the sensors designed in 4.4.2, the place where to apply the electrode is below the device plane, as the disturbances coming from the non-sensing area has to be avoided. For this reason, a hatched electrode has been added to the back of the sensor and connected to the shield electrode, as in Figure 83.



a)



b)

Figure 83. Sensor for moisture measurement (a) with the hatched shield on the back (b).

4.5 Experimental validation

The measurement of moisture content is a subject of interest for many textile industries and for domestic applications. Its measurement is not simple and usually refers to the wet and dry weight of the textiles for an accurate estimation. When drying a textile, the loss in weight is taken as the amount of water and is expressed as a percentage of the mass of the completely dried material [179]. In this study, the reference point for the percentage measurement is bone-dry, defined as the absence of any

moisture in the textile. The mass variation must be less than 1% or 20g compared to the previous measurement taken after a specific drying cycle. In comparison with condition dry, where the fabric is conditioned at defined environmental condition for a fixed time, the bone-dry is independent by the textile type. The moisture content is defined as:

$$MC = \frac{m_{wet} - m_{dry}}{m_{wet}} \cdot 100 [\%] \quad (27)$$

where m_{wet} represents the total mass of the wet textiles and m_{dry} the bone-dry mass.

4.5.1 Textile test

The performance of the sensor is experimentally evaluated using a test bench, shown in Figure 84 with an early version of the sensor prototype. The sensor is placed inside a bucket, supported by two adjustable screws to regulate its height. A thermocouple type K and a humidity sensor model FHAD 46-41L05 are placed inside the bucket and connected to an external logger to measure the environmental temperature and humidity during the tests. The logger used is an Ahlborn Almemo 2890-9. The sensor to be tested is connected to the electronics circuit through the gray cable of 30 cm length, the communication with a PC is done using a wireless module. Two rigid rulers are placed over the bucket to support the layer of textile when placed over the sensor, and to guarantee the repeatability of the positioning.

Four different textiles are used to test the sensor performances on the evaluation of moisture content:

- Cotton
- Wool
- Polyester
- Polycotton 50/50.

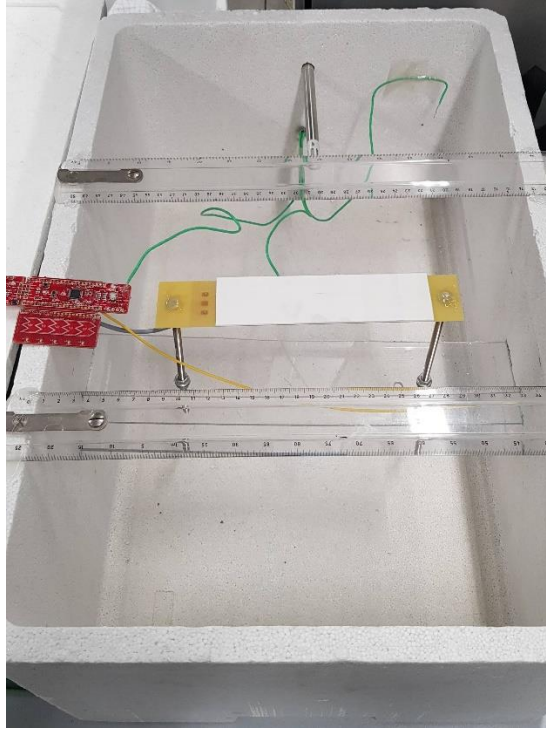


Figure 84. Test bench for testing different types of textiles in a steady condition.

Before the tests are executed, the bone-dry weights of each textile type are recorded using a scale Mettler PE3000. A sequence of drying cycles was executed using an oven until the weight did not vary more than 1%. The values are reported in Table 19.

	Cotton	Polycotton	Wool	Polyester
Condition dry weight	104.8 g	161.5 g	61.0 g	25.8 g
Bone-dry weight	101.5 g	158.7 g	56.6 g	25.6 g

Table 19. Reference weights of the textiles used for the experimental tests.

A testing method has been developed in order to guarantee the repeatability for each test run. First, the textile is bathed in a washer at the lowest temperature of 30 degrees, to not heat the fabric. A short extraction at low speed is performed at the end of the cycle, to spread the water evenly on the textile. Then, the textile is left to dry in a conditioned

chamber until the moisture points foreseen for the measurement are reached. These measurements points are taken with a delta of 10%, starting from 70% till 10%, and with a delta of 5% below 10% moisture content.

Before performing the moisture evaluation with the sensor, the weight of the textile is recorded. When the measurement starts, the textile is placed over the PCB and the rigid supports, leaving it for at least 250 samples recorded by the sensor. The procedure is repeated for five times in the same position to evaluate the repeatability of the measurement. At the end of the five tests series, the weight of the textile is recorded again and the average moisture content value during the measurement is calculated. Finally, the textile is left to dry in the conditioned chamber until the next measurement point. The procedure is summarized in Figure 85.

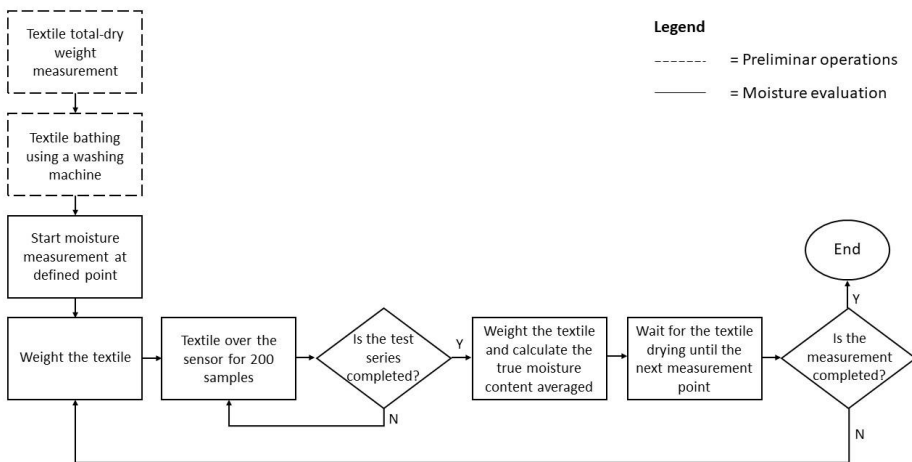


Figure 85. Measurement procedure for textiles moisture evaluation.

The results for the layer of cotton are shown in Figure 86. The count values have been normalized, to show the results for each textile type on the same scale. Each point represents the averaged value of the normalized count for each moisture content analyzed. The black bars represent the standard deviation, both for the count vertically and for the moisture content horizontally. The measurement is repeatable, and the standard deviation is low for every point. The behavior of the sensor with

cotton can be modeled using a regression analysis, with a polynomial equation of the second degree:

$$Count_{NORM} = -0.015 \cdot MC^2 + 2.645 \cdot MC - 14.314 \quad (28)$$

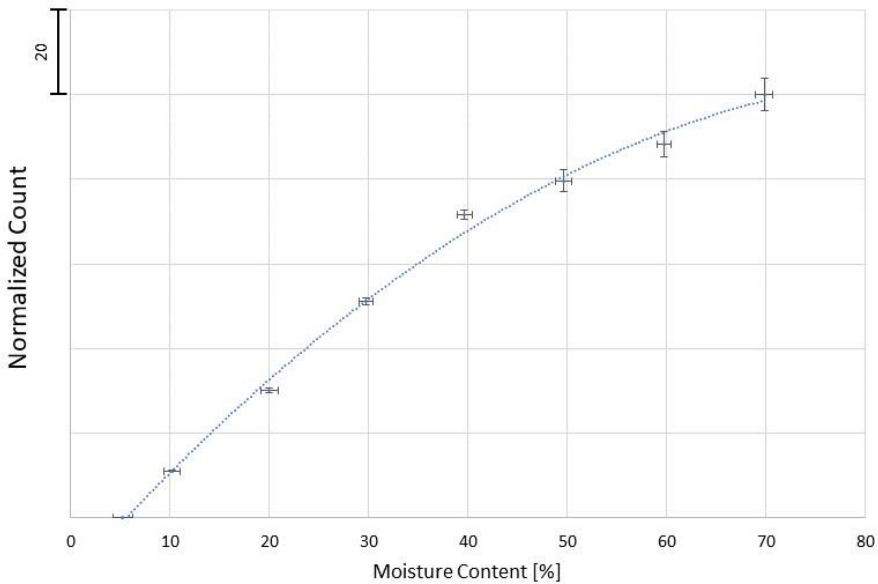


Figure 86. Test results normalized, using cotton.

The results of polycotton are reported in Figure 87. The maximum moisture percentage is 50% because this textile retains less water than the others. This is the highest value possible to guarantee a uniform distribution of the water after the bathing. Compared to cotton, the standard deviation is higher both in moisture content and in count values when the water content is higher than 20%. This is not an issue, since the measured counts does not overlap at different moisture contents. The regression analysis models well the behavior using a second-degree polynomial equation:

$$Count_{NORM} = -0.030 \cdot MC^2 + 3.851 \cdot MC - 19.495 \quad (29)$$

The value of R^2 is 0.991, which means that the model fits well the experimental data.

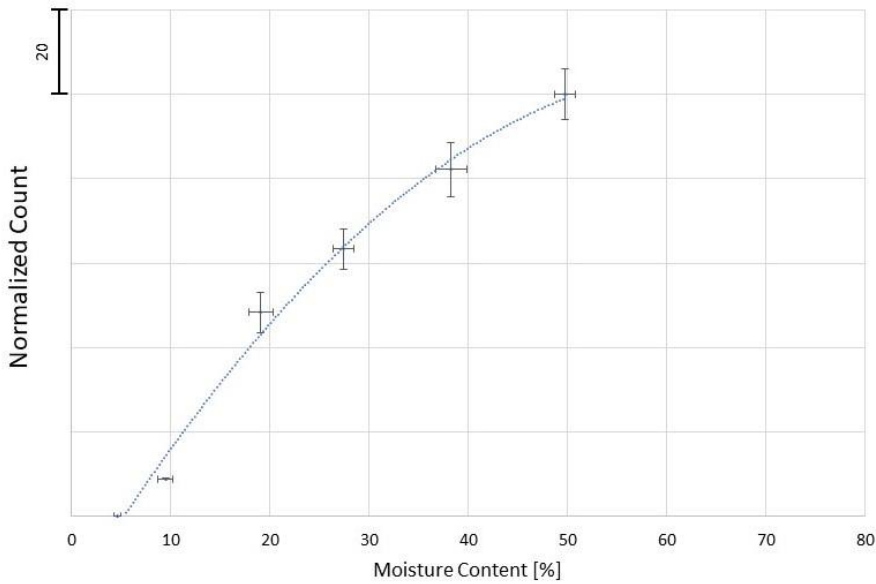


Figure 87. Test results normalized, using polycotton.

When wool is tested, a different trend is visible. The result is shown in Figure 88. The standard deviation is low for all the points, but some values seem to not follow a clear trend. For example, the difference between 50% and 60% is low. The regression analysis models the behavior using a simple linear polynomial equation, as the benefit of using higher grades is not convenient. The equation is:

$$Count_{NORM} = 1.681 \cdot MC - 15.138 \quad (30)$$

The value of R^2 is 0.945, which is still high.

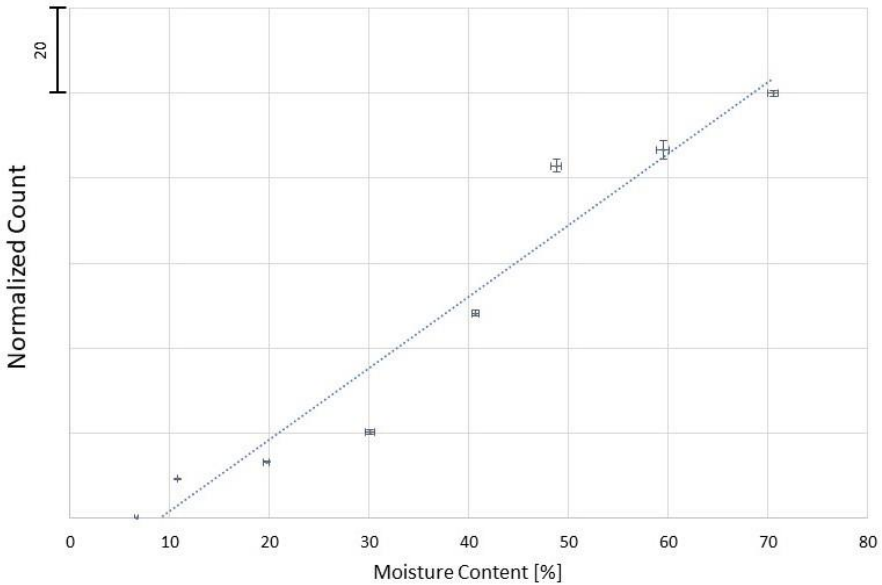


Figure 88. Test results normalized, using wool.

Finally, the result of the tests using polyester is shown in Figure 89. The standard deviation is low for all the points. Compared to the previous experiments, the absolute values of the digital counts are lower under the same moisture content. As for the wool, also in this case the linear model fits well the experimental values:

$$Count_{NORM} = 1.409 \cdot MC + 0.814 \quad (31)$$

The value of R^2 is 0.952. For all the models, this value is close to 1, which means that the equations replicate well the observed data.

All the results from the four textiles are shown in Figure 90 for a comparison. The normalized count values for each moisture content are reported, with the regression models that highlight the trends. Polycotton has the highest normalized count values when compared to the others, probably because of the textile type that influences the trend. The behavior is linear with wool and polyester, while is quadratic with cotton and polycotton. It is also interesting to compare the results with absolute values, as in Figure 91. In this plot, the drying trends of each textiles are different, and this lets to the identification of the textile type.

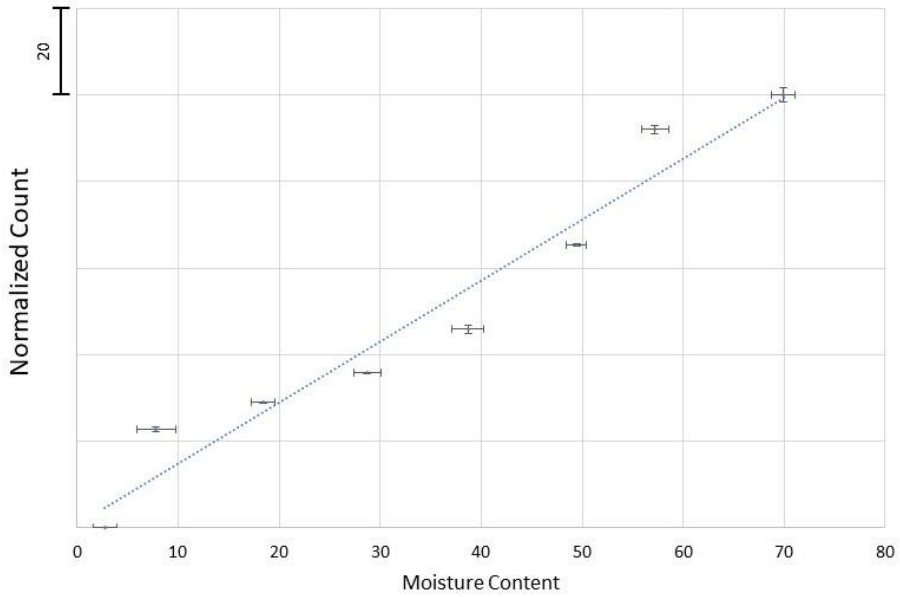


Figure 89. Test results normalized, using pure polyester.

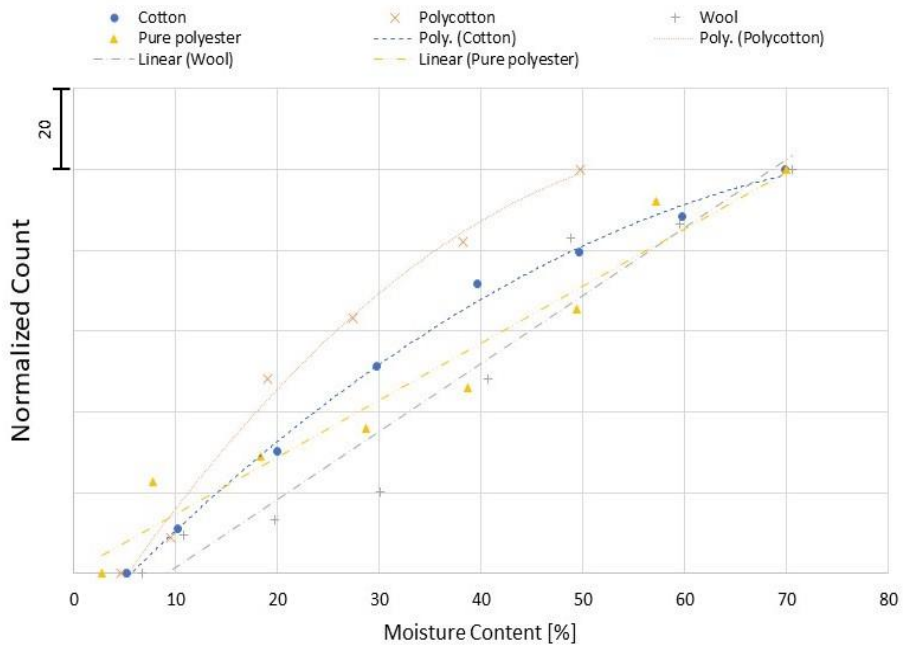


Figure 90. Experimental test results normalized, using four different textiles.

It is also interesting to compare the results with absolute values, illustrated in Figure 91. In this plot, the drying trends of each textiles are

different, and this lets a textile identification as well as the moisture content measurement. Knowing the textiles in the tumble dryer can bring interesting developments for the future, as a more accurate cycle's time estimation and a fabric-based drying process.

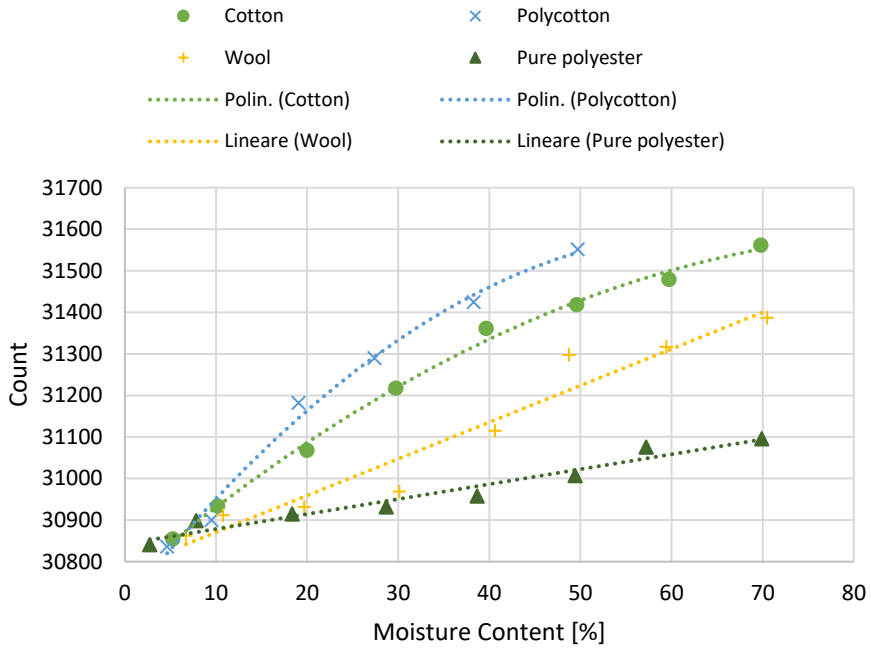


Figure 91. Experimental test results with absolute values, using four different textiles.

To check how far the models are from the experimental data, the residuals analysis is presented in Figure 92. The model for wool is the one that has the highest values and fits less than the others, as already noticed above. The others have low residuals at all the moisture contents, with particularly low numbers at 70%. This means that the models cover well all the moisture range analyzed, giving a good approximation of the experimental data.

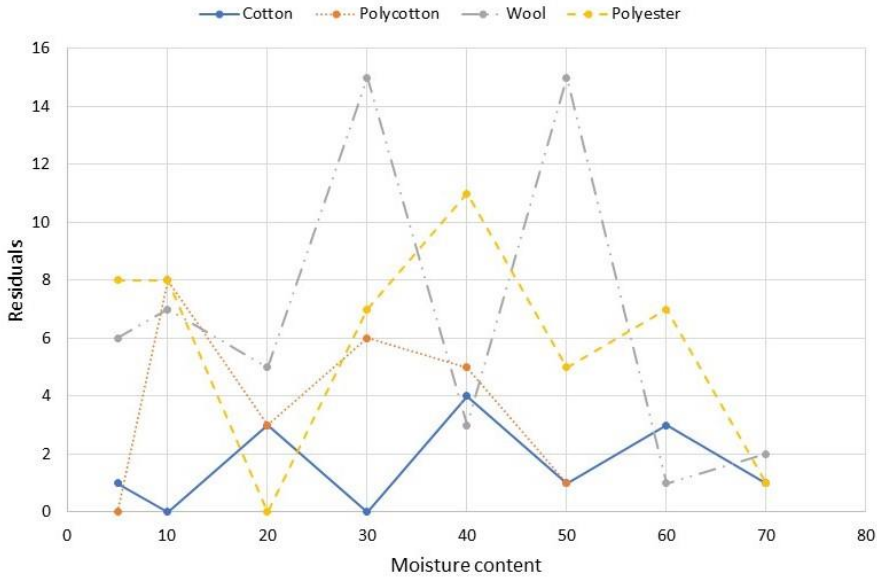


Figure 92. Residual analysis of the four regression models on normalized data.

4.5.2 Harsh conditions test

The analysis performed in the previous section highlighted a good response coming from the sensor, with all the textiles considered for the analysis. The tests have been conducted at environmental temperature and humidity, that is the most common usage for the sensor. It is also interesting to evaluate how the baseline of the measurements varies, when it moves away from a typical condition to a harsh one. For this reason, a test with a climatic chamber has been performed, with high temperatures and humidity.

The sensor is placed into the climatic chamber showed in Figure 93. The temperature and humidity are adjusted using two selectors, which change the intensity of the hot air and of the resistances below the water based on a proportional controller. To check the parameters, a humidity sensor model FHAD 46-41L05 and a thermocouple type K are placed inside the chamber. The quantity of water inside the climatic chamber is manually adjusted to increase or decrease the relative humidity.

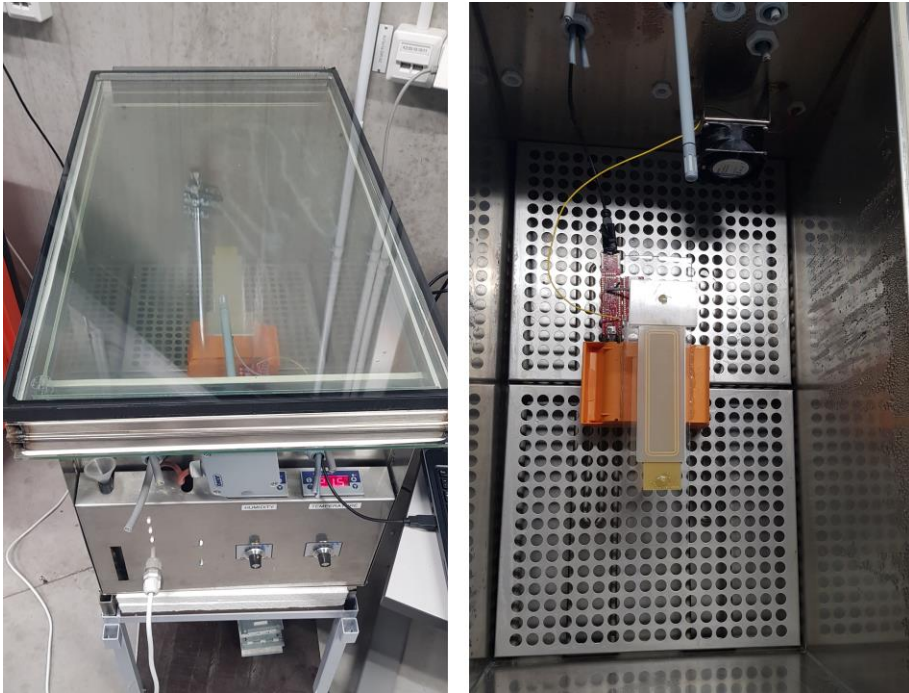


Figure 93. Climatic chamber used for harsh condition test.

The temperature is modified starting from 30°C till 80°C, that is the limit allowed by the electronic components, with a step of 10°C. Five repetitions are logged for each temperature point, with at least 1000 samples each. The temperature and humidity are recorded both at the beginning and at the end of each repetitions.

Two test sequences are performed:

- Increase of the air temperature without water in the chamber, with low values of the relative humidity
- Increase of the air temperature with water in the chamber, with high values of the relative humidity.

The result of the first test sequence is shown in Figure 94. The blue points are the count measurements at different temperatures, while the red line is the variation of the relative humidity. The trend of the count is linear with the temperature increasing. When the relative humidity is high, as shown in Figure 95, the trend is linear but with a slope 1.47 times higher than the previous result. This means that both the temperature and the relative humidity influence the sensor baseline.

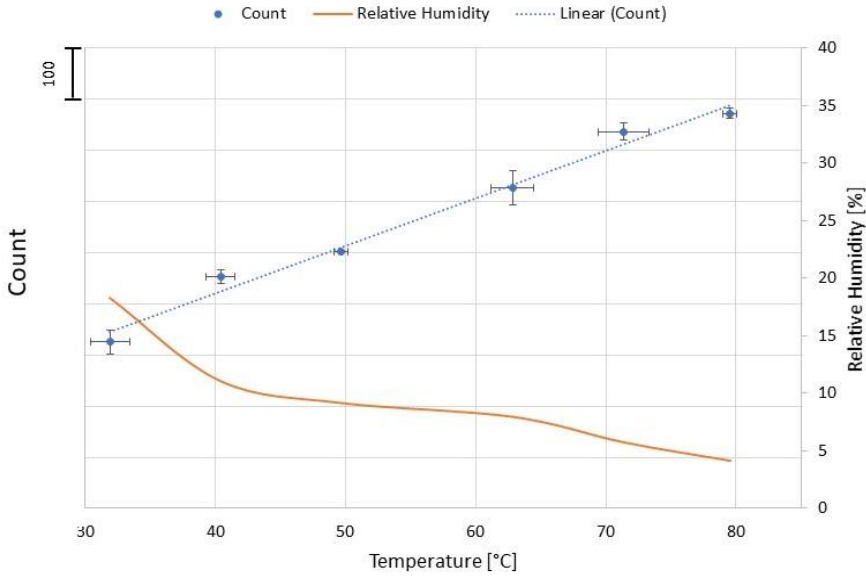


Figure 94. Temperature variation analysis at low relative humidity.

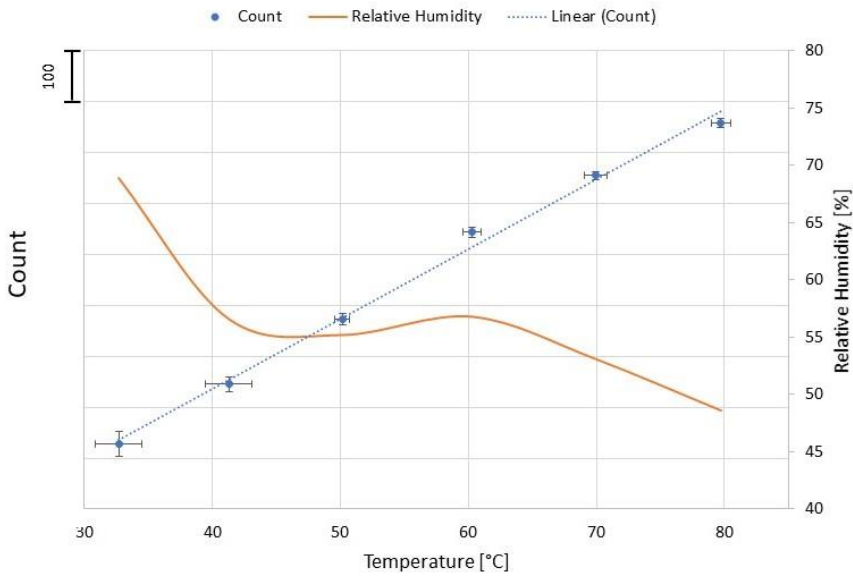


Figure 95. Temperature variation analysis at high relative humidity.

When the two test sequences are compared on the same graph, as in Figure 96, it is possible to notice that the humidity has a high effect only at low temperature, as the two trendlines tend to cross at 80°C. Moreover,

the temperature is the main responsible of the linear trend. In fact, when the temperature is between 50°C and 60°C, the relative humidity is approximately constant and, despite this, the counts increase, continuing to follow the linear trendline in both Figure 94 and Figure 95. Thanks to the linear approximation, it is easy to consider the temperature and humidity effects and to use the sensor also in harsh conditions, modifying accordingly the baseline of the measurement.

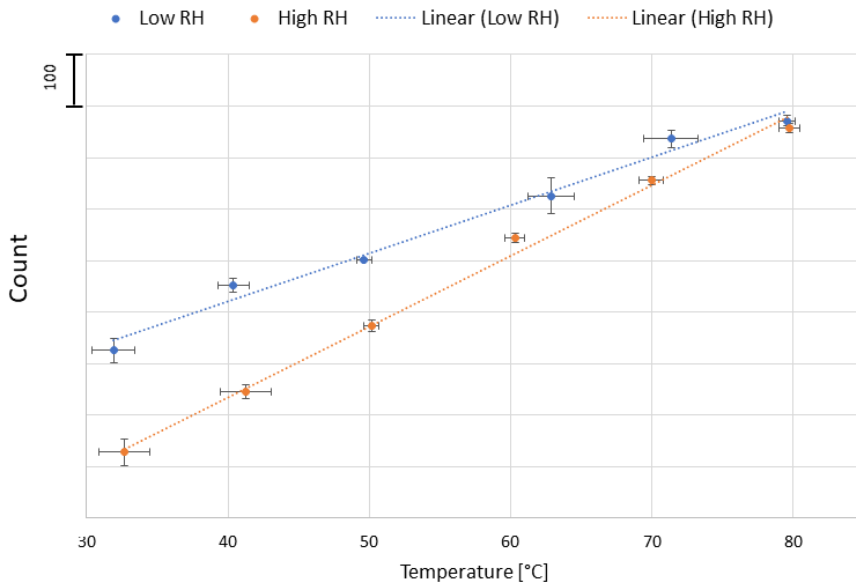


Figure 96. Comparison between the two temperature variations at different relative humidity.

Conclusions and Future Works

This thesis has presented three projects on different fields with the aim to improve the whole process of the laundry cleaning, starting from sorting until drying. The last advances in artificial intelligence and electronics have been applied for laundry products, with a deeper research on the weak points of these technologies for a further improvement and a successful application for the professional business. More specifically, the present thesis has been focused on the improvements of three stages of the cleaning process: sorting of garments, extraction phase at the end of the washing cycle, and moisture measurement during the drying run.

In Chapter 2, a fully automatic robot garment sorting system based on a novel vision recognition streamline has been proposed. The advantage of an autonomous sorting of laundry is to free resources from a time-consuming and risky task, as workers are in contact with contaminated garments. The system is able to automatically separate the items based on the washing program, moving the garments into a basket assigned to a cleaning cycle. The only sensor used is a RGB camera, which detect, classify, extract the color, and find the gripping point for a collaborative robot. The approach is based on a Convolutional Neural Network and its final-layers activations, which recognize clothing categories and locate them for the subsequent color extraction and gripping point detection. The vision streamline is made up of four modules: image acquisition system, image classification, features extraction, and robot sorting platform.

Image acquisition is performed using an industrial camera with a wide optic, able to capture a great amount of light also in indoor environments without the need of an additional illumination.

For the image classification, ResNet50 is fine-tuned using a new custom database, composed by more than 8000 images divided into 16 categories. The dataset has been created from scratch and customized for the required task, to recognize items shown in front of a camera but not worn by people. The final accuracy is 90.8% with a small loss of 0.379, which means that the network correctly predicts a wide number of images with a great confidence. In order to select the proper network for the classification, five CNN has been tested and the training parameters has been optimized for the learning process. The selected architectures are AlexNet, GoogLeNet, VGG16, ResNet50 and Inception v3. The comparison of the relative performance of these networks reveals that the best solution for a fast classification is AlexNet, for an accurate prediction is Inception v3 and a good balance is represented by ResNet50. VGG16 is not a convenient network to use because ResNet50 is faster in both training and prediction time, with even a higher accuracy and lower loss. Moreover, the latter network requires a lot of computational power for the training. The optimization streamline has demonstrated to work well, reaching an improvement of the final accuracy on all the networks. Moreover, an automatic optimization methodology has been proposed, which rely on the Bayesian algorithm. The main advantage is the possibility of investigating more parameters with a wide range of values, to explore more combinations for the optimization process. The disadvantage is that it requires more than 30 trainings to reach a good accuracy, and the fact that is a local optimization process.

Then, the CAM technique is used for the location of the garment inside the image and the subsequent gripping point and color extraction, using also some Image Processing techniques. This methodology has the advantage of avoiding any bounding-box design around the item inside the images, so that the database can be easily updated in the future. Colors were classified based on the Natural color space definition, starting from the CAM area with a background removal using the entropy filter. The final accuracy, calculated on at least 190 images randomly selected from the database for each category, is 91.5%. The gripping point were selected

among the CAM area centroid and the maximum activation value, based on the class performances. The point is inside the garments area 98.7% of the time, which is a surprising result, considering that only a CNN dedicated to image classification is used to extrapolate information.

Finally, the artificial intelligence system has been applied for a sorting application using a cobot, which has the advantage of sharing the same workspace with workers, without the needs of physical barriers. The final accuracy for classification, grip point selection and color are aligned with the ones obtained in each section evaluation, which confirms the validity of the new method. Moreover, the accuracy values for classification and color give the confirmation that the system works also with new garments never seen before by the CNN. An additional test with three garments in pile demonstrated the flexibility of the development system.

For the future developments, the last trial on garments in pile leaves the doors open for an implementation of the system to manage more items together. This can include a new depth sensor, to accurately calculate the gripping height for the robot gripper. On the classification side, the identification of textiles can help to assign with more precision the washing program, also to items that has not been classified in a category yet. It can be obtained using a NIR camera, as in the near-infrared field the textiles have different appearances and can be distinguished. A future research can focus on the definition of the best wavelength and on the development of a cheap camera that can be used for industrial needs. About the classification network, the database should be enlarged with more images in the less performing categories, and new classes should be added for special business sectors that are important in the professional applications, like mops and fire brigade suits.

In Chapter 2, the extraction phase of the washing cycle has been analyzed, as it is important to forecast the residual water content of the garments based on the drum speed and process time. The residual moisture content is the parameter commonly used to evaluate performances of washing machines and it affects also the design of the extraction cycle with an influence on the later drying phase. The goal is to reach a low final retention value, to reduce the energy consumption for

the drying cycle, and to forecast the water content during the extraction to stop it at the right point. The study defines a methodology and provides an experimental model to predict dewatering from the washed load during the spinning cycle of professional washing machines.

Because of the complexity involved in washing machines, the experimental approach was chosen to model dewatering phenomena during extraction cycle and the hypothesis of constant garments composition, constant temperature, filling coefficient and no detergent were considered.

An experimental set up was defined and built in accordance with standards, and repeatability analysis demonstrated the general validity of the procedure on the entire speed and washing capacity range. In fact, the maximum variation in terms of residual moisture content is lower than 0.3% at high speed, compatibly with the accuracy of the sensors.

Water retention time histories at different G-acceleration factor were used to define a polynomial surface model able to predict dewatering performances as a function of t and G , regardless of drum geometry. Best performances occur at high value of G and t , where the water retention value decreases up to 120% in respect with the initial point. G -acceleration factor showed the greatest impact on residual moisture content compared to time. The accuracy of the predictive surface was evaluated calculating the residuals, which were lower than $\pm 2\%$ for all the appliances, when the extraction cycle is longer than 2 minutes.

A scaling analysis showed no considerable influence of the drum shape and capacity on water retention performances over 100G. Therefore, for the shape factor range and the G-acceleration typically adopted on professional washing machines, a unique polynomial surface can be used to predict dewatering performances.

For future developments, further studies are necessary to improve the model in order to take into account the influence of the parameters maintained constant in this analysis: temperature, type of textile, fill factor and detergent.

In Chapter 4, a novel low-cost sensor to estimate textile moisture content, based on self-capacitance, has been proposed. The sensors that

are today used in the professional appliances are not accurate in the range between the condition and bone-dry, for this reason it is necessary an improvement, especially in this area. It is important to have a sensor accurate in the entire range of the drying cycle, as it let to reduce the energy consumption, by avoiding the over drying, and a device that can be easily mounted on every model of tumble dryer. The new developed sensor is based on capacitive sensing which features several advantages, such as low-cost production and contactless measurement. Moreover, self-capacitance gives the advantage to use planar sensor based on one electrode.

An electronic circuit board built for proximity and touch sensing has been selected, with the goal to adapt it for moisture measurements. A wireless device has been connected to communicate with a PC and to allow a flexible positioning of the sensing part. Three different layouts, whose electrodes were printed on a PCB plate, has been evaluated using an impedance analyzer. The sensors were connected using cables of different length and characteristics, and different overlays were tested. The results showed that traces led to lower capacitance when compared to pads and hatch grids. Glass performs better than polycarbonate and a suitable length for the cable is 30 cm to be within the measurement range.

The entire device was evaluated using four different textiles: cotton, polycotton, wool and polyester. The response was different based on the textiles type, with a quadratic trend for cotton and polycotton and a linear relationship for wool and polyester. The models approximate well all the behaviors and the sensor has demonstrated to be repeatable in the entire range of moisture measurement.

Finally, a test sequence was performed in a climatic chamber to verify the effect of temperature and humidity in the sensor measurement. With the increasing of the temperature, the response of the sensor is linear while the relative humidity has a lower effect on the measurement as the temperature grow. This allows the usage of the sensor also in harsh environments, considering the temperature and humidity effects with a baseline modification of the sensor readings.

For future developments, the sensor has to be tried inside a tumble dryer with a real load, both to check the shield is working against the

external disturbances, and to analyze the signal during a drying cycle. Then, based on the moisture curve, a new algorithm to predict the drying time more accurately should be developed, using also the information about the textile and the drying program selected.

Bibliography

- [1] "Electrolux Professional Website." <https://www.electroluxprofessional.com/corporate/our-company-in-brief/> (accessed Oct. 23, 2020).
- [2] "Electrolux Professional OnePro Internal Website." <https://electroluxprofessional.unily.com/sites/our-company/SitePageModern/9201/our-history> (accessed Oct. 23, 2020).
- [3] J. Fox, *Why It Took the Washing Machine So Long to Catch On*. 2017.
- [4] L. M. Maxwell, *Save Womens Lives: History of Washing Machines*. Oldewash, 2003.
- [5] A. J. Fisher, "Drive Mechanism for Washing Machines." 1910.
- [6] A. J. Fisher, "Yielding shaft-coupling," 1919.
- [7] D. J. Cole, F. E. Schroeder, and E. Browning, *Encyclopedia of Modern Everyday Inventions*. 2003.
- [8] C. L. Association, "Coin Laundry Association Industry Overview."
- [9] I. Rüdener *et al.*, "Preparatory Studies for Eco-design Requirements of Energy-using Products Lot 24: Professional Washing Machines, Dryers and Dishwashers," 2011. [Online]. Available: https://circabc.europa.eu/sd/a/5eedd0be-bc43-4506-81b2-2a825eb79e01/Lot24_Dish_T4_ENER_clean_final.pdf.
- [10] D. P. Bockmühl, "Laundry Hygiene - how to get more than clean," *J. Appl. Microbiol.*, 2017, doi: <https://doi.org/10.1111/jam.13402>.
- [11] Miele, "Sinner's Cycle." <https://www.miele.com/en/com/sinners-circle-5149.htm> (accessed Oct. 27, 2020).
- [12] D. L. Carter and D. O. Shah, "The role of surface tension on the residual water content of fabrics," *J. Surfactants Deterg.*, vol. 8, no. 1, pp. 91–94, 2005, doi: 10.1007/s11743-005-0335-5.
- [13] IEC Central Office, "International Standard IEC 60456," 2010.
- [14] G. T. Sampson, "Clothes-drier, U.S. Patent #476416A," 1892.
- [15] C. Froehlich, *Laundry Wisdom: Instructions for a Greener and Cleaner Life*. 2010.
- [16] O. A. Harold, Ed., *Heating & Gas Appliance Merchandising, Volumes 29-30*. New York: Moore Publishing Co., 1957.

- [17] S. Søgaard, *Laundry_Operations*, 2nd ed. Ronne, Denmark: Laundry Logics aps, 2015.
- [18] A. Hickman and B. Sargeant, "Maintain and Operate an Industrial Laundry," 2012.
- [19] L. Donati, E. Iotti, G. Mordonini, and A. Prati, "Fashion product classification through deep learning and computer vision," *Appl. Sci.*, vol. 9, no. 7, pp. 1–22, 2019, doi: 10.3390/app9071385.
- [20] R. Davies and L. Brazendale, "Intelligent Laundry Sorting System for Rest Homes," in *Volume 7: Dynamic Systems and Control; Mechatronics and Intelligent Machines, Parts A and B*, Jan. 2011, pp. 1181–1185, doi: 10.1115/IMECE2011-63212.
- [21] J. Wäldchen and P. Mäder, "Machine learning for image based species identification," *Methods Ecol. Evol.*, vol. 9, no. 11, pp. 2216–2225, Nov. 2018, doi: 10.1111/2041-210X.13075.
- [22] L. Xu, J. S. J. Ren, C. Liu, and J. Jia, "Deep convolutional neural network for image deconvolution," *Adv. Neural Inf. Process. Syst.*, vol. 2, no. January, pp. 1790–1798, 2014.
- [23] F. A. C. Azevedo *et al.*, "Equal numbers of neuronal and nonneuronal cells make the human brain an isometrically scaled-up primate brain," *J. Comp. Neurol.*, vol. 513, no. 5, pp. 532–541, Apr. 2009, doi: 10.1002/cne.21974.
- [24] D. Frejlichowski, P. Czapiewski, and R. Hofman, "Finding Similar Clothes Based on Semantic Description for the Purpose of Fashion Recommender System," in *Lecture Notes in Computer Science (including subseries Lecture Notes in Artificial Intelligence and Lecture Notes in Bioinformatics)*, vol. 9621, 2016, pp. 13–22.
- [25] H. Chen, A. Gallagher, and B. Girod, "Describing clothing by semantic attributes," *Lect. Notes Comput. Sci. (including Subser. Lect. Notes Artif. Intell. Lect. Notes Bioinformatics)*, vol. 7574 LNCS, no. PART 3, pp. 609–623, 2012, doi: 10.1007/978-3-642-33712-3_44.
- [26] B. Willimon, S. Birchfield, and I. Walker, "Classification of clothing using interactive perception," *Proc. - IEEE Int. Conf. Robot. Autom.*, pp. 1862–1868, 2011, doi: 10.1109/ICRA.2011.5980336.
- [27] L. Sun, S. Rogers, G. Aragon-Camarasa, and J. P. Siebert, "Recognising the clothing categories from free-configuration using Gaussian-Process-based interactive perception," *Proc. - IEEE Int. Conf. Robot. Autom.*, vol. 2016-June, pp. 2464–2470, 2016, doi: 10.1109/ICRA.2016.7487399.
- [28] M. Manfredi, C. Grana, S. Calderara, and R. Cucchiara, "A complete system for garment segmentation and color classification," *Mach. Vis. Appl.*, vol. 25, no. 4, pp. 955–969, 2014, doi: 10.1007/s00138-

- 013-0580-3.
- [29] Y. Kalantidis, L. Kennedy, and L. J. Li, "Getting the look: Clothing recognition and segmentation for automatic product suggestions in everyday photos," *ICMR 2013 - Proc. 3rd ACM Int. Conf. Multimed. Retr.*, pp. 105–112, 2013, doi: 10.1145/2461466.2461485.
- [30] X. Wang and T. Zhang, "Clothes search in consumer photos via color matching and attribute learning," *MM'11 - Proc. 2011 ACM Multimed. Conf. Co-Located Work.*, pp. 1353–1356, 2011, doi: 10.1145/2072298.2072013.
- [31] X. Wang, T. Zhang, D. R. Tretter, and Q. Lin, "Personal clothing retrieval on photo collections by color and attributes," *IEEE Trans. Multimed.*, vol. 15, no. 8, pp. 2035–2045, 2013, doi: 10.1109/TMM.2013.2279658.
- [32] M. Yang and K. Yu, "Real-time clothing recognition in surveillance videos," *Proc. - Int. Conf. Image Process. ICIP*, pp. 2937–2940, 2011, doi: 10.1109/ICIP.2011.6116276.
- [33] A. Ramisa, G. Alenyà, F. Moreno-Noguer, and C. Torras, "Learning RGB-D descriptors of garment parts for informed robot grasping," *Eng. Appl. Artif. Intell.*, vol. 35, pp. 246–258, 2014, doi: 10.1016/j.engappai.2014.06.025.
- [34] B. Willimon, I. Walker, and S. Birchfield, "A new approach to clothing classification using mid-level layers," *Proc. - IEEE Int. Conf. Robot. Autom.*, pp. 4271–4278, 2013, doi: 10.1109/ICRA.2013.6631181.
- [35] Z. Li, Y. Sun, F. Wang, and Q. Liu, "Convolutional Neural Networks for Clothes Categories," in *Communications in Computer and Information Science*, vol. 547, 2015, pp. 120–129.
- [36] C. Cao, Y. Du, and H. Ai, "Bag Detection and Retrieval in Street Shots," in *Lecture Notes in Computer Science (including subseries Lecture Notes in Artificial Intelligence and Lecture Notes in Bioinformatics)*, vol. 9516, 2016, pp. 780–792.
- [37] I. Mariolis, G. Peleka, A. Kargakos, and S. Malassiotis, "Pose and category recognition of highly deformable objects using deep learning," *Proc. 17th Int. Conf. Adv. Robot. ICAR 2015*, pp. 655–662, 2015, doi: 10.1109/ICAR.2015.7251526.
- [38] K. Saxena and T. Shibata, "Garment Recognition and Grasping Point Detection for Clothing Assistance Task using Deep Learning*," *Proc. 2019 IEEE/SICE Int. Symp. Syst. Integr. SII 2019*, pp. 632–637, 2019, doi: 10.1109/SII.2019.8700343.
- [39] P. Yildirim and D. Birant, "The Relative Performance of Deep Learning and Ensemble Learning for Textile Object Classification," in *2018 3rd International Conference on Computer Science and*

- Engineering (UBMK)*, Sep. 2018, pp. 22–26, doi: 10.1109/UBMK.2018.8566611.
- [40] C. Q. Huang, J. K. Chen, Y. Pan, H. J. Lai, J. Yin, and Q. H. Huang, “Clothing Landmark Detection Using Deep Networks with Prior of Key Point Associations,” *IEEE Trans. Cybern.*, vol. 49, no. 10, pp. 3744–3754, 2019, doi: 10.1109/TCYB.2018.2850745.
- [41] K. Hori, S. Okada, and K. Nitta, “Fashion image classification on mobile phones using layered deep convolutional neural networks,” *ACM Int. Conf. Proceeding Ser.*, pp. 359–361, 2016, doi: 10.1145/3012709.3016075.
- [42] Z. Liu, P. Luo, S. Qiu, X. Wang, and X. Tang, “DeepFashion: Powering Robust Clothes Recognition and Retrieval with Rich Annotations,” *Proc. IEEE Comput. Soc. Conf. Comput. Vis. Pattern Recognit.*, vol. 2016-Decem, no. 1, pp. 1096–1104, 2016, doi: 10.1109/CVPR.2016.124.
- [43] J. Cychnerski, A. Brzeski, A. Boguszewski, M. Marmołowski, and M. Trojanowicz, “Clothes detection and classification using convolutional neural networks,” *IEEE Int. Conf. Emerg. Technol. Fact. Autom. ETFA*, pp. 1–8, 2017, doi: 10.1109/ETFA.2017.8247638.
- [44] J. Yosinski, J. Clune, Y. Bengio, and H. Lipson, “How transferable are features in deep neural networks?,” *Adv. Neural Inf. Process. Syst.*, vol. 4, pp. 3320–3328, 2014.
- [45] R. R. Selvaraju, M. Cogswell, A. Das, R. Vedantam, D. Parikh, and D. Batra, “Grad-CAM: Visual Explanations from Deep Networks via Gradient-Based Localization,” *Proc. IEEE Int. Conf. Comput. Vis.*, vol. 2017-Octob, pp. 618–626, 2017, doi: 10.1109/ICCV.2017.74.
- [46] Stemmer Imaging GmbH, *The Imaging and Vision Handbook*. 2016.
- [47] Z. Lu and L. Cai, “Paraxial focal length measurement method with a simple apparatus,” *Opt. Express*, vol. 27, no. 3, p. 2044, Feb. 2019, doi: 10.1364/OE.27.002044.
- [48] Basler, “Basler acA2500-60uc Datasheet.” <https://www.baslerweb.com/en/products/cameras/area-scan-cameras/ace/aca2500-60uc/>.
- [49] P. Jiménez, “Visual grasp point localization, classification and state recognition in robotic manipulation of cloth: An overview,” *Rob. Auton. Syst.*, vol. 92, pp. 107–125, 2017, doi: 10.1016/j.robot.2017.03.009.
- [50] G. Cheng, Z. Li, X. Yao, L. Guo, and Z. Wei, “Remote Sensing Image Scene Classification Using Bag of Convolutional Features,” *IEEE Geosci. Remote Sens. Lett.*, vol. 14, no. 10, pp. 1735–1739, 2017, doi: 10.1109/LGRS.2017.2731997.

-
- [51] O. M. Parkhi, A. Vedaldi, C. V. Jawahar, and A. Zisserman, "The truth about cats and dogs," in *2011 International Conference on Computer Vision*, Nov. 2011, vol. 243, no. 3237, pp. 1427–1434, doi: 10.1109/ICCV.2011.6126398.
- [52] Y. Lecun, Y. Bengio, and G. Hinton, "Deep learning," *Nature*, vol. 521, no. 7553, pp. 436–444, 2015, doi: 10.1038/nature14539.
- [53] H. Xiao, K. Rasul, and R. Vollgraf, "Fashion-MNIST: a Novel Image Dataset for Benchmarking Machine Learning Algorithms," Aug. 2017, [Online]. Available: <http://arxiv.org/abs/1708.07747>.
- [54] E. Corona, G. Alenyà, A. Gabas, and C. Torras, "Active garment recognition and target grasping point detection using deep learning," *Pattern Recognit.*, vol. 74, pp. 629–641, 2018, doi: 10.1016/j.patcog.2017.09.042.
- [55] A. Y. Ivanov, G. I. Borzunov, and K. Kogos, "Recognition and identification of the clothes in the photo or video using neural networks," *Proc. 2018 IEEE Conf. Russ. Young Res. Electr. Electron. Eng. ElConRus 2018*, vol. 2018-Janua, pp. 1513–1516, 2018, doi: 10.1109/EIConRus.2018.8317385.
- [56] J. Lu, V. Behbood, P. Hao, H. Zuo, S. Xue, and G. Zhang, "Transfer learning using computational intelligence: A survey," *Knowledge-Based Syst.*, vol. 80, no. January, pp. 14–23, 2015, doi: 10.1016/j.knosys.2015.01.010.
- [57] M. D. d. S. Wanderley, L. de A. E. Bueno, C. Zanchettin, and A. L. I. Oliveira, "The impact of dataset complexity on transfer learning over convolutional neural networks," *Lect. Notes Comput. Sci. (including Subser. Lect. Notes Artif. Intell. Lect. Notes Bioinformatics)*, vol. 10614 LNCS, pp. 582–589, 2017, doi: 10.1007/978-3-319-68612-7_66.
- [58] J. Deng, W. Dong, R. Socher, L.-J. Li, Kai Li, and Li Fei-Fei, "ImageNet: A large-scale hierarchical image database," in *2009 IEEE Conference on Computer Vision and Pattern Recognition*, Jun. 2009, vol. 20, no. 11, pp. 248–255, doi: 10.1109/CVPR.2009.5206848.
- [59] W. Zhi, H. W. F. Yueng, Z. Chen, S. M. Zandavi, Z. Lu, and Y. Y. Chung, "Using Transfer Learning with Convolutional Neural Networks to Diagnose Breast Cancer from Histopathological Images," *Lect. Notes Comput. Sci. (including Subser. Lect. Notes Artif. Intell. Lect. Notes Bioinformatics)*, vol. 10637 LNCS, pp. 669–676, 2017, doi: 10.1007/978-3-319-70093-9_71.
- [60] R. K. Samala, H. P. Chan, L. M. Hadjiiski, M. A. Helvie, K. H. Cha, and C. D. Richter, "Multi-task transfer learning deep convolutional neural network: Application to computer-aided diagnosis of breast cancer on mammograms," *Phys. Med. Biol.*, vol. 62, no. 23, pp. 8894–8908, 2017, doi: 10.1088/1361-6560/aa93d4.

- [61] R. Mormont, P. Geurts, and R. Maree, "Comparison of deep transfer learning strategies for digital pathology," *IEEE Comput. Soc. Conf. Comput. Vis. Pattern Recognit. Work.*, vol. 2018-June, pp. 2343–2352, 2018, doi: 10.1109/CVPRW.2018.00303.
- [62] N. Zhuang, Y. Yan, S. Chen, H. Wang, and C. Shen, "Multi-label learning based deep transfer neural network for facial attribute classification," *Pattern Recognit.*, vol. 80, pp. 225–240, 2018, doi: 10.1016/j.patcog.2018.03.018.
- [63] J. T. Wang, G. L. Yan, H. Y. Wang, and J. Hua, "Pedestrian recognition in multi-camera networks based on deep transfer learning and feature visualization," *Neurocomputing*, vol. 316, pp. 166–177, 2018, doi: 10.1016/j.neucom.2018.07.063.
- [64] P. Wieschollek and H. P. A. Lensch, "Transfer Learning for Material Classification using Convolutional Networks," 2016, [Online]. Available: <http://arxiv.org/abs/1609.06188>.
- [65] V. Chauhan, K. D. Joshi, and B. Surgenor, "Image Classification Using Deep Neural Networks: Transfer Learning and the Handling of Unknown Images," vol. 1, no. December 2016, Springer International Publishing, 2019, pp. 274–285.
- [66] A. Kaya, A. S. Keceli, C. Catal, H. Y. Yalic, H. Temucin, and B. Tekinerdogan, "Analysis of transfer learning for deep neural network based plant classification models," *Comput. Electron. Agric.*, vol. 158, no. January, pp. 20–29, 2019, doi: 10.1016/j.compag.2019.01.041.
- [67] M. Mehdipour Ghazi, B. Yanikoglu, and E. Aptoula, "Plant identification using deep neural networks via optimization of transfer learning parameters," *Neurocomputing*, vol. 235, no. August 2016, pp. 228–235, 2017, doi: 10.1016/j.neucom.2017.01.018.
- [68] Y. Wu, X. Qin, Y. Pan, and C. Yuan, "Convolution neural network based transfer learning for classification of flowers," *2018 IEEE 3rd Int. Conf. Signal Image Process. ICSIP 2018*, pp. 562–566, 2019, doi: 10.1109/SIPROCESS.2018.8600536.
- [69] H. Esmaeili and T. Phoka, "Transfer Learning for Leaf Classification with Convolutional Neural Networks," *Proceeding 2018 15th Int. Jt. Conf. Comput. Sci. Softw. Eng. JCSSE 2018*, pp. 1–6, 2018, doi: 10.1109/JCSSE.2018.8457364.
- [70] A. A. Binguitcha-Fare and P. Sharma, "Crops and weeds classification using convolutional neural networks via optimization of transfer learning parameters," *Int. J. Eng. Adv. Technol.*, vol. 8, no. 5, pp. 2284–2294, 2019.
- [71] Z. Huang, Y. Cao, and T. Wang, "Transfer Learning with Efficient Convolutional Neural Networks for Fruit Recognition," in *2019*

- IEEE 3rd Information Technology, Networking, Electronic and Automation Control Conference (ITNEC)*, Mar. 2019, no. Itnec, pp. 358–362, doi: 10.1109/ITNEC.2019.8729435.
- [72] Q. Dong, S. Gong, and X. Zhu, “Multi-Task curriculum transfer deep learning of clothing attributes,” *Proc. - 2017 IEEE Winter Conf. Appl. Comput. Vision, WACV 2017*, pp. 520–529, 2017, doi: 10.1109/WACV.2017.64.
- [73] J. P. A. Madulid and P. E. Mayol, “Clothing classification using the convolutional neural network inception model,” *ACM Int. Conf. Proceeding Ser.*, vol. Part F1483, pp. 3–7, 2019, doi: 10.1145/3322645.3322646.
- [74] A. Alharthi, “Convolutional Neural Network based on Transfer Learning for Medical Forms Classification,” *Int. J. Adv. Trends Comput. Sci. Eng.*, vol. 8, no. 6, pp. 3405–3411, Dec. 2019, doi: 10.30534/ijatcse/2019/115862019.
- [75] A. Krizhevsky, I. Sutskever, and G. E. Hinton, “ImageNet classification with deep convolutional neural networks,” in *Advances in Neural Information Processing Systems*, 2012, vol. 2, pp. 1097–1105.
- [76] O. Russakovsky *et al.*, “ImageNet Large Scale Visual Recognition Challenge,” *Int. J. Comput. Vis.*, vol. 115, no. 3, pp. 211–252, 2015, doi: 10.1007/s11263-015-0816-y.
- [77] N. Srivastava, G. Hinton, A. Krizhevsky, I. Sutskever, and R. Salakhutdinov, “Dropout: A Simple Way to Prevent Neural Networks from Overfitting,” *ournal Mach. Learn. Res.*, vol. 15, pp. 1929–1958, 2014, [Online]. Available: <http://jmlr.org/papers/v15/srivastava14a.html>.
- [78] C. Szegedy *et al.*, “Going Deeper with Convolutions,” *J. Chem. Technol. Biotechnol.*, vol. 91, no. 8, pp. 2322–2330, 2015, doi: 10.1002/jctb.4820.
- [79] K. Simonyan and A. Zisserman, “Very deep convolutional networks for large-scale image recognition,” *3rd Int. Conf. Learn. Represent. ICLR 2015 - Conf. Track Proc.*, pp. 1–14, 2015.
- [80] K. He, X. Zhang, S. Ren, and J. Sun, “Deep residual learning for image recognition,” *Proc. IEEE Comput. Soc. Conf. Comput. Vis. Pattern Recognit.*, vol. 2016-Decem, pp. 770–778, 2016, doi: 10.1109/CVPR.2016.90.
- [81] S. Hochreiter, “The vanishing gradient problem during learning recurrent neural nets and problem solutions,” *Int. J. Uncertainty, Fuzziness Knowledge-Based Syst.*, vol. 6, no. 2, pp. 107–116, 1998, doi: 10.1142/S0218488598000094.
- [82] Q. Ji, J. Huang, W. He, and Y. Sun, “Optimized Deep Convolutional

- Neural Networks for Identification of Macular Diseases from Optical Coherence Tomography Images,” *Algorithms*, vol. 12, no. 3, p. 51, Feb. 2019, doi: 10.3390/a12030051.
- [83] C. Szegedy, V. Vanhoucke, S. Ioffe, J. Shlens, and Z. Wojna, “Rethinking the Inception Architecture for Computer Vision,” *Proc. IEEE Comput. Soc. Conf. Comput. Vis. Pattern Recognit.*, vol. 2016-Decem, pp. 2818–2826, 2016, doi: 10.1109/CVPR.2016.308.
- [84] G. Aragon-Camarasa, S. B. Oehler, Y. Liu, S. Li, P. Cockshott, and J. P. Siebert, “Glasgow’s Stereo Image Database of Garments,” Nov. 2013, [Online]. Available: <http://arxiv.org/abs/1311.7295>.
- [85] H. Vasa, “Google Images Download.” <https://github.com/hardikvasa/google-images-download>.
- [86] A. Graf, A. Koch-Kramer, and L. Lindqvist, “Instaloder.” <https://github.com/instaloder/instaloder>.
- [87] P. Y. Simard, D. Steinkraus, and J. C. Platt, “Best practices for convolutional neural networks applied to visual document analysis,” in *Seventh International Conference on Document Analysis and Recognition, 2003. Proceedings.*, vol. 1, pp. 958–963, doi: 10.1109/ICDAR.2003.1227801.
- [88] N. V. Chawla, K. W. Bowyer, L. O. Hall, and W. P. Kegelmeyer, “SMOTE: Synthetic Minority Over-sampling Technique,” Jun. 2011, doi: 10.1613/jair.953.
- [89] I. Goodfellow, Y. Bengio, and A. Courville, *Deep Learning*. The MIT Press, 2016.
- [90] K. P. Murphy, *Machine Learning: A Probabilistic Perspective*, 1st ed. The MIT Press, 2012.
- [91] D. P. Kingma and J. Ba, “Adam: A Method for Stochastic Optimization,” Dec. 2014, [Online]. Available: <http://arxiv.org/abs/1412.6980>.
- [92] R. Girshick, J. Donahue, T. Darrell, and J. Malik, “Rich feature hierarchies for accurate object detection and semantic segmentation,” Nov. 2013, [Online]. Available: <http://arxiv.org/abs/1311.2524>.
- [93] M. Pelikan, D. Goldberg, and E. Cantu-Paz, “BOA: The Bayesian optimization algorithm,” *Urbana, Univ. Illinois Urbana-Champaign*, 1999, [Online]. Available: [http://scholar.google.com/scholar?hl=en&btnG=Search&q=intitle:BOA+:+The+Bayesian+Optimization+Algorithm#3%5Cnhttp://scholar.google.com/scholar?hl=en&btnG=Search&q=intitle:BOA:+The+Bayesian+optimization+algorithm+\(IlligAL+Report+No.+99003\)#0](http://scholar.google.com/scholar?hl=en&btnG=Search&q=intitle:BOA+:+The+Bayesian+Optimization+Algorithm#3%5Cnhttp://scholar.google.com/scholar?hl=en&btnG=Search&q=intitle:BOA:+The+Bayesian+optimization+algorithm+(IlligAL+Report+No.+99003)#0).
- [94] J. Maitin-Shepard, M. Cusumano-Towner, J. Lei, and P. Abbeel,

- “Cloth grasp point detection based on multiple-view geometric cues with application to robotic towel folding,” in *2010 IEEE International Conference on Robotics and Automation*, May 2010, pp. 2308–2315, doi: 10.1109/ROBOT.2010.5509439.
- [95] T. Rasheed, A. A. Khan, and J. Iqbal, “Feature extraction of garments based on Gaussian mixture for autonomous robotic manipulation,” *2017 1st Int. Conf. Latest Trends Electr. Eng. Comput. Technol. INTELLECT 2017*, vol. 2018-Janua, pp. 1–6, 2018, doi: 10.1109/INTELLECT.2017.8277629.
- [96] A. Ramisa, G. Alenyà, F. Moreno-Noguer, and C. Torras, “Using depth and appearance features for informed robot grasping of highly wrinkled clothes,” *Proc. - IEEE Int. Conf. Robot. Autom.*, pp. 1703–1708, 2012, doi: 10.1109/ICRA.2012.6225045.
- [97] K. Yamazaki, “Grasping point selection on an item of crumpled clothing based on relational shape description,” in *2014 IEEE/RSJ International Conference on Intelligent Robots and Systems*, Sep. 2014, pp. 3123–3128, doi: 10.1109/IROS.2014.6942994.
- [98] Q. Gao, Z. Li, and J. Pan, “A Visual Detection and Location Method for Soft Fabrics,” *IOP Conf. Ser. Mater. Sci. Eng.*, vol. 612, no. 3, 2019, doi: 10.1088/1757-899X/612/3/032085.
- [99] T. Ziegler, J. Butepage, M. C. Welle, A. Varava, T. Novkovic, and D. Kragic, “Fashion landmark detection and category classification for robotics,” *2020 IEEE Int. Conf. Auton. Robot Syst. Compet. ICARSC 2020*, pp. 81–88, 2020, doi: 10.1109/ICARSC49921.2020.9096071.
- [100] V. Gupta *et al.*, “Using Transfer Learning and Class Activation Maps Supporting Detection and Localization of Femoral Fractures on Anteroposterior Radiographs,” *Proc. - Int. Symp. Biomed. Imaging*, vol. 2020-April, pp. 1526–1529, 2020, doi: 10.1109/ISBI45749.2020.9098436.
- [101] Y. Sun, S. Dai, J. Li, Y. Zhang, and X. Li, “Tooth-marked tongue recognition using gradient-weighted class activation maps,” *Futur. Internet*, vol. 11, no. 2, pp. 1–12, 2019, doi: 10.3390/fi11020045.
- [102] W. E. Fathy and A. S. Ghoneim, “A deep learning approach for breast cancer mass detection,” *Int. J. Adv. Comput. Sci. Appl.*, vol. 10, no. 1, pp. 175–182, 2019, doi: 10.14569/IJACSA.2019.0100123.
- [103] A. Esteva *et al.*, “Dermatologist-level classification of skin cancer with deep neural networks,” *Nature*, vol. 542, no. 7639, pp. 115–118, Feb. 2017, doi: 10.1038/nature21056.
- [104] A. Kwásniewska, J. Rumiński, and P. Rad, “Deep features class activation map for thermal face detection and tracking,” *Proc. - 2017 10th Int. Conf. Hum. Syst. Interact. HSI 2017*, pp. 41–47, 2017, doi: 10.1109/HSI.2017.8004993.

- [105] B. Zhou, A. Khosla, A. Lapedriza, A. Oliva, and A. Torralba, "Learning Deep Features for Discriminative Localization," *Proc. IEEE Comput. Soc. Conf. Comput. Vis. Pattern Recognit.*, vol. 2016-Decem, pp. 2921–2929, 2016, doi: 10.1109/CVPR.2016.319.
- [106] R. C. Gonzalez, R. E. Woods, and S. L. Eddins, *Digital Image Processing using Matlab*. Prentice Hall, 2003.
- [107] Samsung, "Washing cycle for Samsung washing machine." <https://www.samsung.com/uk/support/home-appliances/what-wash-cycle-should-i-use-for-my-samsung-washing-machine/>.
- [108] Miele, *Operating instructions for washing machines*, Nr. 10 834. .
- [109] T. P. Tho and N. T. Thinh, "Design and development of the sorting system based on robot," *ICCAS 2015 - 2015 15th Int. Conf. Control. Autom. Syst. Proc.*, pp. 1639–1644, 2015, doi: 10.1109/ICCAS.2015.7364620.
- [110] D. Q. Thuyet, Y. Kobayashi, and M. Matsuo, "A robot system equipped with deep convolutional neural network for autonomous grading and sorting of root-trimmed garlicks," *Comput. Electron. Agric.*, vol. 178, no. April, p. 105727, 2020, doi: 10.1016/j.compag.2020.105727.
- [111] International Standard, *Clothes washing machines for household use – Methods for measuring the performance*, 5.0. International Electrotechnical Commission, 2017.
- [112] J. Zheng, "The new direction of computational fluid dynamics and its application in industry The new direction of computational fluid dynamics and its application in industry," 2018.
- [113] S. Rief, E. Glatt, E. Laourine, D. Aibibu, C. Cherif, and A. Wiegmann, "Modeling and CFD-simulation of woven textiles to determine permeability and retention properties," *Autex Res. J.*, vol. 11, no. 3, pp. 78–83, 2011.
- [114] A. Szymkiewicz, "Mathematical Models of Flow in Porous Media," in *Modelling Water Flow in Unsaturated Porous Media Accounting for Nonlinear Permeability and Material Heterogeneity*, Springer, 2013, pp. 9–47.
- [115] T. N. Narasimhan and P. A. Witherspoon, "An integrated finite difference method for analyzing fluid flow in porous media," *Water Resour. Res.*, vol. 12, no. 1, pp. 57–64, 1976, doi: 10.1029/WR012i001p00057.
- [116] R. H. Brooks and A. T. Corey, "Hydraulic properties of porous media," in *Hydrology papers Colorado State University*, vol. 3, Colorado State University, Fort Collins, Colorado, 1964, pp. 1–25.
- [117] A. Cheng and M. Gulliksson, "Finite Difference Methods for Saturated-unsaturated Flow in Porous Media," Sundsvall, 2003.

- [118] C. Brasquet and P. Le Cloirec, "Pressure drop through textile fabrics - experimental data modelling using classical models and neural networks," *Chem. Eng. Sci.*, vol. 55, no. 15, pp. 2767–2778, 2000, doi: 10.1016/S0009-2509(99)00549-7.
- [119] L. Loeb, "Water Retention by Cotton Fabric under Compressional Loading," *Text. Res. J.*, vol. 35, no. 7, pp. 621–625, 1965, doi: 10.1177/004051756503500706.
- [120] A. Salehi Rad, S. M. Hosseini Varkiyani, and M. Haghghat Kish, "Water retention in hollow fibres nonwoven mat," *J. Text. Inst.*, vol. 104, no. 9, pp. 994–1002, 2013, doi: 10.1080/00405000.2013.770957.
- [121] C. E. Mongan, "Validity of Darcy's Law Under Transient Conditions," Washington, 1985. doi: 10.3133/pp1331.
- [122] E. Ghane, N. R. Fausey, and L. C. Brown, "Non-Darcy flow of water through woodchip media," *J. Hydrol.*, vol. 519, no. PD, pp. 3400–3409, 2014, doi: 10.1016/j.jhydrol.2014.09.065.
- [123] C. T. S. Beckett and C. E. Augarde, "Prediction of soil water retention properties using pore-size distribution and porosity," *Can. Geotech. J.*, vol. 50, no. 4, pp. 435–450, 2013, doi: 10.1139/cgj-2012-0320.
- [124] M. Castellini, S. Di Prima, and M. Iovino, "An assessment of the BEST procedure to estimate the soil water retention curve: A comparison with the evaporation method," *Geoderma*, vol. 320, no. January, pp. 82–94, 2018, doi: 10.1016/j.geoderma.2018.01.014.
- [125] S. Maggi, "Estimating water retention characteristic parameters using differential evolution," *Comput. Geotech.*, vol. 86, pp. 163–172, 2017, doi: 10.1016/j.compgeo.2016.12.025.
- [126] E. Ebrahimi, H. Bayat, M. R. Neyshaburi, and H. Zare Abyaneh, "Prediction capability of different soil water retention curve models using artificial neural networks," *Arch. Agron. Soil Sci.*, vol. 60, no. 6, pp. 859–879, 2014, doi: 10.1080/03650340.2013.837219.
- [127] R. Moosavizadeh-Mojarrad and A. R. Sepaskhah, "Predicting soil water retention curve by artificial neural networks," *Arch. Agron. Soil Sci.*, vol. 57, no. 1, pp. 3–13, 2011, doi: 10.1080/03650340903222302.
- [128] A. Reatto, E. M. da Silva, A. Bruand, E. S. Martins, and J. E. F. W. Lima, "Validity of the Centrifuge Method for Determining the Water Retention Properties of Tropical Soils," *Soil Sci. Soc. Am. J.*, vol. 72, no. 6, p. 1547, 2008, doi: 10.2136/sssaj2007.0355N.
- [129] F. Saboya, S. Tibana, C. R. Marciano, A. B. Ribeiro, W. N. Sterck, and E. D. Avanzi, "Determination of soil-water retention curve for a young residual soil using a small centrifuge," *18th Int. Conf. Soil*

- Mech. Geotech. Eng.*, no. 1937, pp. 1175–1178, 2013.
- [130] M. C. Caputo and J. R. Nimmo, “Quasi-steady centrifuge method for unsaturated hydraulic properties,” *Water Resour. Res.*, vol. 41, no. 11, pp. 1–5, 2005, doi: 10.1029/2005WR003957.
- [131] Q. Cheng, J. Wang, J. McNeel, and P. Jacobson, “Water Retention Value Measurements of Cellulosic,” *BioResources*, vol. 5, pp. 1945–1954, 2010.
- [132] S. Petrulyte and R. Baltakyte, “Investigation into the wetting phenomenon of terry fabrics,” *Fibres Text. East. Eur.*, vol. 16, no. 4, pp. 62–66, 2008.
- [133] S. Petrulyte and R. Baltakyte, “Static water absorption in fabrics of different pile height,” *Fibres Text. East. Eur.*, vol. 74, no. 3, pp. 60–65, 2009.
- [134] S. Trabelsi, A. W. Kraszewski, and S. O. Nelson, “New calibration technique for microwave moisture sensors,” *IEEE Trans. Instrum. Meas.*, vol. 50, no. 4, pp. 877–881, 2001, doi: 10.1109/19.948292.
- [135] P. Li, B. Wang, and J. Jing, “The application of microwave detecting textile moisture content,” *2010 Int. Conf. Intell. Comput. Technol. Autom. ICICTA 2010*, vol. 3, no. 3, pp. 706–709, 2010, doi: 10.1109/ICICTA.2010.249.
- [136] E. Terzic, J. Terzic, R. Nagarajah, and M. Alamgir, “A neural network approach to fluid quantity measurement in dynamic environments,” *A Neural Netw. Approach to Fluid Quant. Meas. Dyn. Environ.*, vol. 9781447140, pp. 1–138, 2012, doi: 10.1007/978-1-4471-4060-3.
- [137] J. C. Gamio, “A comparative analysis of single- and multiple-electrode excitation methods in electrical capacitance tomography,” *Meas. Sci. Technol.*, vol. 13, no. 12, pp. 1799–1809, Dec. 2002, doi: 10.1088/0957-0233/13/12/301.
- [138] A. Fuchs, H. Zangl, M. J. Moser, and T. Bretterkieber, “Capacitive sensing in process instrumentation,” *Metrol. Meas. Syst.*, vol. XVI, no. 4, pp. 557–568, 2009.
- [139] C.-T. Chiang and Y.-C. Huang, “A Semicylindrical Capacitive Sensor With Interface Circuit Used for Flow Rate Measurement,” *IEEE Sens. J.*, vol. 6, no. 6, pp. 1564–1570, Dec. 2006, doi: 10.1109/JSEN.2006.883847.
- [140] W. H. Ko and Qiang Wang, “Touch mode capacitive pressure sensors for industrial applications,” in *Proceedings IEEE The Tenth Annual International Workshop on Micro Electro Mechanical Systems. An Investigation of Micro Structures, Sensors, Actuators, Machines and Robots*, pp. 284–289, doi: 10.1109/MEMSYS.1997.581828.

-
- [141] N. Anandan and B. George, "A Wide-Range Capacitive Sensor for Linear and Angular Displacement Measurement," *IEEE Trans. Ind. Electron.*, vol. 64, no. 7, pp. 5728–5737, Jul. 2017, doi: 10.1109/TIE.2017.2677308.
- [142] Junseok Chae, H. Kulah, and K. Najafi, "A monolithic three-axis micro-g micromachined silicon capacitive accelerometer," *J. Microelectromechanical Syst.*, vol. 14, no. 2, pp. 235–242, Apr. 2005, doi: 10.1109/JMEMS.2004.839347.
- [143] H.-K. Lee, S.-I. Chang, and E. Yoon, "Dual-Mode Capacitive Proximity Sensor for Robot Application: Implementation of Tactile and Proximity Sensing Capability on a Single Polymer Platform Using Shared Electrodes," *IEEE Sens. J.*, vol. 9, no. 12, pp. 1748–1755, Dec. 2009, doi: 10.1109/JSEN.2009.2030660.
- [144] K. Bal and V. K. Kothari, "Measurement of dielectric properties of textile materials and their applications," *Indian J. Fibre Text. Res.*, vol. 34, no. 2, pp. 191–199, 2009.
- [145] G. Mander and M. Arora, "Design of capacitive sensor for monitoring moisture content of soil and analysis of analog voltage with variability in moisture," *Recent Adv. Eng. Comput. Sci. RAECS 2014*, pp. 6–8, 2014, doi: 10.1109/RAECS.2014.6799646.
- [146] A. Fuchs, M. J. Moser, H. Zangl, and T. Bretterkieber, "Using Capacitive Sensing To Determine the Moisture Content of Wood Pellets – Investigations and Application," *Int. J. Smart Sens. Intell. Syst.*, vol. 2, no. 2, pp. 293–308, 2009, doi: 10.21307/ijssis-2017-352.
- [147] S. Wu, B. Zhang, Y. Tian, S. Zhou, and H. Ma, "A grain moisture model based on capacitive sensor," *J. Phys. Conf. Ser.*, vol. 1074, no. 1, p. 012120, Sep. 2018, doi: 10.1088/1742-6596/1074/1/012120.
- [148] S. Zuk, A. Pietrikova, and I. Vehec, "Capacitive touch sensor," *Microelectron. Int.*, vol. 35, no. 3, pp. 153–157, Jul. 2018, doi: 10.1108/MI-12-2017-0071.
- [149] M. K. Ramasubramanian and K. Tiruthani, "A capacitive displacement sensing technique for early detection of unbalanced loads in a washing machine," *Sensors*, vol. 9, no. 12, pp. 9559–9571, 2009, doi: 10.3390/s91209559.
- [150] S. Tsuji and T. Kohama, "Tactile and proximity sensor using self-capacitance measurement on curved surface," *Proc. IEEE Int. Conf. Ind. Technol.*, no. c, pp. 934–937, 2017, doi: 10.1109/ICIT.2017.7915485.
- [151] Y. Kojima *et al.*, "Low-cost soil moisture profile probe using thin-film capacitors and a capacitive touch sensor," *Sensors (Switzerland)*, vol. 16, no. 8, pp. 1–14, 2016, doi: 10.3390/s16081292.

- [152] M. E. Casada and P. R. Armstrong, "Wheat moisture measurement with a fringing field capacitive sensor," *Trans. ASABE*, vol. 52, no. 5, pp. 1785–1791, 2009, doi: 10.13031/2013.25197.
- [153] K. Chetpattananondh, T. Tapoanoi, P. Phukpattaranont, and N. Jindapetch, "A self-calibration water level measurement using an interdigital capacitive sensor," *Sensors Actuators, A Phys.*, vol. 209, pp. 175–182, 2014, doi: 10.1016/j.sna.2014.01.040.
- [154] P. Li, L. Sun, and J. Jing, "Methods research and analysis of non-contact measurement to the moisture content of textile material," *Adv. Mater. Res.*, vol. 562–564, pp. 1205–1208, 2012, doi: 10.4028/www.scientific.net/AMR.562-564.1205.
- [155] B. Côté, C. Forget, N. Thérien, and A. D. Broadbent, "Measuring the Water Content of a Textile Fabric Using a Radio Frequency Sensor," *Text. Res. J.*, vol. 61, no. 12, pp. 724–728, 1991, doi: 10.1177/004051759106101205.
- [156] E. Cleve, E. Bach, and E. Schollmeyer, "Using chemometric methods and NIR spectrophotometry in the textile industry," *Anal. Chim. Acta*, vol. 420, no. 2, pp. 163–167, 2000, doi: 10.1016/S0003-2670(00)00888-6.
- [157] R. Bhunjun and R. W. Vogt, "Sensor system for contactless and online moisture measurements," *IEEE Trans. Instrum. Meas.*, vol. 59, no. 11, pp. 3034–3040, 2010, doi: 10.1109/TIM.2010.2046692.
- [158] Q. Smit, B. J. P. Mortimer, and J. Tapson, "General purpose self-tuning capacitance sensor [for oil recycling and soil moisture measurement application]," in *IMTC/98 Conference Proceedings. IEEE Instrumentation and Measurement Technology Conference. Where Instrumentation is Going (Cat. No.98CH36222)*, 2002, vol. 2, pp. 1074–1078, doi: 10.1109/IMTC.1998.676889.
- [159] G. Bresseur, B. Brandstätter, and H. Zangl, "State of the art of robust capacitive sensors," *ROSE 2003 - 1st IEEE Int. Work. Robot. Sens. 2003 Sens. Percept. 21st Century Robot.*, pp. 3–6, 2003, doi: 10.1109/ROSE.2003.1218702.
- [160] O. Bolshunova and A. Korzhev, "Sensors for automatic moisture measurement of bulk and liquid materials," *2nd Int. Conf. Ind. Eng. Appl. Manuf. ICIEAM 2016 - Proc.*, pp. 1–4, 2016, doi: 10.1109/ICIEAM.2016.7910928.
- [161] Y. Xu, W. Yi, and K. Jwo, "Research on the electrical model of a capacitive soil moisture sensor," *Appl. Mech. Mater.*, vol. 261–262, pp. 917–925, 2013, doi: 10.4028/www.scientific.net/AMM.260-261.917.
- [162] A. Rende and M. Biage, "Characterization of capacitive sensors for measurements of the moisture in irrigated soils," *Rev. Bras. Ciências Mec. Brazilian Soc. Mech. Sci.*, vol. 24, no. 3, pp. 226–233, 2002, doi:

- 10.1590/S0100-73862002000300012.
- [163] K. Xu, Q. Sheng, X. Zhang, P. Li, and S. Chen, "Design and calibration of the unilateral sensitive soil moisture sensor," *IEEE Sens. J.*, vol. 15, no. 8, pp. 4587–4594, 2015, doi: 10.1109/JSEN.2015.2423697.
- [164] B. A. Albrecht, C. H. Benson, and S. Beuermann, "Polymer capacitance sensors for measuring soil gas humidity in drier soils," *Geotech. Test. J.*, vol. 26, no. 1, pp. 3–11, 2003, doi: 10.1520/GTJ11101J.
- [165] Y. Liu, C. Xinrong, M. Haomiao, and S. Yuyao, "Improved Method for Modeling in Capacitive Grain Moisture Sensor," in *CCTA 2014: Computer and Computing Technologies in Agriculture VIII*, 2015, pp. 144–150, doi: 10.1007/978-3-319-19620-6_18.
- [166] B. Bailey and T. L. Phelps, "The Capacitance of Textile Materials in Relation to Moisture Content," *Text. Res. J.*, vol. 9, no. 3, pp. 101–113, Jan. 1939, doi: 10.1177/004051753900900302.
- [167] M. Pourová, R. Zajíček, L. Oppl, and J. Vrba, "Measurement of dielectric properties of moisture textile," *Proc. 14th Conf. Microw. Tech. Com. 2008*, 2008, doi: 10.1109/COMITE.2008.4569904.
- [168] J. L. Spencer-Smith, "An electrical method for measuring the moisture contents of fabrics," *J. Text. Inst. Trans.*, vol. 26, no. 11, pp. T336–T340, 1935, doi: 10.1080/19447023508661662.
- [169] M. Peeters, "Independent Evaluation of the Dry Mass and the Moisture Content of Running Textile Yarns with a Capacity-Type Meter," *Text. Res. J.*, vol. 39, no. 12, pp. 1081–1088, 1969, doi: 10.1177/004051756903901201.
- [170] S. M. Smirnov, Y. I. Dorogov, and A. Ternyuk, "Measurement of the moisture content of fiber in a layer of variable thickness," *Meas. Tech.*, vol. 13, no. 9, pp. 1417–1419, Sep. 1970, doi: 10.1007/BF00982024.
- [171] D. D. Cerovic, J. R. Dojcilovic, K. A. Asanovic, and T. A. Mihajlidi, "Dielectric investigation of some woven fabrics," *J. Appl. Phys.*, vol. 106, no. 8, 2009, doi: 10.1063/1.3236511.
- [172] Q. ying Xu and L. kun Yang, "Design of the instrument of measuring moisture ratio in textile fibre based on integrate circuit CAV424," *Adv. Mater. Res.*, vol. 571, pp. 676–679, 2012, doi: 10.4028/www.scientific.net/AMR.571.676.
- [173] T. Kohama and S. Tsuji, "Tactile and proximity measurement by 3D tactile sensor using self-capacitance measurement," *2015 IEEE SENSORS - Proc.*, vol. 3, pp. 1–4, 2015, doi: 10.1109/ICSENS.2015.7370565.
- [174] J. O'Dowd, A. Callanan, and G. Banarie, "Capacitive Sensor Interfacing Using Sigma-Delta Techniques," in *IEEE Sensors, 2005.*

- p. 951, doi: 10.1109/ICSENS.2005.1597858.
- [175] B. Liu, Z. Hoseini, K.-S. Lee, and Y.-M. Lee, "On-Chip Touch Sensor Readout Circuit Using Passive Sigma-Delta Modulator Capacitance-to-Digital Converter," *IEEE Sens. J.*, vol. 15, no. 7, pp. 3893–3902, Jul. 2015, doi: 10.1109/JSEN.2015.2403132.
- [176] Y. Kawahara, S. Hodges, B. S. Cook, C. Zhang, and G. D. Abowd, "Instant inkjet circuits: lab-based inkjet printing to support rapid prototyping of UbiComp devices," in *Proceedings of the 2013 ACM international joint conference on Pervasive and ubiquitous computing - UbiComp '13*, 2013, p. 363, doi: 10.1145/2493432.2493486.
- [177] F. Reverter, X. Li, and G. C. M. Meijer, "Liquid-level measurement system based on a remote grounded capacitive sensor," *Sensors Actuators A Phys.*, vol. 138, no. 1, pp. 1–8, Jul. 2007, doi: 10.1016/j.sna.2007.04.027.
- [178] D. Wang, "Capacitive Sensing: Ins and Outs of Active Shielding," 2015.
- [179] J. G. Montalvo and T. M. Von Hoven, "Review of standard test methods for moisture in lint cotton," *J. Cotton Sci.*, vol. 12, no. 1, pp. 33–47, 2008.

Appendix A

This appendix includes the code of the classification system and for the color and gripping point extraction.

```
clear all
close all
clc
addpath(genpath(pwd))      % Add folder and subfolders to
path
load washProg.mat         % Load variables for washing
programs

Load ResNet50 Test 3 trained for garments classification with 16
categories.
load net_resnet50_16cat.mat
net = net_resnet50_16;
% analyzeNetwork(net)

Extract network features
inputSize = net.Layers(1).InputSize(1:2); % Size of images
accepted by the CNN
classes = net.Layers(end).Classes; % Number of
classification classes
layerName = 'activation_49_relu'; % Name of the
ReLU layer

Create camera input and acquire an image
vid = videoinput('gentl', 1, 'RGB8'); % Create a video
object
src = getselectedsource(vid); % Get the video
object created before
src.BalanceWhiteAuto = 'Continuous'; % Auto balance the
white in the image
src.ExposureAuto = 'Once';
src.GainAuto = 'Continuous';
im = getsnapshot(vid);
load cameraParams_Lj4.mat
```

```
im = undistortImage(im,cameraParams);
```

Image Classification

Classify the image using the trained network

```
imResized = imresize(im, [inputSize(1), inputSize(1)]);  
% Resize the image to the CNN input  
[pred,prob] = classify(net, imResized); % Prediction of  
actual image  
imageActivations = activations(net, imResized, layerName);  
% Extract activations of cross-entropy layer
```

Class Activation Map

```
% Average of the activations for each channel  
avg = mean(imageActivations, [1 2]); % Mean of activation  
values for each channel  
scores = squeeze(avg); % Create a vector with the means of  
each channel
```

```
% Activations weighted on fully-connected layer  
fcWeights = net.Layers(end-2).Weights; % Extract weights of  
the fully-connected layer  
fcBias = net.Layers(end-2).Bias; % Extract bias of  
the fully-connected layer  
scores = fcWeights*scores + fcBias; % Class activations  
weighted on the extracted weights
```

```
% Extract the three highest weights  
[~, classIds] = maxk(scores,3); % Find the indices  
of the 3 biggest weighted activations
```

```
% Create the class activation map for the highest class  
weightVector = shiftdim(fcWeights(classIds(1), :), -1); %  
Extract the weight of the class predicted  
CAM = sum(imageActivations .* weightVector, 3); %  
CAM of the predicted class
```

```
% CAM represent the sum of the 2048 activations weighted with  
the fully connected weights of  
% the predicted class.
```

Top 3 class labels and related class scores

```
scores = exp(scores)/sum(exp(scores));           % Output of the
softmax layer for every class
maxScores = round(scores(classIds)*100,2);      % Accuracy of
the prediction for the Top 3 classes
labels = classes(classIds);                    % Labels of the
Top 3 classes
```

Plot Class Activation Map

```
figure()
% Show the original image
subplot(1,2,1)
imshow(im)
% Show the class activation map
subplot(1,2,2)
CAMshow(im, CAM)
% Title
title([string(labels) + ', ' + string(maxScores) + '%'])
```

Gripping point

Find the gripping point as the maximum value of the CAM

```
imSize = size(im);                             % Extract
the size of the image
CAMres = imresize(CAM, imSize(1:2));           % Resize
the activation map to the image size
[maxCAM, indCAM] = max(CAMres(:));             % Indices
of the maximum value of CAM
[rGrip, cGrip] = ind2sub(imSize(:, :, 1), indCAM); % Convert
the linear index into row and column

% Show the position of the gripping point
CAMshowMarker(im, CAMres, [cGrip rGrip])      % Show the
image with CAM and the marker position
```

Preliminary operations for color identification

Image Pre-processing

```
% Convert to grayscale
imGray = rgb2gray(im);
imshow(imGray, [])
title('Image converted to grayscale')
imGraySize = size(imGray);
```

Binarize Image

```
% Create binary image using texture segmentation
entropyOutput = entropyfilt(imGray); % Entropy filter,
value of each pixel
imshow(entropyOutput,[])
title('Entropy filtered output')
imBW = entropyOutput > 4.3; % Apply threshold
imshow(imBW);
title('Binary image with entropy filter')
```

```
% Remove small objects
properties = regionprops(imBW, 'Area');
properties = sortProperties(properties, 'Area');
minArea = imGraySize(1)/12;
maxArea = properties.Area;
imBW = bwpropfilt(imBW, 'Area', [minArea maxArea]);
imshow(imBW)
title('Small objects removed')
```

Boundaries detection

```
imBound = bwboundaries(imBW);
figure, imshow(imGray)
hold on
visboundaries(imBound, 'LineWidth', 1)
title('Border using texture segmentation')
```

CAM boundary extraction

```
CAMim = imresize(CAM, imGraySize(1:2)); % Resize the
activation map to the grayscale image size
CAMim = normalizeImage(CAMim); % Normalize the
image so to have values between 0 and 1
CAMbin = CAMim > 0.75; % Create a binary
image starting from CAM
imshow(CAMbin) % Show the binary
image
title('CAM converted in binary')
```

```
% Count the number of CAM found and select the biggest
[~, nAreas] = bwlabel(CAMbin)
if nAreas > 1
    CAMbin = bwareafilt(CAMbin, 1,4);
    imshow(CAMbin)
    title('CAM selected from all the areas')
```

```

else % If there is only one CAM
    CAMbin = CAMim > 0.7; % Use a bigger threshold
    imshow(CAMbin)
    title('CAM with threshold 1')
end

```

Find the gripping point as the centroid of the CAM

```

CAMprop = regionprops(CAMbin, 'Centroid');
% Plot in the grayscale image
imMarker = insertMarker(imGray,
    round(CAMprop.Centroid), 'x', 'Size', 40, 'Color', 'red');
figure, imshow(imMarker)
title('Gripping point from area centroid of CAM mask')

```

Extract the borders from the binary image

```

CAMBound = bwboundaries(CAMbin, 'noholes');
imshow(imGray)
hold on
visboundaries(CAMBound, 'LineWidth', 1)
title('CAM Border on original Grayscale Image')

```

Area for color identification

Merge the borders obtained from the grayscale image with the one extracted from the CAM

```

% Concatenate the boundaries
allBound = [imBound; CAMBound];
imshow(imGray)
hold on
visboundaries(allBound, 'LineWidth', 1)
title('Merged borders on Grayscale Image')

```

Create a new mask with the areas present inside the CAM

```

% Create a new mask with the same image size
mask = true(imGraySize);

% Add all the borders as 0 logic element to the previous
mask
for b = 1:length(allBound) % Number of borders
    identified
        for p = 1:length(allBound{b}) % Number of pixel for
            each border
                ind = allBound{b}(p,:); % Extract pixels row
                and column
                mask(ind(1), ind(2)) = 0; % Mask false on the
                borders
            end
        end
    end

```

```
    end
end

% Remove the areas outside the CAM from the mask
mask = logical(mask .* CAMbin);

% Select the bigger area of the mask
colorBW = bwareafilt(mask, 1,4);

% Apply morphological opening to smooth the borders
s = strel('disk', 5);
colorBWopen = imopen(colorBW, s);
figure, imshowpair(colorBW, colorBWopen, 'falsecolor')

% Show the final border on the original image
colorBound = bwboundaries(colorBWopen, 'noholes');
imshow(imGray)
hold on
visboundaries(colorBound, 'LineWidth', 1)
title('Border of the color extraction area')
```

Color identification

Apply the mask to the RGB resized image and find the median values for each channel

```
% Show the original RGB image masked
maskedRgbImage = bsxfun(@times, im, cast(colorBWopen,
'like', im));
figure, imshow(maskedRgbImage)
title('RGB image with mask applied on it')
```

Color identification using the mask on the RGB image

```
% Extract the three channels from the image
redCh = im(:,:,1);
greenCh = im(:,:,2);
blueCh = im(:,:,3);

% Extract the pixel values applying the color mask
redValue = redCh(colorBWopen);
greenValue = greenCh(colorBWopen);
```



```

blueValue = blueCh(colorBWopen);

% Median value for each channel (average works better)
avgRed = double(median(redValue, 'all'))/255;
avgGreen = double(median(greenValue, 'all'))/255;
avgBlue = double(median(blueValue, 'all'))/255;

% Color identification
[color, ~] = colnames('Natural', [avgRed, avgGreen,
avgBlue]);
color = string(color{1});
fprintf('The color of garment is: %s', color)

```

Washing Program

Main program

```

white = 'White'; % Variable to set washing
temperature
catPred = string(pred); % Convert the prediction
from CNN into a string
idx = find (catOrd == catPred); % Find the index for
washing program and temperature
Prog = wProg(idx); % Washing Program

```

Temperature

```

if colDep(idx) == 1 % If the category is color dependent
    if color == white
        Temp = num2str(tempWhite(idx));
        ProgFinal = strcat(Prog,Temp);

    else
        Temp = num2str(tempCol(idx));
        ProgFinal = strcat(Prog,Temp);

    end
elseif colDep(idx) == 0 && ~isnan(tempWhite(idx)) % If the
category is not color dependent
    Temp = num2str(tempWhite(idx));
    ProgFinal = strcat(Prog,Temp);

else % If the category is not color dependent and a
temperature is not set
    ProgFinal = Prog;
end

```

```
fprintf('The washing program is %s', ProgFinal)
```

Support functions

Visualize the CAM

```
function CAMshow(im, CAM)
% INPUT:
% 1- Original image
% 2- Class Activation Map of the same image

% Scale and normalize the CAM to the original image size
imSize = size(im);           % Extract the size of
the image
CAM = imresize(CAM, imSize(1:2)); % Resize the activation
map to the image size
CAM = normalizeImage(CAM);    % Normalize the image
so to have values between 0 and 1
CAM(CAM < 0.2) = 0;         % Remove small
activations

% Adapt the CAM to the Jet color map
CAM = CAM*255;              % Scale CAM values from
0-1 to 0-255
jetmap = jet(255);         % Create jet colormap
with 255 values (like RGB)
scalemap = linspace(0,1,255)'; % Vector to scale the
color intensity of the jet colormap
cmap = jetmap.*scalemap;   % Create the jet color
map that will be used to convert
                           % the CAM in RGB
CAM = ind2rgb(uint8(CAM), cmap)*255;% Convert CAM values to
integer and then to RGB on jet colormap

% Combine the original image with the CAM converted on RGB
combinedImage = double(rgb2gray(im))/2 + CAM;
combinedImage = normalizeImage(combinedImage)*255;
imshow(uint8(combinedImage)); % Convert to integer
and then show the image
colormap(gca, cmap);
% colorbar(gca)
end
```

Normalize the image to have the pixel values between 0 and 1

```
function N = normalizeImage(I)
minimum = min(I(:));
maximum = max(I(:));
N = (I-minimum)/(maximum - minimum);
end
```

Visualize the Class Activation Map with a marker in the position of the gripping point

```
function CAMshowMarker(im, CAMres, position)
% INPUT:
% 1- Original image
% 2- Class Activation Map of the same image
% 3- Marker position

% Scale and normalize the CAM to the original image size
CAMres = normalizeImage(CAMres);           % Normalize the
image so to have values between 0 and 1
CAMres(CAMres < 0.2) = 0;                 % Remove small
activations

% Adapt the CAM to the Jet color map
CAMres = CAMres*255;                       % Scale CAM
values from 0-1 to 0-255
jetmap = jet(255);                         % Create jet colormap
with 255 values (like RGB)
scalemap = linspace(0,1,255)';           % Vector to scale the
color intensity of the jet colormap
cmap = jetmap.*scalemap;                  % Create the jet color
map that will be used to convert
                                           % the CAM in RGB
CAMres = ind2rgb(uint8(CAMres), cmap)*255;% Convert CAM
values to integer and then to RGB on jet colormap

% Combine the original image with the CAM converted on RGB
combinedImage = double(rgb2gray(im))/2 + CAMres;
combinedImage = uint8(normalizeImage(combinedImage)*255);
imMarker = insertMarker(combinedImage, position, 'x',
'Size',80, 'Color', 'white');
figure()
imshow(imMarker)
```

```
end
```

Sort properties

```
function properties = sortProperties(properties, sortField)
% Compute the sort order of the structure based on the sort
field.
[~,idx] = sort([properties.(sortField)], 'descend');

% Reorder the entire structure.
properties = properties(idx);
end
```